Solid State Spectroscopy I
— IR, VUV, etc. —

(BL1B, 5B, 6A1, 7B, 8B1)

(BL1B)

Vacuum-ultraviolet reflectance spectroscopy of transition-metal oxides

Tsuyoshi KIMURA[1], Shigeki MIYASAKA[1], Kenya OHGUSHI[1], Masakazu MATSUBARA[1], Takeshi GOTOU[1], and Yoshinori TOKURA[1,2,3]

[1] *Department of Applied Physics, University of Tokyo, Tokyo 113-8656*

[2] *Correlated Electron Research Center (CERC), National Institute of Advanced Industrial Science and Technology (AIST), Tsukuba 305-8562*

[3] *Spin Superstructure Project, ERATO, Japan Science and Technology Corporation (JST), Tsukuba 305-8562*

One of the most important characteristics for the correlated electron systems is the drastic re-construction of electronic structure over an energy scale of eV with changes of temperature, doping concentration, and/or external field. Therefore, optical reflectivity measurement over a wide energy range and the optical conductivity spectra derived from the reflectivity spectra provide us with very useful information about the strongly correlated electron systems.

In this beam time, we measured the reflectivity spectra of several transition-metal oxides, including Mn-, Ni-, Co-, Mo- and V-oxides, for an energy range of 4 eV < E < 35 eV at room temperature using the beam line BL1B. The measured reflectivity data, together with the lower-energy data below 6 eV, were used to derive the optical conductivity spectra or dielectric function via the Kramers-Kronig analysis. As an example, the imaginary part of the dielectric function of single-layered manganite crystals, $Nd_{1-x}Sr_{1+x}MnO_4$ (x=0.67, 0.75, 0.82) are shown below.

At low temperatures, this system undergoes the doping-induced crossover between the charge-ordered zigzag-type ferromagnetic state ($x \leqq 0.75$) and the charge-disordered one-dimensional ferromagnetic (C-type antiferromagnetic) one ($0.75<x<0.90$), which arise from the e_g-orbital ordering of alternate d_{3x2-r2}/d_{3y2-r2} and coherent d_{3x2-r2}, respectively. As shown in the figure, the ε_2 spectra for x=0.67 and 0.75 are distinctly different from that for x=0.82 even at room temperature, which is above the spin-, charge- and orbital-ordering temperature. These spectral features are attributed to robust spin-, charge- and orbital-correlation in this system.

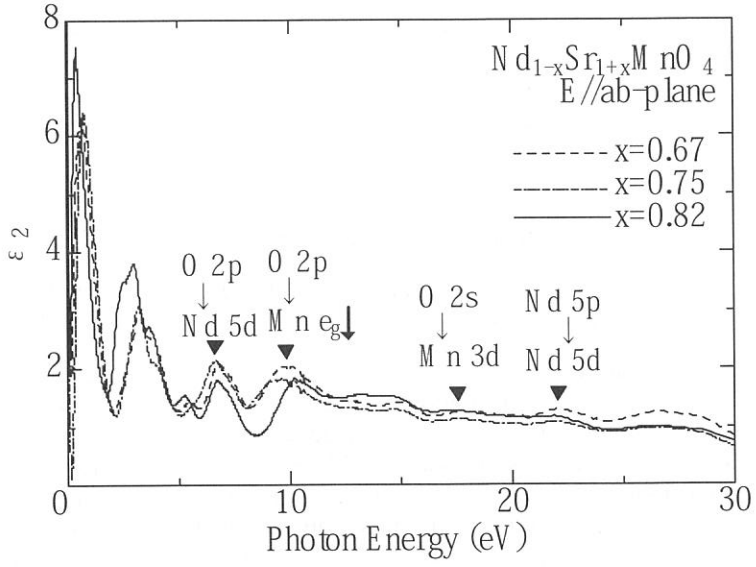

(BL-1B)

VUV Spectroscopy on Condensed Oxygen under Pressure

Yuichi Akahama, Masaki Harada, Souichi Nose and Haruki Kawamura

Department of Material Science, Graduate School of Science, Himeji Institute of Technology, 3-2-1, Koto, Kamigohri, Hyogo 678-1297

Introduction

The physical and chemical properties of condensed oxygen have been of considerable interest for many years because of its simple and fundamental molecular magnetism. For liquid oxygen, up to now, many arguments about the formation of O_4 molecular units have been made while it has been revealed that vibronically induced excitations of O_2 pairs from $2^3\Sigma_g^-$ to $2^1\Delta_g$ make liquid oxygen blue. (The potential-energy diagram of O_2[1] is shown in Fig. 1). More recently, metal-insulator transition has been reported in highly condensed oxygen and superconductivity has been observed in the molecular-metal phase. (The P-T phase diagram of oxygen[2] is shown in Fig. 2.) In such phenomena, the intermolecular interaction between O_2 molecules will play a main role. Therefore, it is important to understand the interaction from the viewpoint of chemical bonding of molecules. However, there has been no report of the study on electronic spectra of condensed oxygen in the VUV region under pressure.

In this report, VUV absorption spectra of condensed oxygen are presented up to 13 GPa for the discussion of the intermolecular interaction between O_2 molecules.

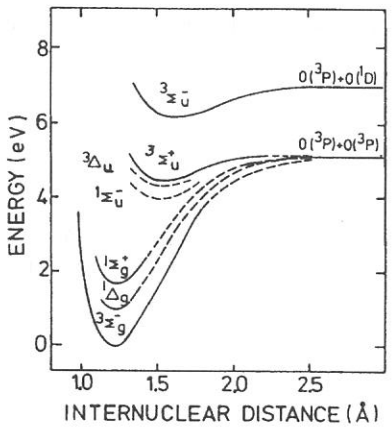

Fig.1 Potential-energy diagram of the O_2 molecular states[1].

Experimental

The VUV absorption measurements were developed over the wide pressure range from gaseous state at 1 atm to solid state at 13 GPa at room temperature using the VUV source on the BL-B1 beam line, at UVSOR in IMS. For applying pressure, a sapphire or a type IIA diamond anvil high-pressure cell was used. Liquid oxygen was loaded in a sample chamber of the pressure cell, and pressure was regulated at 300 K based on a ruby pressure scale. Error of estimated pressure was ±0.05 GPa. Raman shift due to the intramolecular vibration (O_2 vibron) was also used to determine the sample pressure. The thickness and diameter of the sample chamber were about 27-35 μm and 100-200 μm, respectively. The oxygen sample in solid phases was polycrystalline. Transmitted light through the oxygen sample and the anvils were collected with a detector of a photo multiplier.

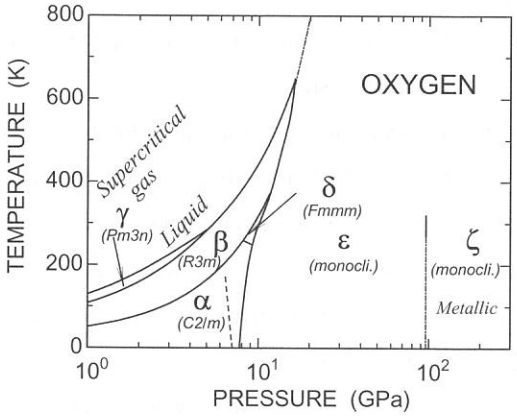

Fig. 2 Phase diagram of oxygen[2].

Results and Discussion

Figure 3(a) shows the typical absorption spectra of condensed oxygen at pressure up to 1.5 GPa at 300 K. The spectra were measured using the sapphire anvil cell. At first experimental run, pressure was increased from 0.95 GPa to 1.5 GPa, and then decreased to 0.05 GPa. At second run, pressure was increased from 0.13 GPa to 1.0 GPa. By applying pressure, the thickness of the sample, which was estimated from the thickness of the recovered gasket after compression, decreased from 35 μm to about 27 μm. Very strong absorption was observed in VUV region of 5-7 eV. At lower pressure than 0.13 GPa, the on-set of the absorption locates above 6.5 eV and agrees with that of the absorption spectrum of low-pressure gas at about 1 Pa. Maximum absorption coefficient observed in the experiments was about 7×10^2 cm^{-1}. The absorption band corresponds to the Schumann-Runge system of the $^3\Sigma_g^- \rightarrow {}^3\Sigma_u^-$ transition. The prominent feature of the spectra is a dramatic low-energy shift of the absorption edge with increasing pressure. The pressure dependence of the absorption edge is illustrated in Fig. 4. The

absorption edge shifts from 6.5 eV to 5.0 eV at pressure between 0.13 and 0.5 GPa. Under such pressures, the sample is in a supercritical gas state and the state is actually dominated by the intermolecular interaction. However, it is unlikely that the energy of the $^3\Sigma_g^- \rightarrow {}^3\Sigma_u^-$ transition decreases more than 1.5 eV by van der Waals like interaction because its interaction is order of 0.1 eV. It should be considered that a new absorption band occurs in the VUV region. The band energy corresponds to the Herzberg band. Therefore, one probable explanation for the origin of the absorption band is that the Herzberg system of the $^3\Sigma_g^- \rightarrow {}^3\Sigma_u^+$ transition becomes allowed as a result of an intermolecular interaction such as the formation of O_4 molecular units as involving a symmetrical change in the electron orbit. Because the system is forbidden by a parity selection rule and its absorption is extremely weak.

The absorption spectra at higher pressure to 13 GPa at 300 K shown in Fig. 3(b) were collected using the diamond anvil cell with two experimental runs. As increasing pressure up to 13 GPa at 300 K, the oxygen crystallized in the rhombohedral β–O_2 at 6.0 GPa. The β-O_2 transformed to the orthorhombic δ-O_2 at 9.5 GPa, and further to the monoclinic ε-O_2 at 10 GPa. The edge of the strong VUV absorption shifts the low-energy side monotonically with pressure and reaches 3.5 eV at 12.7 GPa. The pressure dependence of the absorption edge of the ε-O_2 is consistent with a previous report[3] and the energy of the edge finally decreases 0.8 eV just before the metal-insulator transition to ζ-O_2 at 96 GPa[3]. The optical gap corresponds to the energy gap of the solid oxygen and the metallization is caused by a closure of the gap. In order to understand the metallization, it is indispensable to clarify the mechanism of the new VUV absorption. The spectra also indicate additional absorption bands at 2.2-2.4 eV, 2.7-3.0 eV, and 3.5-3.8 eV. These bands, which move to higher energies by about 0.02 eV/GPa, are assigned to the $2^3\Sigma_g^- \rightarrow 2^1\Delta_g$, $2^3\Sigma_g^- \rightarrow {}^1\Delta_g + {}^1\Sigma_g^+$, and $2^3\Sigma_g^- \rightarrow 2^1\Sigma_g^+$ transitions, respectively. The behavior well agrees with the previous report[4].

In conclusion, a strong VUV absorption with an on-set of 5.0 eV was newly found for condensed oxygen in this study. The absorption occurred in supercritical gas state, where the intermolecular interaction actualizes. The interaction must be remove the selection rule of Herzberg system with a perturbation to the symmetry of electron orbits. Since the VUV absorption of oxygen molecules has a significant meaning for life, making clear the absorption mechanism is next our subject.

References

[1] G.Herzberg, Molecular Spectra and Molecular Structure I. Spectra of Diatomic Molecules (Van Nostrand, Prinston, 1950).

[2] Y.Akahama *et al.* Phys. Rev. B**64**(2001) 0541051.

[3] M.Nicol & K.Syassen, Phys. Rev.B**28**(1983)1201.

[4] S.Desgreniers *et al.* J.Phys. Chem. **94**(1990)1117.

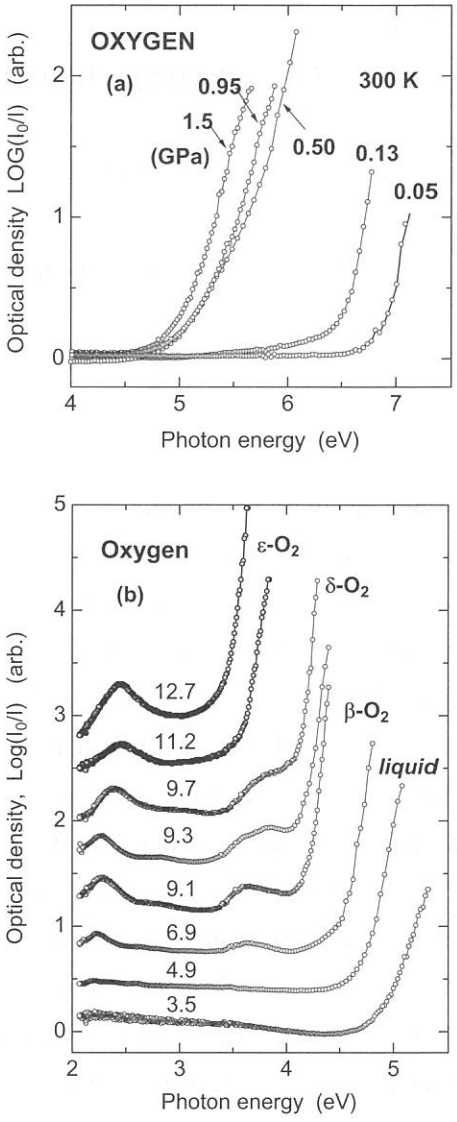

Fig. 3 Pressure dependence of absorption spectra of condensed oxygen, (a) at lower pressure using a sapphire anvil cell, and (b) at higher pressure using a diamond anvil cell.

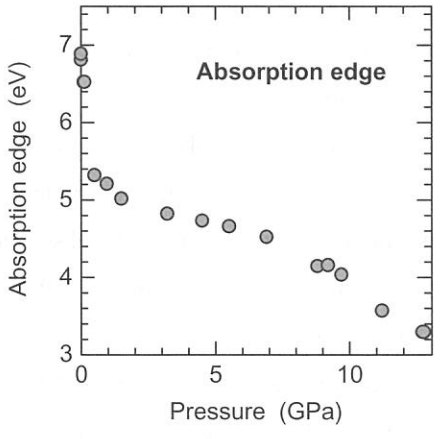

Fig. 4 Pressure dependence of the absorption edge of condensed oxygen.

(BL1B)

VUV Optical Spectra of Hydrogen-Bonded Ferroelectrics CsH_2PO_4

T. FUYUKI, N. OHNO, K. SASAKI and K. DEGUCHI[A]

Division of Electronics and Applied Physics, Osaka Electro-Communication University, Neyagawa 572-8530

[A]*Department of Materials Science, Shizuoka Institute of Technology, Fukuroi, Shizuoka 437-8555*

Cesium dihydrgen phosphate, CsH_2PO_4 (CDP) is one of hydrogen-bonded ferroelectric materials. Below the transition temperature T_C≃150 K, the spontaneous polarization P_S takes place along the *b*-axis, showing a first-order structural phase transition from a monoclinic $P2_1/m$ to orthorhombic $P2_1$ [1]. Replacing the hydrogen by deuteron, T_C increases from 150 K to 270 K. The advantage of targeting CDP is that the hydrogen bond linking PO_4^{3-} tetrahedra are in quasi-one-dimensional network separated by Cs^+ ions, in contrast to well known KH_2PO_4 (KDP) with three-dimensional linkage of the hydrogen bonds.

In the present study, reflection and absorption spectra of CDP have been investigated in the VUV region by using polarized synchrotron radiation at the BL1B beam line. The single crystals of CDP were grown at ～50 ℃ by slow cooling of a saturated aqueous solution after several times of recrystallization [2], and the specimens were cleaved just before the optical measurements.

Figure 1 shows the reflection spectra of CDP for polarization parallel to the crystallographic *b*-axis (***E***//***b***) and the *c*-axis (***E***//***c***) measured at 12 K. By comparing the previous reports of the reflection spectra of KDP [3,4], structures of the energy region from 8 to 15 eV are quite similar to those of CDP. Consequently, the A, B, C and D peaks are certainly ascribed to the transitions due to the anions, namely, $[H_2PO_4]^-$ complex ions. The sharp reflection peak A is observed at 9.64 eV for ***E***//***b*** and at 9.43 eV for ***E***//***c***, and the spectral profile is quite similar to that of the structure of KDP at ～10 eV. It is to be noted that the structure A observed for CDP exhibits more appreciable anisotropy. The structures observed in the region from 15 to 22 eV are shifted in energy with about 5 ～8 eV higher than the structures in the reflection spectra of KDP, but the spectral profile and the polarization dependence are quite similar to those of KDP. Therefore, these structures are originated from the transitions in cationic Cs^+ ions.

Figure 2 shows the fundamental absorption spectra of CDP at various temperatures. At 12 K the absorption edge starts at ～7.4 eV, shifting to the lower energy side with increasing temperature. It is also found that the logarithmic plot of the fundamental absorption tail gives a straight line above 50 K, indicating that the Urbach rule holds for the absorption tail of CDP. We have obtained the small value of the high- temperature steepness parameter σ_0= 0.37.

We have investigated the energy shift of the absorption tail at around T_C, and the anomalous shift was observed at T_C. Figure 3 shows the temperature dependence of the absorption-edge energy in CDP determined at α=100 cm^{-1}. As clearly seen in Fig. 3, the absorption-edge energy above T_C shows a small temperature shift compared with that below T_C. Such an anomalous shift has been also found at the absorption edge of KDP [5].

Therefore, it is concluded that the ferroelectric phase transition in hydrogen-bonded ferroelectrics influences the fundamental absorption edge.

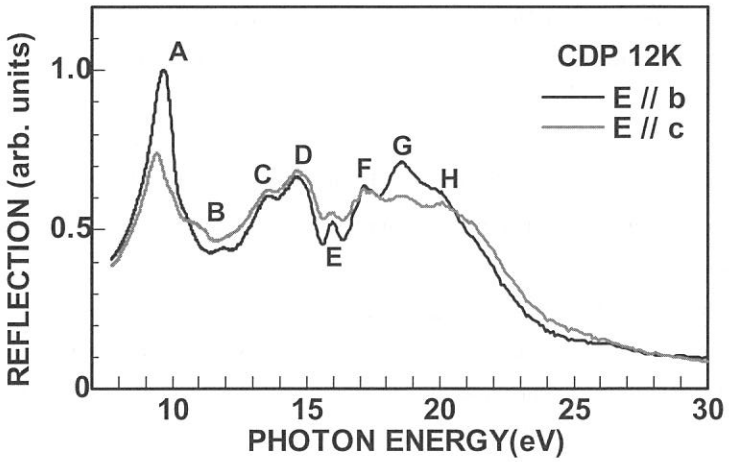

Fig. 1. Reflection spectra of CDP measured at 12K.

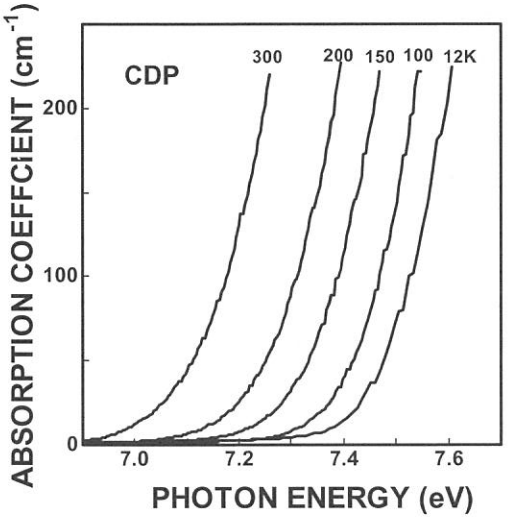

Fig. 2. Absorption edge spectra of CDP at various temperatures.

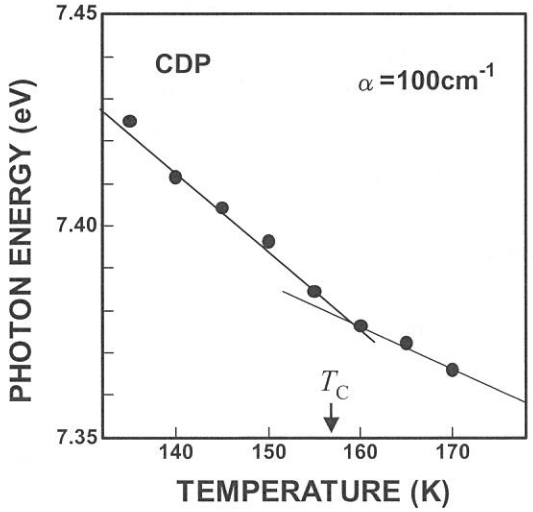

Fig. 3. Temperature dependence of the absorption tail energy of CDP determined at α=100 cm^{-1}.

REFERENCES

[1] A. Levstik, R. Blinc, P. Kadaba, S. Cizlkov, I. Lvstik and C. Filipic, Solid State Commun. **16** (1975) 1339.

[2] K. Deguchi, E. Okaue and E. Nakamura, J. Phys. Soc. Jpn. **51** (1982) 3569.

[3] S. Saito, K. Wada and R. Onaka, J. Phys. Soc. Jpn. **37** (1974) 711.

[4] S. Matsumoto, M. Fujisawa and S. Suga, J. Electron Spectrosc. Relat. Phenom. **79** (1987) 615.

[5] S. Saito and R. Onaka, Ferroelectrics **21** (1978) 553.

(BL1B)

Photoionization of Adsorbed Dye below Aliphatic Acid Monolayer at the Aqueous Solution Surface

Toshio Ishioka, Akira Harata, and Yoshihiko Hatano

Department of Molecular and Material Sciences, Kyushu University,
Kasugakoen 6-1, Kasuga-shi, Fukuoka 816-8680, Japan

Introduction

Photoionization of molecules has been of great importance both in fundamental and applied sciences. Such studies have been in progress with powerful photon sources such as lasers and synchrotron radiation (SR).[1] SR has a complementary as compared with laser radiation to study photoionization of molecules not only in the gas phase but also in the condensed phase or at the surface to characterize molecular states or to analyze photoionization mechanisms.

A solute in a bulk solution is known to photoionize at a lower photon energy than the ionization potential in the gas phase due to neighboring solvent molecules around a solute molecule. However, photoionizing behavior of adsorbed molecules at an aqueous solution surface has hardly studied even though there are a wide variety of surface-active molecules and their adsorption behavior has a great importance in physical chemistry, biochemistry, environmental chemistry, and technology. It seems that the mechanism of the photoionization of a molecule at the liquid surface is different from that in the gas phase or in the bulk liquid phase but it has not been clarified due to a lack of precise experimental results.

Furthermore, it is not clarified also how a solute interacts on photoionization with solvent molecules or surface-active species and how much distance from surface the solute molecule participate in that. In this study, photocurrent induced by the single-photon ionization of a water-soluble rhodamine dye with and without aliphatic acid is measured in a cell that is specially designed for solution surfaces. The photoionization process and the state of the rhodamine dye molecules are discussed by acid density dependence of photoionization current.

Experimental

The experimental setup is illustrated in Figure 1. The monochromated synchrotron light (4-8 eV) was obtained from BL1B at the UVSOR facility and emitted from the chamber to the He-purged cell through an MgF_2 window.

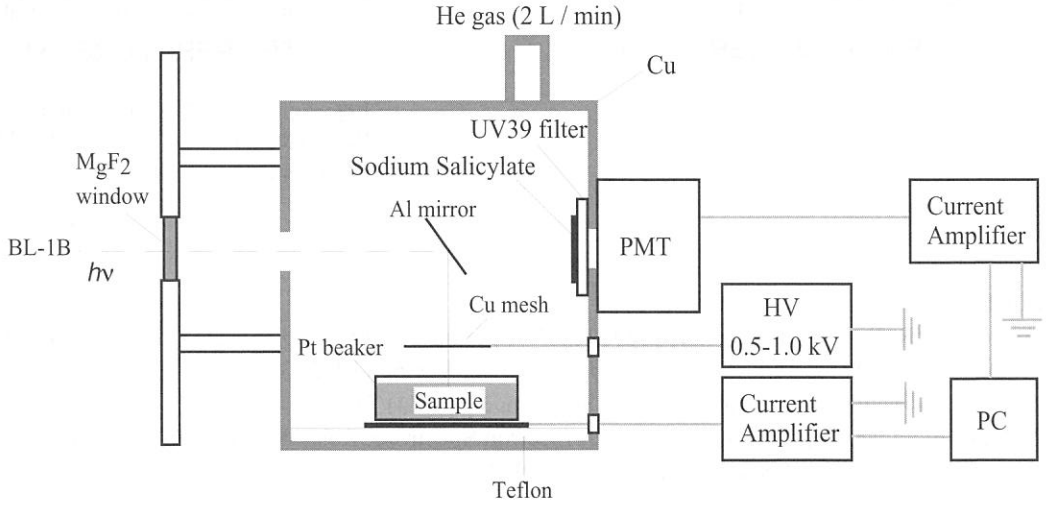

Figure 1 Schematic illustration of experimental setup for single-photon ionization on the water surface.

The emitted light was reflected on an Al mirror and vertically irradiated on the aqueous solution surface through a Cu-mesh electrode. The electrode was set at 5 mm high above the liquid surface and high voltage (500-1000 V) was applied to the electrode so that emitted electrons were trapped. The sample solutions were composed of surface-active dye (rhodamine B, 10 μM), a buffer electrolyte (HCl, pH 1.0), and water. The aqueous solution surface was modified with aliphatic acid (arachidic acid, $C_{19}C_{39}CO_2H$) by spreading as a benzene solution. The added amount was approximately within two monolayers at maximum that is calculated by the assumption that close-packed layer was formed on the aqueous solution surface. The photocurrent (~100 fA) was measured by a picoammeter (Model 617, Keithley) and the incident photon intensity was monitored by measuring fluorescence intensity from sodium salicylate plate by a photomultiplier tube (1P28, Hamamatsu Photonics).

Results and Discussion

Typical photon energy dependence of measured current is shown in Figure 2. The intensities are normalized with the SR photon intensities. The photocurrent for the surface of pure buffer solution and aliphatic acid is not detected in this experimental accuracy. Without aliphatic acid on the surface of Rhodamine B solution, the current increases steeply with the photon energy above the threshold energy, 5.6 eV, which coincides with the previous report of the photoionization threshold of rhodamine B on the water surface.[2] By adding aliphatic acid on the solution surface, the current increases in the same manner and no remarkable changes are observed on the threshold energy. However, the intensity remarkably increases when a small amount of acid is added (~0.2 monolayer) and then decreases to a constant value above monolayer formation level (Figure 3). These experimental results can not be explained by a simple model that is described by the uniform monolayer formation and simple electron scattering through the aliphatic monolayer because this model needs monotonous decrease of photoionizaion current upon film formation. Changes of a surface structure such as aggregate formation and accumulation of dyes around the aggregate is one of the possible explanations for such behavior. We do not have enough data to discuss the surface structure at this stage and further experiments such as spatially microscopic two-photon ionization and fluorescence microscopy at the surface are now in progress.

References

1. Y. Hatano, *Phys. Rep.*, **1999**, *313*, 109.
2. T. Ishioka, K. Seno, A. Harata, and Y. Hatano, *UVSOR Activity Report 2001*, 104.

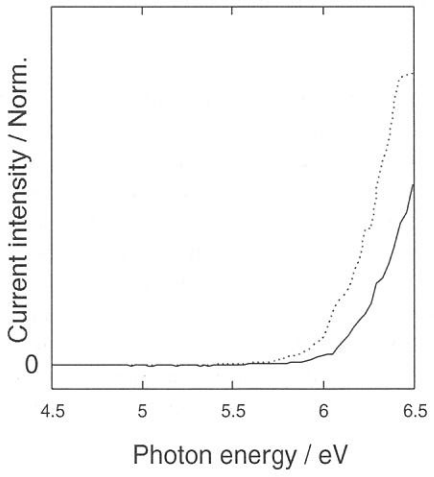

Figure 2. Photon energy dependence of measured photocurrent from the Rhodamine B aqueous solution surface.
Solid line: rhodamine B aqueous solution surface
Broken line: rhodamine B aqueous solution surface modified with arachidic acid (0.2 monolayer)

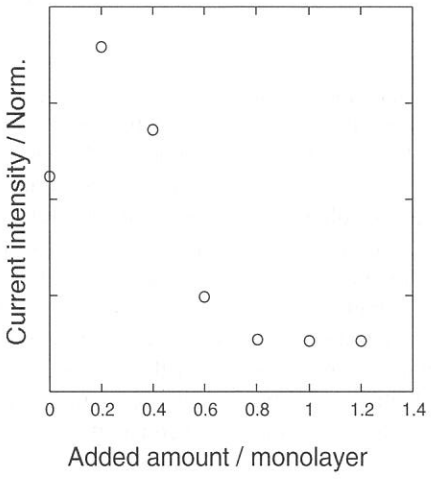

Figure 3. Effect of arachidic acid addition on the photocurrent from the surface of rhodamine B aqueous solution.

(BL1B)

Optical Band Gap Energy of High-permittivity Hafnium and Zirconium Silicates

Hiromitsu KATO, Tomohiro NANGO, and Yoshimichi OHKI

Department of Electrical Engineering and Bioscience,
Waseda University, Shinjuku-ku, Tokyo 169-8555.

Amorphous hafnium silicate and zirconium silicate films were successfully deposited by simple plasma-enhanced chemical vapor deposition. The source materials are tetraethoxysilane (TEOS: $Si(OC_2H_5)_4$) and a hafnium alkoxide [$Hf(O\text{-}i\text{-}C_3H_7)_4$] or a zirconium alkoxide [$Zr(O\text{-}i\text{-}C_3H_7)(C_{11}H_{19}O_2)_3$]. Oxygen, used as a carrier and oxidation gas, was excited with a rf power of 13.56 MHz through capacitive coupling. The TEOS was vaporized and transported at 70 °C into the "tail flame" of the oxygen plasma. The TEOS flow rate was controlled with a mass-flow controller. The hafnium or zirconium alkoxide was vaporized and transported at 220 °C into the oxygen plasma. Argon was used as a carrier and diluent gas for each alkoxide vapor and its flow rate was controlled with a mass-flow controller. A CaF_2 crystal transparent to 9.9 eV (125 nm) was used as a substrate for vacuum ultraviolet (VUV) absorption measurements. The substrate temperature was kept constant at 400 °C during the deposition. By changing the flow rate of argon from 5 to 50 sccm, four kinds of hafnium films shown in Table I were deposited. Another film deposited without using TEOS was also prepared as a reference. Similarly, five zirconium films were deposited including one reference deposited without using TEOS. Furthermore, one more film was deposited for reference without using alkoxides. During the deposition, the flow rates of oxygen and TEOS were kept constant at about 0.71 and 1.0 sccm, respectively. The total pressure changed from 40 to 65 Pa depending on argon flow rate.

The deposited films were examined by X-ray photoelectron spectroscopy (XPS) using Mg $K\alpha$ ($h\nu$ = 1253.6 eV) X-rays. The VUV absorption spectra were measured by a Shimadzu UV-3100 spectrophotometer for only sample ZC, while they were observed using synchrotron radiation (SR) operated in a multi-bunch mode (BL1B Line, UVSOR, Institute for Molecular Science, Okazaki, Japan) for all the other samples. All measurements were done at room temperature.

By XPS analyses, the deposited samples HC1 to HC4 or ZC1 to ZC4 were found to be silicate films with O-Si and O-Hf bonds or those with O-Si and O-Zr bonds. It was also found that the films are represented by the formula $Hf_xSi_{(1-x)}O_y$ or $Zr_xSi_{(1-x)}O_y$ with the elementary compositions shown in Table I.

Figure 1 shows the VUV absorption spectra of the silicates. The onset of the interband photon absorption between the valence band and the conduction band shifts to a lower energy as the hafnium or zirconium content increases. No specific absorption due to defect states or impurities is detected below the onset energy. The fact that the onset spreads out over a wide energy region indicates that the deposited films are amorphous with structural randomness. Since the films are amorphous, the interband absorption can be expressed by the following equation:

$$\alpha h\nu \propto (h\nu - E_{opt})^2, \qquad \text{------(1)}$$

where α, $h\nu$, and E_{opt} are the absorption coefficient, photon energy, and optical band gap energy, respectively. By replotting the data shown in Fig. 1 in accordance with Eq. (1), the values of E_{opt} are estimated as shown in Fig. 2. If we compare the values of E_{opt} between the films with the same x, the hafnium silicate has a larger value than the zirconium silicate. The value of E_{opt} decreases monotonically as x increases in both silicates. This is reasonable since the band gap of HfO_2 or that of ZrO_2 is far narrower than SiO_2. However, if we go into detail, E_{opt} decreases rapidly up to x = 0.6 and then stays almost constant. It is known that the nonbonding O 2p states form the top of the valence band of SiO_2 and that the Si-O antibonding states form the bottom of its conduction band. In the case of ZrO_2, the O 2p states form the top of the valence band as in the case of SiO_2, but the antibonding d-states of zirconium form the lowest conduction band states. Therefore, the rapid decrease in E_{opt} with an increase in x in the case of the zirconium silicate is considered to be due to the increase in the d-state electrons. When x is higher than 0.6, it seems that the bottom of the conduction band is fully formed by the Zr d-states, resulting in the constant E_{opt}.

Table I Source alkoxide and elementary ratios of the deposited films.

Sample	Alkoxide	Elementary ratio (atomic %)			$Hf_x Si_{(1-x)}O_y$	
		Hf	Si	O	x	y
HC1	HA, T	13	20	67	0.39	2.0
HC2	HA, T	18	16	66	0.53	1.9
HC3	HA, T	20	12	68	0.63	2.1
HC4	HA, T	23	8.6	68	0.73	2.2
HC	HA	33	---	67	1.0	2.0
---	---	Zr	Si	O	$Zr_x Si_{(1-x)}O_y$	
ZC1	ZA, T	8.5	25	66	0.25	2.0
ZC2	ZA, T	13	23	64	0.36	1.8
ZC3	ZA, T	17	16	67	0.52	2.0
ZC4	ZA, T	20	15	65	0.57	1.9
ZC	ZA	33	---	67	1.0	2.0
SC	T	---	33	67	0	2.0

HA: hafnium alkoxide, ZA: zirconium alkoxide, T: TEOS

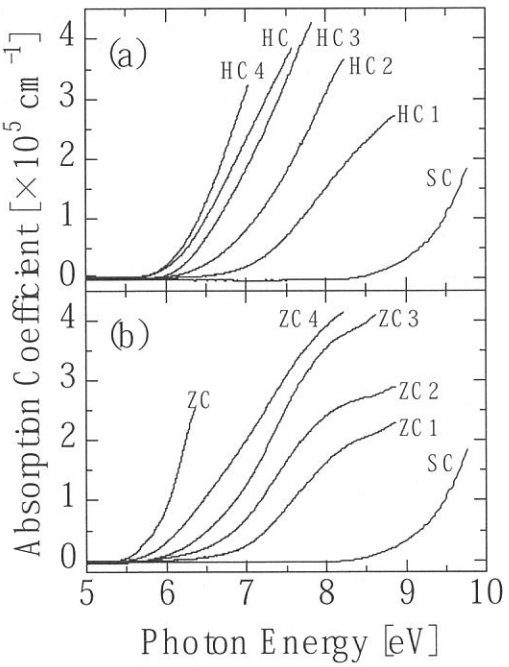

Fig. 1. VUV absorption spectra of $Hf_xSi_{(1-x)}O_y$ (a) and $Zr_xSi_{(1-x)}O_y$ (b).

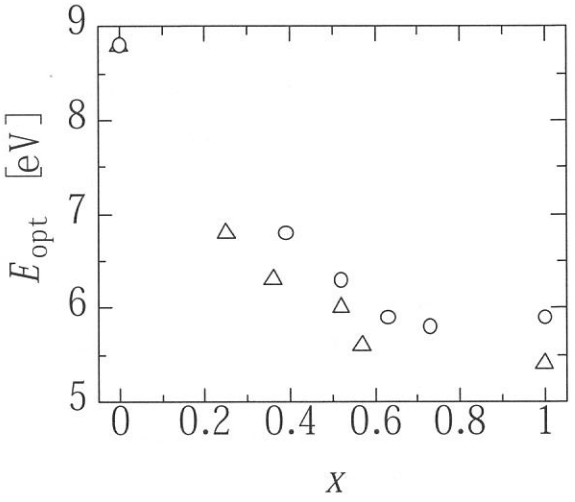

Fig. 2. Optical band gap energy (E_{opt}) estimated from the VUV absorption spectra as a function of the composition x. Circles and triangles indicate the data obtained for $Hf_xSi_{(1-x)}O_y$ and $Zr_xSi_{(1-x)}O_y$, respectively.

(BL1B)

Optical Absorption Bands of Tl^+ Centers Doped in Ammonium Halides with the CsCl Structure

Taketoshi KAWAI and Satoshi HASHIMOTO

Department of Environmental Sciences, Faculty of Science, Osaka Women's University, Daisen- cho, Sakai City, Osaka 590- 0035, Japan

When the Tl^+ ions are doped in alkali halides with the NaCl structure, the absorption bands called A, B and C from the lower energy side are observed in the energy region below the fundamental absorption edge of the host crystals. The A, B and C bands have it's origin in the intraionic transitions corresponding to $^1S_0 \rightarrow {}^3P_1$ (spin-orbit allowed), $^1S_0 \rightarrow {}^3P_2$ (vibration induced) and $^1S_0 \rightarrow {}^1P_1$ (dipole allowed), respectively [1,2]. On the other hands, the absorption bands of the Tl^+ centers doped in cesium halides having the CsCl structure are remarkably different from those of NaCl-type alkali halides doped with the Tl^+ centers [3- 7]. What is the cause of the difference of the absorption spectra between NaCl- and CsCl- type alkali halide crystals doped with the Tl^+ centers? In order to make the problem clear, further optical studies of the Tl^+ centers doped in ionic crystals with the CsCl crystal structure are needed.

Ammonium halides are the same ionic crystals as alkali halides and have the CsCl structure at low temperature with an exception of NH_4F. Though ammonium halides are an attractive host material for the Tl^+ ions, optical properties of the Tl^+ centers doped in the ammonium halides are comparatively less studied [8- 11], especially in the vacuum ultraviolet energy region. Optical studies of ammonium halides doped with the Tl^+ centers will provide useful information on the Tl^+ centers doped in ionic crystals with the CsCl structure.

Single crystals of $NH_4Cl:Tl^+$ were grown from saturated aqueous solution containing various TlCl concentrations from 10^{-2} to 10^{-6} mole %. Urea was added into the solution as a habit modifier in order to obtain the good cube shaped samples. For the optical measurements, the light source of 2.0～25 eV was obtained from the 270 MeV electron storage ring of the synchrotron radiation from a BL- 1B beam line of UVSOR. The absorption spectra were measured by using a 1 m monochromator of Seya- Namioka type.

Figure 1 shows the absorption spectra of the $NH_4Cl:Tl^+$ and $NH_4Br:Tl^+$ crystals with lower concentrations of the Tl^+ ions. In $NH_4Cl:Tl^+$ and $NH_4Br:Tl^+$, absorption bands with the lowest peak energy are observed at 4.88 and 5.22 eV, having halfwidths of 65 and 77 meV, respectively. The most intense absorption bands are observed at 5.98 eV for $NH_4Cl:Tl^+$ and at 6.59 eV for $NH_4Br:Tl^+$. Their absorption intensities are about six times as large as those of the respective lowest bands. The intensity ratio is similar to those of the C to A absorption bands in NaCl- type alkali halides doped with the Tl^+ centers. Therefore, the lowest energy and most intense absorption bands are assigned to the A and C bands, respectively. Several weak absorption bands appear in the energy region between the A and C absorption bands.

Figure 2 shows the absorption spectra of $NH_4Cl:Tl^+$ and $NH_4Br:Tl^+$ with higher concentrations of the Tl^+ centers. In the high energy region above the A absorption bands, successive absorption bands are observed in both crystals. The bands appear at 5.07, 5.26, and 5.45 eV for $NH_4Br:Tl^+$, and at 5.42 and 5.61 eV for $NH_4Cl:Tl^+$. The energy interval among these bands is about 190 meV and their absorption intensity become smaller with increasing photon energy. Such the successive absorption bands have been observed in the molecular crystals such as anthracene and perylene but not in alkali halides doped with the Tl^+ centers. In the molecular crystals, the successive absorption bands are attributed to the transition accompanied with the internal

vibrations of the molecules: the vibronic absorption transitions [12]. Since the energy interval among these bands in $NH_4Cl:Tl^+$ and $NH_4Br:Tl^+$ is independent on the halogen ions, we ascribe the successive absorption bands to the intracation transitions accompanied with the internal vibrations in the NH_4^+ ion which is the next nearest-neighbor cation of the Tl^+ ion. In $NH_4Cl:Tl^+$, the small humps are observed at the high energy region above the C absorption bands. The small humps may be also the bands due to the vibronic absorption transitions for the C bands.

References

[1] A. Ranfagni, D. Mugnai, M. Bacci, G. Viliani and M. P. Fontana: Advances in Physics **32** (1983) 823.

[2] P. W. M. Jacobs: J. Phys. Chem. Solids **52** (1991) 35.

[3] S. Masunaga, I. Morita and M. Ishiguro: J. Phys. Soc. Jpn. **21** (1966) 638.

[4] K. Asami, T. Naka and M. Ishiguro: phys. stat. sol. (b) **104** (1981) 145.

[5] M. I. Stillman, P. W. M. Jacobs, K. Oyama Gannon and D. J. Simkin: phys. stat. sol. (b) **124** (1984) 261.

[6] E. Mihokova, V. Nagirnyi, M. Nikl, A. Stolovich, G. P. Pazzi, S. Zazubovich and V. Zeplin: J. Phys. : Condensed Matter **8** (1996) 4301.

[7] T. Kawai, N. Ichimura and S. Hashimoto: phys. stat. sol. (b) **227** (2001) 587.

[8] R. A. Forman and W. S. Brower: J. Lumin. **4** (1971) 98.

[9] N. L. Pathak and S. C. Sen: phys. stat. sol. (a) **24** (1974) 415.

[10] M. K. Murzakhmetov and T. A. Kuketaev: Optics and Spectroscopy **79** (1995) 245.

[11] T. Kawai and S. Shimanuki: J. Phys. Soc. Jpn **67** (1998) 2960.

[12] M. Pope and C. E. Swenberg: *Electronic processes in organic crystals*, (Oxford University Press, New York, 1982) Chap.1,

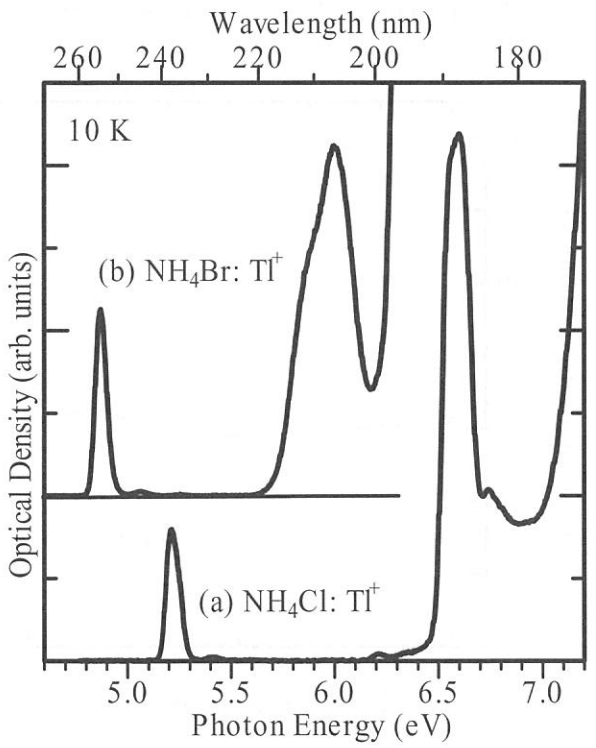

Figure 1 Absorption spectra of (a)$NH_4Cl:Tl^+$ and (b)$NH_4Br:Tl^+$ with lower concentrations of the Tl^+ centers

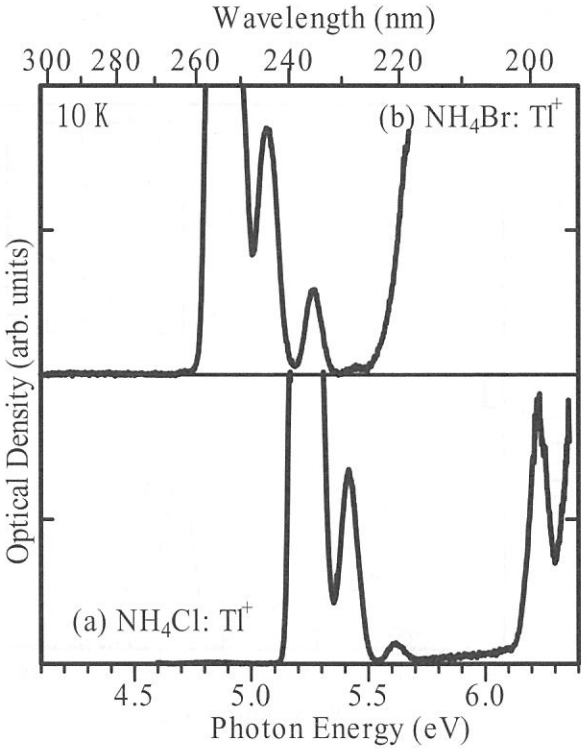

Figure 2 Absorption spectra of (a)$NH_4Cl:Tl^+$ and (b)$NH_4Br:Tl^+$ with higher concentrations of the Tl^+ centers

(BL-1B)

PL Excitation Spectra of $CaMgSi_2O_6:Eu^{2+}$ Phosphor.

T. Kunimoto*, S. Honda, E. Hata, T. Ishisaka, K. Ohmi and S. Tanaka

Dept. of Electrical and Electronic Eng., Tottori University
Koyama, 4-101, Tottori, Japan, 680-8552
**Venture Business Laboratory, Kobe Univerisity*
Rokkodai, 1-1, Nada, Kobe, Japan, 657-8501

Recently, plasma display panels (PDPs) have been used in high-definition television (HDTV) applications. However, there are some serious problems to be solved. Luminous efficiency and lifetime of PDPs are directly related to the performance of phosphors used in PDPs, thus higher efficiency, higher stability against high-temperature processes, and a long lifetime against vacuum-UV (VUV) irradiation are major concerns in selecting suitable phosphors for PDPs. Current VUV phosphors, $BaMgAl_{10}O_{17}:Eu^{2+}$ (BAM), which is currently used as the blue PDP phosphor, shows serious deterioration by the heating processes for binder burn-off, and by the plasma environment during operation. BAM has some deterioration processes for thermal treatment[1-3] and VUV irradiation[4]. These problems are probably caused by the crystal structure of BAM(β-alumina structure: two-dimensional layer structure) and by the Eu^{2+} site in BAM[5]. Recently, many attempts have been made by researchers to understand the detailed bulk structure around Eu^{2+} using ^{151}Eu Mössbauer[6], neutron diffraction[7], and optical spectroscopy[8]. Recently, some examinations for the improvement of BAM have been performed by changing the chemical composition[9]. However well-stabilized BAM has never been obtained to date. One possibility for overcoming the degradation problems is to replace host crystals with other stable compounds. Recently, We reported new blue emitting Eu^{2+} activated silicate phosphors $CaMgSi_2O_6:Eu^{2+}$ ($CMS:Eu^{2+}$) for VUV excitation[10]. $CaMgSi_2O_6$ has a one-dimensional-like structure and its Ca site is tightly enclosed by eight oxide ions of double Si_2O_6 chains and MgO_6 units. Thus, there is a possibility that $CaMgSi_2O_6$ has a stable structure in comparison with BAM. In this report, we show the PLE spectra of $CMS:Eu^{2+}$ phosphor powder and phosphor paste.

$CMS:Eu^{2+}$ phosphor powders were synthesized by a solid state reaction. The fired products were analyzed by the X-ray powder diffraction (XRD) measurements using Cu$K\alpha$ radiation. PLE spectra of $CMS:Eu^{2+}$ were measured a synchro-

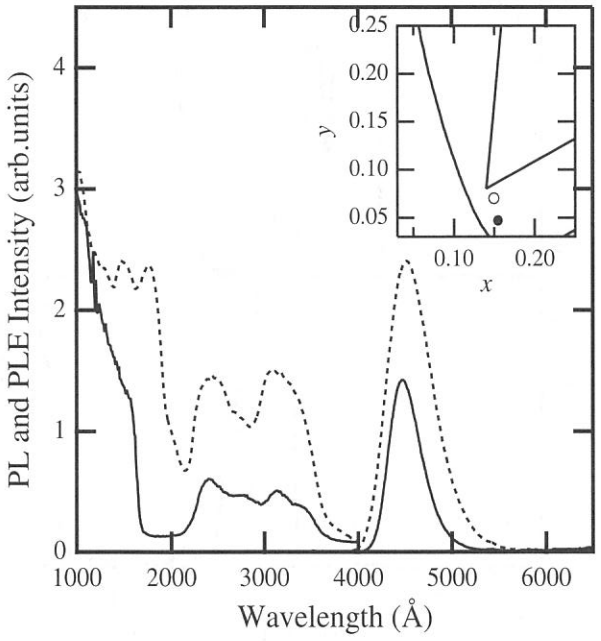

Fig. 1 PL and PLE spectra of $CMS:Eu^{2+}$(solid line). PL and PLE spectra of BAM are shown as a refarence (dotted line).

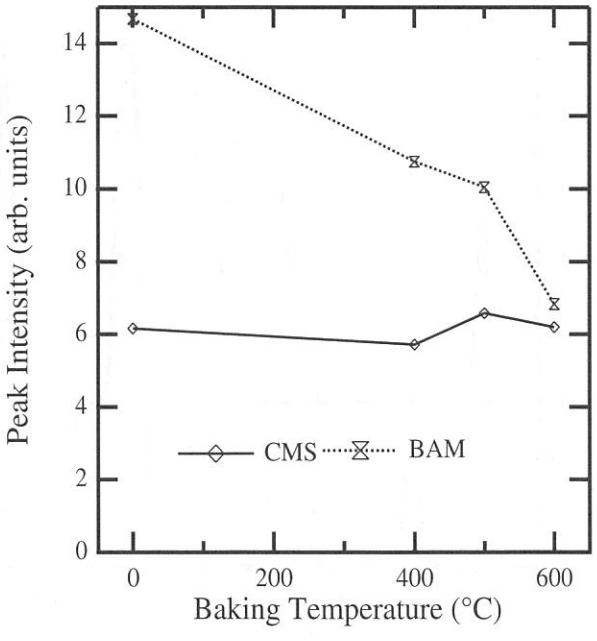

Fig. 2 PL peak intensity of baked phosphor paste of $CMS:Eu^{2+}$ as a function of baking temperature.

tron radiation source BL-1B beam line. Excitation spectra were corrected for the spectral distribution of the light source and the instrumental response using sodium salicylate as a standard.

Figure 1 shows the PL and PLE spectra of the obtained powder which was obtained by firing the stoichiometric mixture with 2 mol % Eu ion at 1200 °C. PL and PLE spectra of BAM are also shown in Fig. 1 as a reference. CMS:Eu^{2+} shows a broad emission peak at about 4470 Å and its bandwidth is narrower than that of BAM. The CIE color coordinates of emission spectra of CMS:Eu^{2+} and BAM are shown in the inset of Fig. 1. These CIE color coordinates are obtained as (x, y) = (0.155, 0.047) for CMS:Eu^{2+} and (x, y) = (0.150, 0.070) for BAM. This shows that a wider color gamut is obtained using CMS:Eu^{2+}. As shown in Fig. 1, several PLE bands were observed. One component, which lies in the wavelength region shorter than 1650 Å for CMS:Eu^{2+} and shorter than 2100 Å for BAM, is due to the host interband transition. Other components, which lie in the 2200 to 3600 Å region, are due to the $4f^7$ to $4f^65d$ transition of Eu^{2+} ion. The PLE intensity of Eu^{2+} direct excitation of CMS:Eu^{2+} is approximately 30 % of that of BAM, nevertheless the PLE intensity of host excitation of CMS:Eu^{2+} is approximately 50 % of that of BAM at 1470 Å, which is the wavelength of the resonance line of Xe discharge. Thus CMS:Eu^{2+} is considered to be appropriated to VUV phosphor. In addition, the edge position of the interband transition of CMS:Eu^{2+} lies at about 1600 Å, which is shorter than that of BAM. Therefore, the absorption coefficient of CMS at 1470 Å seems to be smaller than that of BAM as shown in Fig. 1, in other words, the penetration depth of VUV photon in CMS is longer than that of BAM. This suggests that the absorption coefficient at 1470 Å of $CaMgSi_2O_6$ crystal will be more suitable than that of $BaMgAl_{10}O_{17}$ crystal. The absorbed energy of excitation radiation therefore easily transfers to the Eu^{2+} ions near the surface layer, resulting in the suppression of the formation of an amorphous surface layer.

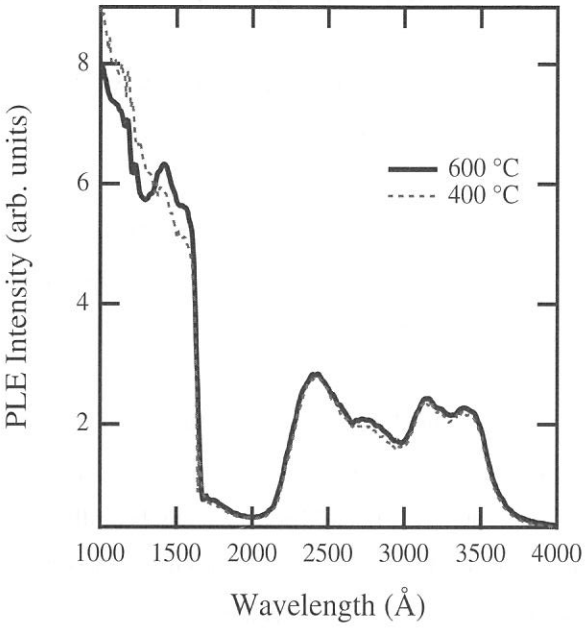

Fig. 3 PLE spectra of CMS:Eu^{2+} phosphor paste baked at 400 °C (dotted line) and 600 °C (solid line).

To examine the characteristic after the heating process, we performed the baking of phosphor paste which is made of the mixture of vehicles and our CMS:Eu^{2+} or commercial BAM. The PL intensity of BAM decreases on increasing the baking temperature as shown in Fig. 2. On the contrary, CMS:Eu^{2+} paste maintains almost the same PL intensity after baking, and PLE spectra of CMS:Eu^{2+} phosphor paste is almost same at any baking temperature as shown in Fig. 3. PLE spectra of BAM indicate that host and direct excitation bands significantly decrease after baking.[11] The BAM paste therefore exhibits deterioration which should be due to the deoxidation of the host lattice[2] and oxidation of Eu^{2+} activators[1]. The lower degree of deterioration of CMS:Eu^{2+} paste is considered to be due to the strong chemical bonding of CMS. Finally phosphor pastes of first-firing specimens show an equivalent peak intensity to that of the baked BAM paste.

In summary, PLE spectra of synthesized CMS:Eu^{2+} phosphors were observed and their resistance against thermal process and VUV irradiation were discussed.

References

[1] S. Oshio, T. Matsuoka, S. Tanaka and H. Kobayashi, J. ElectroChem. Soc.,**145** (1998) 3903.
[2] C. Okazaki, M. Shiiki, M. Komatsu and T. Suzuki, Proc. of IDW'00, (2000) 869.
[3] S. Zhang and H. Uchiike, Proc. of IDW'00, (2000) 865.
[4] M. Ishimoto, N. Iwase, S. Tadaki, S. Fukuta and K. Betsui, Ext. Abst. of the Fifth Int. Conf. of Display Phosphors., (1999) 361.
[5] N. Kijima, Display and Imaging 7 (1999) 225 (in Japanese).
[6] K. Mishra, M. Raukas, M. Boolchand, A. Ellens, to be published.
[7] S.R. Jansen, Thesis, Technical University, Eindhoven, 1998 (Chapter5)
[8] A. Ellens, F. Zwaschka, F. Kummer, A. Meijerink, M. Raukas and K. Mishra, J. Lumin. **93** (2001) 147
[9] S. Zhang, M. Kokubo, H. Fujii and H. Uchiike, SID'01 Digest, (2001) 414.
[10] T. Kunimoto, A. Daud, R. Yoshimatsu, K. Ohmi, S. Tanaka and H. Kobayashi, Extended Abstract of the Sixth Int. Conf. of Display Phosphors. (2000) 21.
[11] T. Kunimoto, R. Yoshimatsu, K. Ohmi, S. Tanaka and H. Kobayashi IEICE Trans. Electron., **E85-C**, (2002) 1888.

(BL1B)

Reflectivity Spectra of Spinel $MgAl_2O_4$ Crystals with Different Origins

H. KUNISAKI, T. MARUYAMA, Y. INABE, M. KOIKE and M. ITOH

Department of Electrical and Electronic Engineering, Shinshu University, Nagano 380-8553

M. FUJITA

Japan Coast Guard Academy, Wakaba, Kure 737-8512

R. MIZUNO and H. NAKAGAWA

Department of Electrical and Electronics Engineering, Fukui University, Fukui 910-8507

Spinel $MgAl_2O_4$ has been the subject of intense study for a long time, because it is a typical example of a large class of inorganic solids with similar structures. The crystal structure of $MgAl_2O_4$ is cubic, fcc, with the space group O_h^7. Each Mg^{2+} ion is tetrahedrally coordinated to four O atoms, while each Al^{3+} ion is surrounded by six octahedrally distributed O atoms. The reflectivity spectra of this material have been measured only by Bortz and French [1] for a geological sample at room temperature. In the present study, we have measured the reflectivity spectra of $MgAl_2O_4$ crystals with different origins at a temperature of 9 K.

All the synthesized crystals used in this experiment were transparent, while the natural crystal was filmy red like ruby. The specimens were mounted on the cupper holder of a cryostat of He-flow type. The reflectivity spectra were measured under the configuration of near-normal incidence.

Figure 1 shows the reflectivity spectrum of a $MgAl_2O_4$ crystal, which was grown from molten PbO-PbF_2 solution by the flux method. The largest crystals were obtained in the temperature range 1220-1250°C with B_2O_3 used to limit the evaporation rate. The sample surface observed here was an as-grown <111> face.

In Fig. 2 is shown the reflectivity spectrum of a $MgAl_2O_4$ crystal, which was prepared by the floating zone (FZ) method using an infrared imaging furnace with a 2-kW Xe lamp. Starting materials were 99.99% pure MgO and Al_2O_3 in the ratio of 1:1. The x-ray analysis showed that the sample is a single crystal without any trace of MgO or Al_2O_3 crystalline mixture. The sample surface was mechanically polished, its orientation being not clear.

Figure 3 shows the reflectivity spectrum of a $MgAl_2O_4$ crystal, which was prepared by the Verneuil method in the Shinkosha Co., Ltd. The <100>-oriented surface was obtained by optical polishing.

In Fig. 4 is shown the reflectivity spectrum of a natural crystal of $MgAl_2O_4$. That was found in Mogok, Myanmar. The reflection measurement was performed on the as-grown <111> surface.

A sharp peak appears at 7.8 eV for all samples. This is attributed to the lowest exciton transition of $MgAl_2O_4$. The exciton band is most clearly observed in natural crystal. Spinel is well known to be highly prone to cation disorder; i.e., some Mg^{2+} ions may exchange positions with Al^{3+} ions. This problem is particularly severe in synthetic spinels. Natural crystals have less cation disorder. Furthermore, synthetic spinels are often removed from the stoichiometric composition. It is supposed that these lattice imperfections cause a broadening of the exciton band in Figs. 1-3.

The humps and peaks below 7.0 eV in Fig. 3 are due to the reflection from the rear surface of sample, because the rear surface of Verneuil-crystal is polished parallel to the front surface. A weak structure is

observed at around 6.2 eV in Figs. 1 and 2. Similar structure is also seen even in natural crystal (Fig. 4). The origin is not clear at present.

The electronic structure of $MgAl_2O_4$ has been studied theoretically by means of the first-principles self-consistent orthogonalized linear combination of atomic orbital method [2]. According to Ref. [2], the calculated band gap is indirect and equal to 6.51 eV. The valence band is mainly constructed by the O 2*p* state, while the conduction band is composed of the *s* orbitals of all atoms in the cell. From the present observation, we estimate the band-gap energy to be about 8.5 eV. The broad structure above 10 eV is not so different from sample to sample, and could be attributed to the allowed transition from the O 2*p* state to the hybridized *s* states.

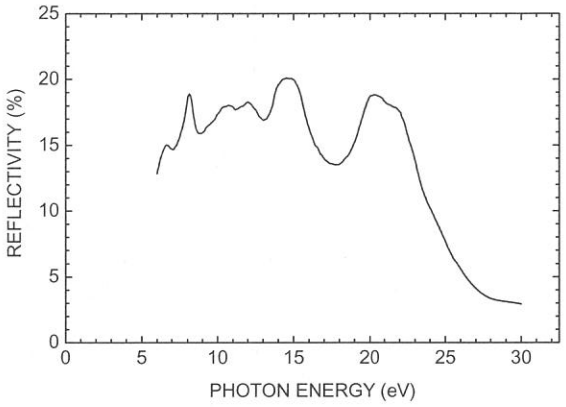

Fig.1 Reflection spectrum of a flux-crystal

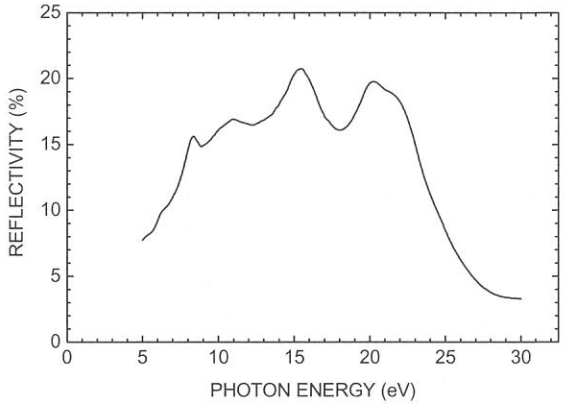

Fig. 2 Reflection spectrum of an FZ-crystal

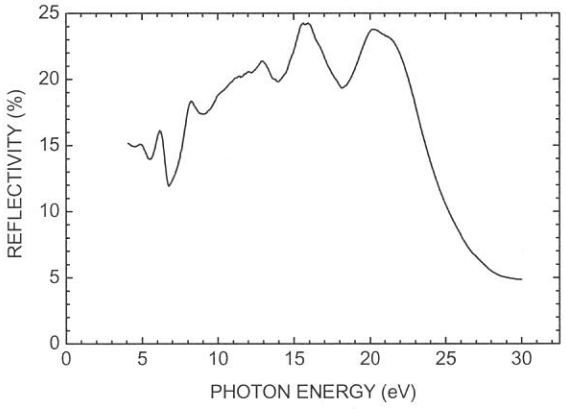

Fig. 3 Reflection spectrum of a Verneuil-crystal

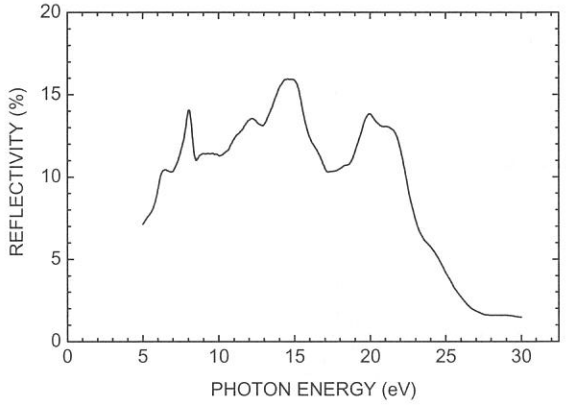

Fig. 4 Reflection spectrum of a natural crystal

The authors would like to thank Professor S. Oishi and Mr. K. Mochizuki for supplying the single $MgAl_2O_4$ crystal grown by the Verneuil method.

References

[1] M. L. Bortz and R. H. French: Appl. Phys. Lett. **55** (1989) 1955.

[2] Y. -N. Xu and W. Y. Ching: Phys. Rev. B **43** (1991) 4461.

(BL1B)

Optical spectra of $ZnGeN_2$ grown on sapphire substrate

T. Misaki, A. Wakahara, H. Okada and A. Yoshida

Toyohashi University of Technology, Tempaku-cho, Toyohashi 441-8580, Japan

Zinc germanium dinitride ($ZnGeN_2$) is one of the II-IV-V_2 compound semiconductors. II-IV-V_2 compounds are derived from III-V compounds by replacing the group-III element with group-II and group-IV elements. The atomic arrangement of the group-II and group-IV elements in II-IV-N_2 compounds has ordered structure, and the symmetry changes from wurtzite to orthorhombic structure with space group of $Pna2_1$ (pseudo-wurtzite structure) [1, 2]. From the analogy of II-IV-P_2 and/or II-IV-As_2 compounds, II-IV-N_2 compounds are expected to have a large optical non-linearity, and thus, $ZnGeN_2$ has a potential for applications in optical band-pass and/or band-rejection filters, second harmonic generators, optical mixers, and parametric oscillators, as well as other chalcopyrite compounds [3]. Recently, epitaxial growth of $ZnGeN_2$ was succeeded on GaN/sapphire [4] or sapphire substrates [5], and absorption edge, excitonic luminescence, and its temperature dependence were reported [5]. Other fundamental properties such as optical spectra, band structure, and effective mass, however, have not been well investigated. In this work, we measure the reflectance spectra of $ZnGeN_2$ over the photon energy range of 2 to 120eV. The optical constants such as the complex index of refraction and the complex dielectric constants have been investigated by means of Kramers-Kronig analysis of reflectance data. The anisotropy of optical properties for $ZnGeN_2$ was also investigated.

$ZnGeN_2$ films were directly grown on r-plane sapphire substrates by remote-plasma enhanced metalorganic vapor phase epitaxy (RPE-MOVPE). The film thickness of $ZnGeN_2$ used in the present study was about 0.2μm. Reflection high-energy electron diffraction (RHEED) pattern revealed that the $ZnGeN_2$ film is single crystal with pseudo-wurtzite structure. From the electron and X-ray diffraction measurements, no other phases such as Zn_3N_2, Ge_3N_4, and Zn_2GeO_4, could not be detected, and the lattice structure of $ZnGeN_2$ films has the space group $Pna2_1$, which is most stable structure expected from the density functional theory (DFT) calculation. The epitaxial relationship were $ZnGeN_2(010)/\alpha\text{-}Al_2O_3(10\text{-}12)$ and $ZnGeN_2[100]//\alpha\text{-}Al_2O_3[11\text{-}20]$. The anisotropy of optical properties for $ZnGeN_2$ can be investigated, because the c-axis of $ZnGeN_2$ epitaxial layer is parallel to the surface. The incident angle was set to be 15° away from the normal direction of the sample surface. The optical constants were determined from the reflectance $R(E)$ and the phase $\theta(E)$ which was calculated by the Kramers-Kronig analysis of the reflectance spectra. Since the spectral region of the reflectance measurements is always bounded ($2\ \text{eV} \le E \le 120\ \text{eV}$ in our measurements), it becomes necessary to extrapolate the reflectance $R(E)$ to infinite energies in order to estimate the phase $\theta(E)$. Below the low energy limit of the measurements ($E \le 2$ eV), the reflectance was assumed to be constant. While the reflectance was taken to be proportional to E^{-4} as in the free electron gas for the energy lager than the high energy limit [6-8].

Figure 1 shows the reflectance spectra of $ZnGeN_2$ epitaxial layer at room temperature in the photon energy range of 2 to 120 eV. The reflectance peaks were observed at 3.9, 5.7. 7.2, 10.3, 13.5, 24, 54 eV when the electric vector $\boldsymbol{E}$ is perpendicular to c-axis. The reflectance spectrum as the electric vector $\boldsymbol{E}$ is parallel to c-axis

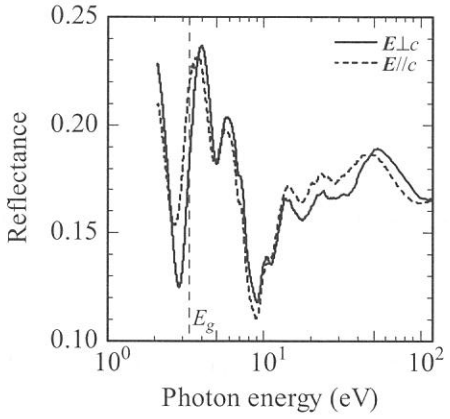

Fig. 1 Spectral dependence of the reflectance for $ZnGeN_2$. The solid line indicates the electric vector is perpendicular to the c-axis, and the broken line represents the one is parallel.

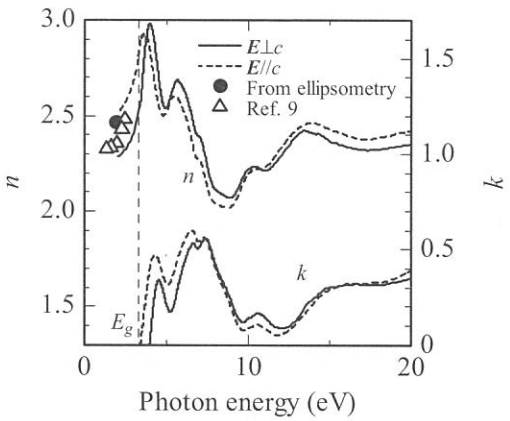

Fig. 2 Spectral dependence of the real and imaginary parts of the refractive index, n and k for $ZnGeN_2$. Filled circle indicates the refractive index n by ellipsometry for the same sample. Triangle indicates the refractive index n by the transmission interference spectra and rutile prism coupling measurements [9].

is similar, but only the peaks at 3.9 and 50eV were shifted to low energy (3.7 and 50 eV). From the optical absorption and photoluminescence measurements, band gap of $ZnGeN_2$ was 3.3 eV at room temperature. Below the band gap (2 eV $\leq E \leq$ 3.3 eV), the interference of $ZnGeN_2$ was occurred. The influence of this interference was removed to refer to the reflectance of GaN in order to apply Kramers-Kronig analysis.

Figure 2 shows the real and imaginary parts of the refractive index, n and k of $ZnGeN_2$. The extinction coefficient k rises up at about 3.3 eV, which is corresponding to the band gap energy of $ZnGeN_2$. The anisotropy of refractive indexes n and k were similar to the reflectance spectra, in which some peaks are shifted to lower energy. From ellipsometry measurement, the refractive index n on the same sample was found to be 2.46±0.12 at the wavelength of 632.8 nm. On the refractive index n below the band gap energy, the value calculated from the reflectance data agree with that measured by ellipsometry. This fact indicates that the revision of the reflectance spectra that, is referred to reflectance data of GaN is reasonable. The refractive index n spectra are similar to other reports [9]. It is well known that the macroscopic quantity most directly related to transitions in the electronic structure is the imaginary part of the dielectric constant ε_2. Its spectral dependence reflects features of the energy band structure. Figure 3 shows the real and imaginary parts of the dielectric constant, ε_1 and ε_2 for $ZnGeN_2$. They exhibit anisotropy in two directions. The peak shift below 10 eV by changing the direction of the electric vector $\boldsymbol{E}$ can be observed. The spectral dependence of the imaginary parts of the dielectric constant ε_2 for $ZnGeN_2$ from theoretical calculations by means of the local density approximation (LDA) to the density functional theory is shown in Fig. 4. See the spectral positions of main peaks for experimental and theoretical value of $\varepsilon_2(E)$ in the region E $\leq$ 15eV, there is a reasonable agreement between experimental and theoretical, although the intensity of the theoretical peaks is higher than of those in experimental spectra because the theoretical spectra were derived in the single-particle scheme [10].

References

[1] S. Limpijumnong, S.N. Rashkeev, and W.R.L. Lambrecht, MRS Internet J. Nitride Semicond. Res. **4S1** (1999) G6.11.
[2] T. Misaki, X. Wu, A. Wakahara, and A. Yoshida, IPAP Conf. Series **1** (2000) 685.
[3] For a review see MRS Bulletin **23**, No.7 (1998).
[4] L.D. Zhu, P.H. Maruska, P.E. Norris, P.W. Yip, and L.O. Bouthillette, MRS Internet J. Nitride Semicond. Res. **4S1** (1999) G3.8.
[5] T. Misaki, K, Tsuchiya, D, Sakai, A. Wakahara, H. Okada, and A. Yoshida, phys. stat. sol. (c) **0** (2002) 188.
[6] M. Cardona, Phys. Rev. **140** (1965) A651.
[7] Q. Guo, H. Ogawa, and A. Yoshida, J. Electron Spectrosc. Relat. Phenom. **79** (1996) 9.
[8] Q. Guo, M. Nishio, and H. Ogawa, Phys. Rev. B **55** (1997) R15987.
[9] L.D. Zhu, P.E. Norris, and L.O. Bouthillette, Mat. Res. Soc. Symp. Proc. **607** (2000) 291.
[10] C. Wang, and B.M. Klein, Phys Rev. B **24** (1981) 3417.

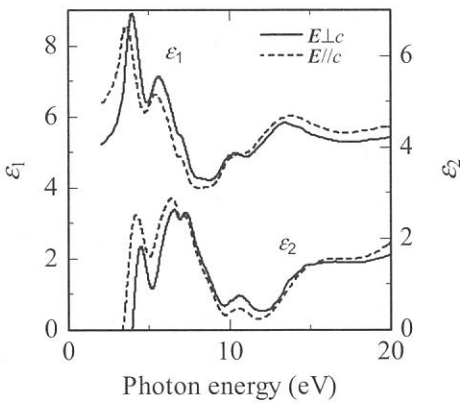

Fig. 3 Spectral dependence of the real and imaginary parts of the dielectric constant, ε_1 and ε_2 for $ZnGeN_2$.

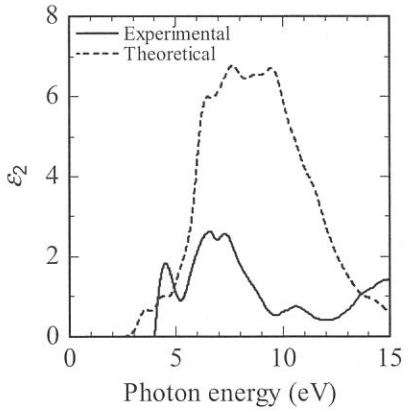

Fig. 4 Spectral dependence of the imaginary parts of the complex dielectric constant, ε_2 for $ZnGeN_2$ from theoretical calculations.

(BL-1B)

Excitation and Fluorescence Spectra of Polyethylene Terephthalate Films

Isuke OUCHI and Ikuo NAKAI[A]

Faculty of Engineering, Tokushima Bunri University, Shido, Kagawa, 769-2193
[A] Faculty of Engineering, Tottori University, Koyama, Tottori, 680-8552

In the early observation of electron-excited emission of a polyethylene terephthalate (PET) film, a braod peak at 380 nm with a shoulder at 325 nm was reported[1]. This shoulder at 325 nm corresponded to the fluorescence peak at 330 nm of dimethyl terephthalate (DMT), monomer of PET, and originated in the lowest energy absorption of PET peaking at 300 nm; whereas, the braod peak around 390 nm was difficult to be identified. Numerous work on photo-excited emission of PET has been made since then for various purposes; whereas the interpretation for the corresponding peak at 390 nm has not been agreed. Ground state dimers in the amorphous phase of PET have been most supported as its origin, from the comparison with the solution fluorescence of PET, for instance; whereas this has not explained the fact that the DMT crystals fluoresce at the same wavelength region. Regardless of its nature, the fluorescence peak at 390 nm must be originated from a corresponding absorption or energy migration. We pointed out in the past that there were faint absorptions in amorphous PET films at 341 nm and 358 nm, corresponding to the excitation peak at 343 nm and to the broad shoulder at 358 nm[2]. Also, long ago, we demonstrated the change of the fluorescence peak at 365-390 nm together with a transmission at 340 nm, as a function of exposure time of a mercury lamp[3]. In this report, we describe some of the observations relevant to the nature of the fluorescence peak at 390 nm.

Sample films of PET and polyethylene naphthalate (PEN) were prepared at the pilot plant of the Film Research Laboratory of Teijin Limited; undrawn, uniaxially drawn and biaxially drawn films of 60-100 μm were utilized. In addition, pieces of undrawn films of 100 μm were supplied by use of various polymerization methods. No fillers were used for both series.

Measurements were made at BL-1B, where a Seya-Namioka type monochromator was equipped. For the measurements of ordinary fluorescence or excitation, Yb-Jobin-MIC mono-chromator, which was placed outside of the vacuum chamber was utilized. Overall excitation spectra were taken without filter nor monochromator for emitted light; here, the observed intensity was the sum of all the light of various wavelengths emitted from the sample and reached the detector through its window. Here, one concerns the wavelengths effective to cause luminescence, regardless of the energy of emission.

Fig.1 shows the overall excitation spectra of uniaxially drawn PET and PEN films. As observed before, fluorescence intensity of PEN is greater than PET by more than 5 times. Although there must be a considerable scattering which appears as background, a big difference is evident between PEN and PET; peak positions of excitation spectra of PEN relate to its absorption spectra in some manner, while those of PET do not look so. Namely, very small excitation peaks are found at 197 nm and 243 nm, which correspond to the peak positions of intense third and second absorption bands of PET, respectively. Some of the absorbed photon energy at these wavelengths are radiated through the lowest energy band at 300 nm, while a majority of them must be lost through non-radiative routes. Relatively more intense excitation is clearly seen at 320 nm with a shoulder at 340 nm. The wavelength of 320 nm is in the tail of the first absorption band peaking at 300 nm, and, at the same time, in the faint absorption peak

of 340nm. Hence, the excitation at 320 nm causes two kinds of emission, one peaking at 330-340 nm which is the intrinsic fluorescence of PET molecules originating in the first absorption band at 300 nm, and one peaking at 365-390 nm; the latter originates partially in the energy migration from the first excited state of PET and partially in the faint absorption at 340 nm.

Separate measurements for undrawn PET films, using Shimadzu Fluorescence Spectromter RF5300-PC, made it clear that the polymerization methods gave a slight difference in the shape of these faint absorption at 341 nm and 358 nm, and also in the shape of the fluorescence peaking at 390 nm. From these facts, together with some other results, we consider that the major origin of the faint absorption around 340 nm which generate fluorescence at 390 nm is a kind of degraded polymers which are possibly generated, by a very slight amount, during the polymerization and extrusion processes, rather than the ground state dimers which many reseachers have maintained.

The anisotropy found in the 320-340 nm peak in Fig 1 (a) is related to that in the transmission spectra shown in Fig. 2. Identification of the origin of the faint absorption at 341 nm and 358 nm must be conformed to this anisotropy, which is yet to be made.

1) D.H. Phillips and J.C. Schug, J. Chem. Phys., 50 (1969) 3297.
2) I. Ouchi, Polym. J., 15 (1983) 225.
3) I. Ouchi, M. Hosoi and F. Matsumoto, J. Appl. Polym. Sci., 20 (1976) 1983.

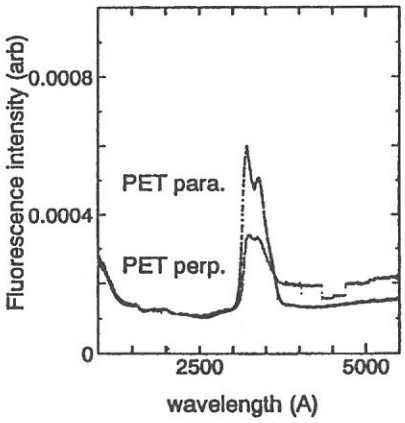

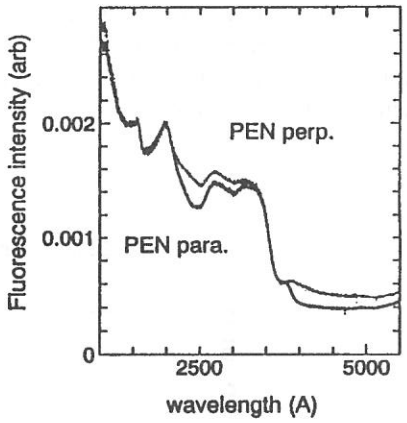

Fig.1 Integrated excitation spectra (a) (top, left): uniaxially drawn PET film. (b) (top, right): PEN.

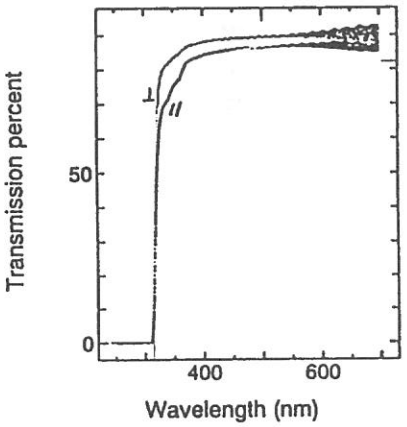

Fig.2. (bottom):Transmission spectra of A uniaxially drawn PET film.

(BL1B)

Optical property of Ce^{3+} ion doped $LiCaAlF_6$ crystal in vacuum ultraviolet region

H. Takahashi, M. Sakai[1], S. Ono[1], N. Sarukura[1], H. SATO[2] and T. FUKUDA[2]

Department of Photo Science, The Graduate University for Advanced Studies, Shonan Village, Hayama 240-0193, Japan

[1]Institute for Molecular Science (IMS), Myodaiji, Okazaki 444-8585, Japan

[2]Institute of Multidisciplinary Research for Advanced Materials, Tohoku University, Katahira 2-1-1, Aoba-ku, Sendai 980-8577, Japan

The development of solid-state ultraviolet laser has attracted a great deal of attention due to its potential applications including environmental sensing, engine-combustion diagnostics, and medical analysis. From the application viewpoint, Ce ion doped fluoride crystals are recognized as promising candidates, since it provide efficient ultraviolet (UV) laser emission with broadband tunability. The main advantage of $LiCaAlF_6$ (LiCAF) and $LiSrAlF_6$ (LiSAF) among the many fluoride crystals is its strong absorption spectrum at around 270 nm, which can be efficiently pumped by the fourth harmonics of Nd:YAG laser. Moreover, using LiCAF is even more attractive than LiSAF because the solarization effect is significantly reduced. Recently, all-solid-state amplifier system has been successfully demonstrated by using Ce:LiCAF crystal as an ultraviolet gain medium. [1-3] In order to improve the laser performance, it is necessary to investigate this material from the spectroscopic point of view. Here, we investigated the Photoluminescence (PL), Photoluminescence excitation (PLE), and Transmission spectra of Ce:LiCAF in VUV region. It is found that the optical excitation from the valence band of LiCAF crystal to the highest ^2D excited state of Ce^{3+} can be utilized as an efficient excitation channel to obtain the ultraviolet emission of 4f – 5d transition in the activated Ce^{3+}.

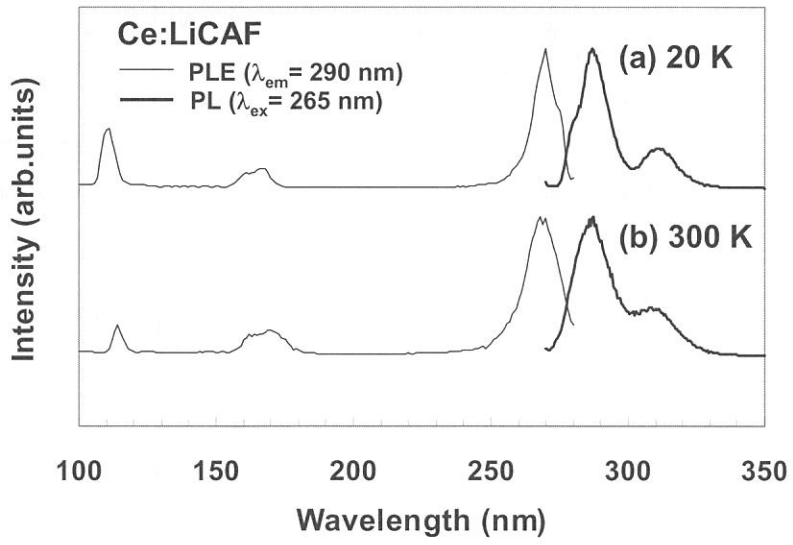

Fig. 1 PL (λ_{ex} = 265 nm) and PLE (λ_{em} = 290 nm) spectra of Ce:LiCAF crystral at (a) 20 K and (b) 300 K.

Figure 1 presents the PL and PLE spectra of Ce:LiCAF crystal measured at 20 K and 300 K. The optical axis of LiCAF crystal was set parallel to the polarization of UVSOR light for generating intense UV emission. For PL measurement, the excitation wavelength was set at 265 nm, which corresponds to the excitation with the fourth harmonics of Nd:YAG laser. The PLE spectra were obtained by monitoring the intensity of 290-nm emission with the bandpass filter and a photo multiplier. The PL spectrum at 300 K consists of the bands at around 288 nm and 310 nm. These luminescence peaks are the transitions from the lowest excited state to the $^2F_{5/2}$ and $^2F_{7/2}$ ground states of Ce^{3+}. At 20 K, the 288-nm band is slightly split, and its bandwidth

becomes narrow. This result is explained by the small electron-phonon coupling at 20 K, which leads to the separation of three energy levels in the $^2F_{5/2}$ band. A schematic diagram of the energy level for Ce:LiCAF crystal is shown in Fig. 2. The optical transitions of 288-nm and 310-nm emissions correspond to (A) and (B) in Fig. 2. The PLE spectra consist of three peaks at around 112 nm, 165 nm, and 265 nm. The 112-nm spectrum exhibits a clear shift toward the shorter-wavelength side with varying temperature from 300 K to 20 K. In contrast, the peak positions of 165-nm and 265-nm spectra are nearly identical and exhibit small temperature-dependent shift. Many researchers have extensively studied the 265-nm spectrum, and its origin is identified to be the optical transition from ground state of the $^2F_{5/2}$ to the lowest ^2D excited states of Ce^{3+}. For 165-nm spectrum, two peaks are clearly observed. This result imply that the origin of this absorption is the transition from ground state of the $^2F_{5/2}$ to the lowest ^2D excited states of Ce^{3+}, which has two separated energy levels in LiCAF crystal. It is well known that the bandgap of LiCAF crystal increases with decreasing temperature. From the result of the temperature-dependent shift, the origin of 112-nm spectrum is considered to be the transition from the valence band of LiCAF crystal to the highest ^2D excited states of Ce^{3+}. The optical transition of 112 nm, 165 nm, and 265 nm are shown as (C), (D), and (E) in Fig. 2.

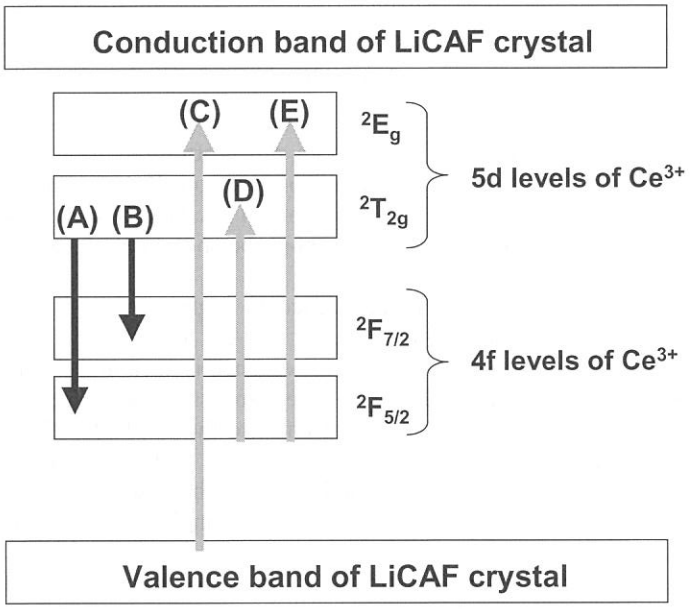

Fig.2 Schematic diagram of the energy levels for Ce:LiCAF crystal. The arrows present the optical transition for emission (black) and absorption (gray).

In summary, we have presented the optical properties of Ce:LiCAF crystal in VUV region. The three excitation-channels are observed to induce ultraviolet laser emission due to 4f-5d transition of Ce^{3+}. For the 180-nm and the 260-nm, their origins are the transition from ground level of $^2F_{5/2}$ to the ^2D excited states of Ce^{3+}. In contrast, the 110-nm spectrum is due to the transition from the valence band of LiCAF crystal to the ^2D excited state of Ce^{3+}.

Reference

[1] N. Sarukura, Z. Liu, H. Ohtake, Y. Segawa, M. A. Dubinskii, R. Y. Abdulsabirov, S. L. Korableva, A. K. Naumov and V. V. Semashko: Opt. Lett, **22** (1997) 994.

[2] Z. Liu, S. Izumida, H. Ohtake, N. Sarukura, K. Shimamura, N. Mujilatu, S. L. Baldochi and T. Fukuda: Jpn. J. Appl. Phys, **37** (1998) L1318.

[3] Z. Liu, T. Kozeki, Y. Suzuki, N. Sarukura, K. Shimamura, T. Fukuda, M. Hirano, and H. Hosono: Opt. Lett, **26** (2001) 301.

[4] S. Ono, Y. Suzuki, T. Kozeki, H. Murakami, H. Ohtake, N. Sarukura, H. Sato, S. Machida, K. Shimamura and T. Fukuda: Appl. Opt, **41** (2002) 7556.

(BL1B)

Two-Photon Spectroscopy of Core Excitons in BaF_2 with Synchrotron Radiation and Laser

T. Tsujibayashi[a], J. Azuma[b], Y. Inabe[c], M. Itoh[c], T. Takaoka[d], M. Watanabe[d], O. Arimoto[e], S. Nakanishi[f], H. Itoh[f], and M. Kamada[g]

[a]*Department of Physics, Osaka Dental University, Hirakata 573-1121*
[b]*Department of Physics, Kyoto University, Kyoto 606-8502*
[c]*Department of Electrical & Electronic Engineering, Shinshu University, Nagano 380-8553*
[d]*Department of Fundamental Sciences, Kyoto University, Kyoto 606-8501*
[e]*Department of Physics, Okayama University, Okayama 700-8530*
[f]*Department of Advanced Materials Science, Kagawa University, Takamatsu 760-8526*
[g]*Synchrotron Light Application Research Center, Saga University, Saga 840-8502*

We have constructed a spectroscopic system in which both synchrotron radiation (SR) and laser are used as light sources [1-3]. A combination of the wide spectral range of SR, from X-ray to infrared, and the high power of lasers is a powerful tool for investigating dynamical behaviors of excitations in inner-shell electronic states of solids. Non-linear spectroscopy such as two-photon and pump-probe spectroscopy can be applicable to solids in this system.

BaF_2 is known as a scintillator with 5.6-eV luminescence in high-energy physics. The luminescence is observed under excitation with photons above the threshold of 17.8 eV. This energy corresponds to that between the outermost core state to the conduction band [4]. The luminescence is attributed to the transition of a valence electron to the hole in the outermost core state, where an Auger process is suppressed since the energy released by the transition is not enough to excite another valence electron to the conduction band. The luminescence is known as Auger-free luminescence (AFL) or cross luminescence. Since AFL is related to core holes, it should be a good probe to examine the relaxation of core electrons and holes. We have so far reported laser-induced AFL of BaF_2 [3, 5]. In this paper, we report the temporal behavior of AFL, changing the SR energy across the excitation threshold of the luminescence.

The block diagram of the measuring system is depicted in Fig. 1. The 1.55-eV laser light was guided to the sample by a 50-m-long optical fiber. This enables the measurement with use of SR and a laser at other beam lines, such as BL7B where a 3-m normal incidence monochromator is equipped. The duration of the pulse was stretched from 160 fs to about 0.3 ns during the travel through the fiber. The temporal behavior of AFL was obtained through the time-correlated single photon counting method. The pulse shapes of the laser and SR are

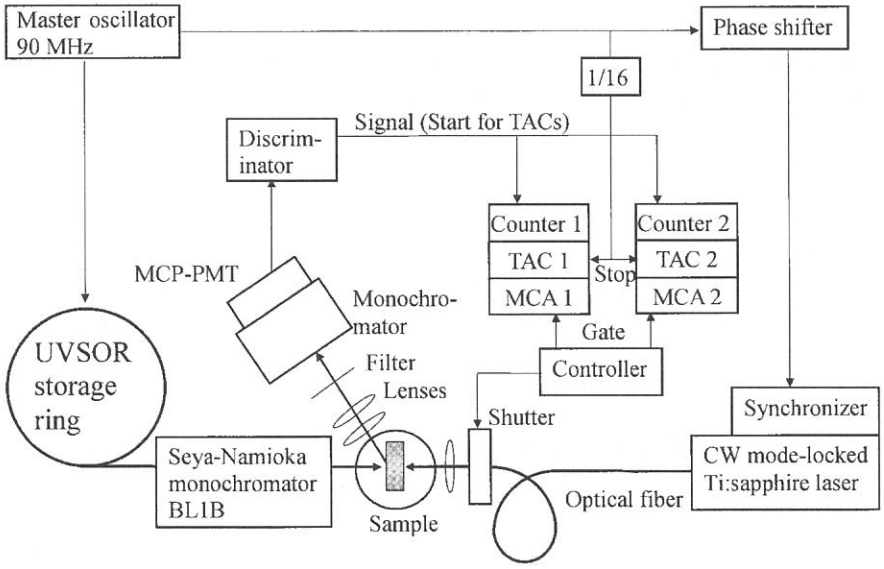

Fig. 1 The block diagram of the experimental setup.

shown by broken and solid lines, respectively, in the top panel of Fig. 2. As shown in Fig. 1, MCA1 and MCA2 accumulated the signal when the shutter was open and closed, respectively. Obtained temporal behaviors of AFL through MCA1 and MCA2 are depicted with broken and solid curves, respectively, in the lower panels of Fig. 2. Photon energies of SR were 17.0, 17.8, and 18.2 eV for panels (a), (b), and (c), respectively. The temperature of the sample was kept at 295 K.

In panel (a), the excitation photon energy is lower than both the lowest core exciton energy of 17.2 eV and the threshold of AFL excitation. Besides AFL, the crystal of BaF_2 has another luminescence band at 4.1 eV caused by the decay of self-trapped excitons (STEs). This band has wide spectral width and its high-energy tail overlaps with the AFL band. The STE luminescence is observed as the background with a long life time in both curves of panel (a) with the same intensity. A fast component is also seen in the panel, whose origin is not clear at present. There is a possibility that it is not luminescence of the sample, but is caused by the scatter of the excitation light beams.

Solid and broken curves of panel (c) are reproduced by convoluting the excitation pulse shapes with an exponential function with a decay time of 0.8 ns which is the lifetime of AFL so far reported. The integrated intensity of the broken curve is slightly larger than that of the solid curve. Two-photon absorption may increase the number of core holes at the expense of photon-absorption by valence electrons.

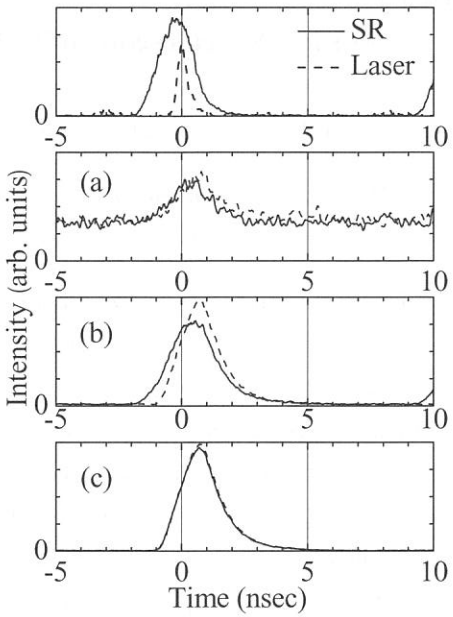

Fig. 2 Top panel: pulse shapes of SR (solid line) and laser light (broken line). Lower panels: temporal behaviors of AFL under excitation exclusively with SR (solid lines) and with SR and laser (broken lines).

The solid curve of panel (b) has two components: one is the ordinary AFL and the other has the same pulse shape as that of the excitation SR pulse. The broken curve consists exclusively of the ordinary AFL. The laser irradiation seems to change the fast component of the solid curve into the ordinary AFL. This might be due to two-photon absorption similarly to the case of panel (c). However, it should be noticed that the change in the time response of the luminescence ranges prior to the arrival of the laser pulse. We must assume accumulated defects or relaxed exciton states [6, 7] which are made by SR pulses irradiating the sample in a 90-MHz repetition and have a longer lifetime than the interval of the excitation pulses. Laser pulses may excite and remove such relaxed excitons or something generated by SR pulses with photon energies in the core exciton absorption region.

References

[1] S. Asaka *et al.*: Rev. Sci. Instrum. **69** (1998) 1931.
[2] S. Asaka *et al.*: UVSOR Activity Report **26** (1999) 34.
[3] T. Tsujibayashi *et al.*: UVSOR Activity Report **28** (2001) 112; ibid **29** (2002) 124.
[4] M. Itoh *et al.*: Solid State Commun. **65** (1988) 523.
[5] J. Azuma *et al.*: Nucl. Instrum. & Methods A **467-8** (2001) 1455.
[6] M. Watanabe *et al.*: UVSOR Activity Report **26** (1999) 66.
[7] M. Kamada and M. Itoh.: Phys. Rev. B **65** (2002) 245104.

(BL1B)

Optical Spectroscopy of $CaF_2:Ce^{3+}$ Crystals Codoped with Li^+ and Na^+

M. Yamaga [1], S. Yabashi [1], Y. Masui [1], H. Takahashi [2], M. Sakai [2] and N. Sarukura [2]

[1] *Department of Mathematical and Design Engineering, Gifu University, Gifu, 501-1193, Japan*
[2] *Institute for Molecular Science, Okazaki, 444-8585, Japan*

While laser action has been reported on interconfigurational transitions in $LiYF_4:Ce^{3+}$ [1] and $LiCaAlF_6:Ce^{3+}$ [2], it has not been achieved for Ce^{3+} doped alkaline earth fluorides in spite of their high energy band gaps. We report on interconfigurational *4f – 5d* absorption and luminescence, as well as temperature dependent X-band EPR measurements for $CaF_2:Ce^{3+}$co-doped with Na^+ and Li^+. A modified defect distribution is revealed, which is due to the presence of the Li^+ and Na^+ co-dopants. For both Li and Na co-doping, tetragonal and orthorhombic symmetry centers have been observed. It is notable that the *g*-values of the tetragonal center, whilst not those of the regular $C_{4v}(F^-)$ center, have the same value irrespective of whether Na^+ or Li^+ co-doping is used. The orthorhombic center consists of an alkali ion in the nearest-interstitial site along the [110] direction giving an overall point group symmetry of C_{2v} for Li^+ /Na^+ co-doping.

Figure 1 shows the absorption spectrum of Na^+ co-doped $CaF_2:Ce^{3+}$ in the range of 100-500 nm at 300 K. *Non* site-selective Ce^{3+} luminescence in the Na^+ co-doped $CaF_2:Ce^{3+}$ has two broadbands A and B centered at 320 and 360 nm with excitation of 300 and 330 nm, respectively, as shown in Fig.2. Narrowband excitation monitoring the 320 nm peak shows the $^2T_2$ and ^2E levels of the excited configuration at 190 and 300 nm respectively. Due to the absence of crystal-field splitting attributable to a significant non-cubic field, we attribute this to the tetragonal center observed in the EPR measurements. The narrowband excitation spectrum of the tail of the luminescence at 380 nm reveals a three fold splitting of the $^2T_2$ level and a two-fold splitting of the ^2E level. As such we attribute this to the C_{2v} center. The measured fluorescence decay times yield a $5d(^2E)$ lifetime of 39 ns for the tetragonal center and 46 ns for the orthorhombic center. Analogous results are obtained for $CaF_2:Ce^{3+}:Li^+$.

Reference

[1] T.D.J. Ehrlich, P.F. Moulton and R.M. Osgood, Opt. Lett. **4**, (1978) 184.

[2] C.D. Marshall, J.A. Speth, S.A. Payne, W.F. Krupke, G.J. Quarles, V. Castillo and B.H.T. Chai, J. Opt. Soc. Am. B. **11**, (1994) 2054.

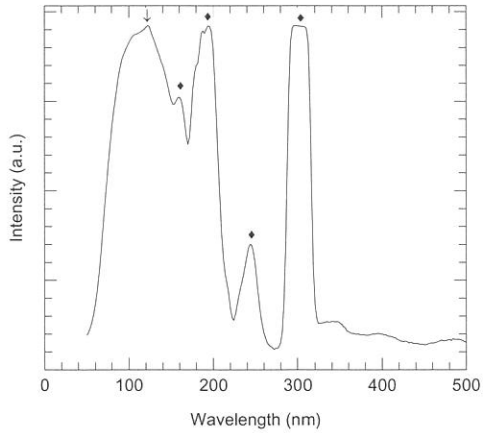

Fig.1 Absorption spectrum of $CaF_2:Ce^{3+}:Na^+$ at 300 K

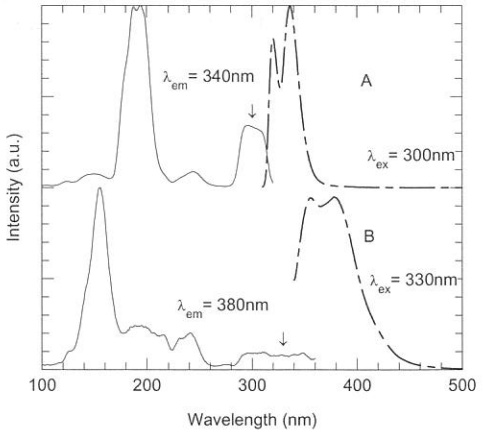

Fig.2 Luminescence and excitation spectra of $CaF_2:Ce^{3+}:Na^+$ at 300 K

(BL5B)

Magnetic Kerr Rotation Spectra of Co/Cu Multilayer around $M_{2,3}$ Edges of Co and Cu

K. Saito, T. Ejima, T. Hatano and M. Watanabe

Institute of Multidisciplinary Research for Advanced Materials, Tohoku University
Katahira 2-1-1, Aoba-ku, Sendai 980-8577, Japan

The magnetic Kerr rotation measurement on Co/Cu multilayer was carried out around $M_{2,3}$ edges of Co and Cu, at room temperature. The instrument consists of a goniometer, permanent magnets and a rotating analyzer equipped with Al/YB_6 and Mo/Si multilayer polarizers.[1] The sample was a [Co(1.8 nm)/Cu(2 nm)]$_{20}$/Co(1.8 nm) multilayer grown by ion beam sputtering on a Si wafer, which was magnetically uncoupled. In the measurement, the longitudinal Kerr configuration was applied and the angles of incidence were fixed at 65° and 80°.

Figures 1 and 2 show the magnetic Kerr rotation spectra of Co/Cu multilayer around $M_{2,3}$ edges of Co and Cu, respectively. In the figures, dots represent experimental results. In Fig.1, the solid curves represent the results by calculation, in which the off-diagonal element of dielectric constant of Co is that of bulk Co obtained previously by us.[1] The calculated results are in agreement with the experimental ones. In Fig.2, the rotation around $M_{2,3}$ edges of Cu is found. This means that Cu is also magnetized, though it is not magnetic material in usual form. The detailed discussion will be made in the near future.

References

1) K. Saito, M. Igeta, T. Ejima, T. Hatano and M. Watanabe, Surf. Rev. Lett. **9** (2002) 943.

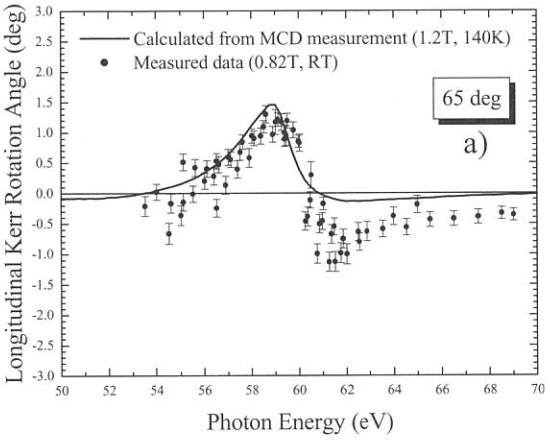

Fig. 1. Longitudinal Kerr rotation angle spectra of Cu (1.8 nm)/Co (2 nm) multilayer for *s*-polaruzed incident light around Co $M_{2,3}$ absorption edges, at angles of incidence of a) 65° and b) 80°.

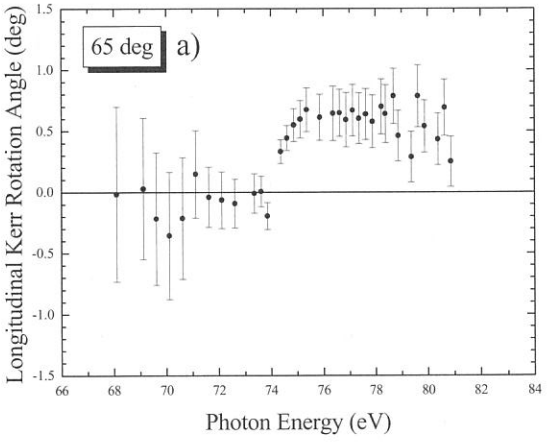

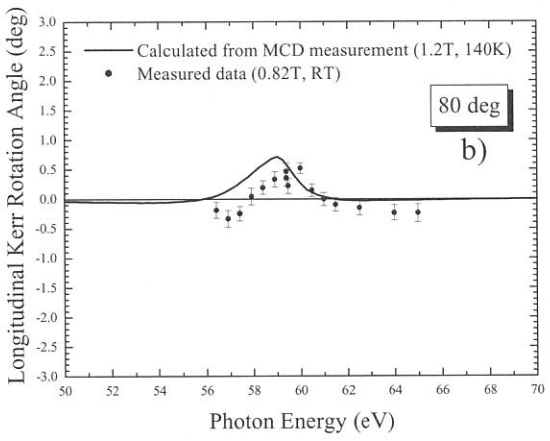

Fig. 2. Longitudinal Kerr rotation angle spectra of Cu (1.8 nm)/Co (2 nm) multilayer for *s*-polaruzed incident light around Cu $M_{2,3}$ absorption edges, at angles of incidence of a) 65° and b) 80°.

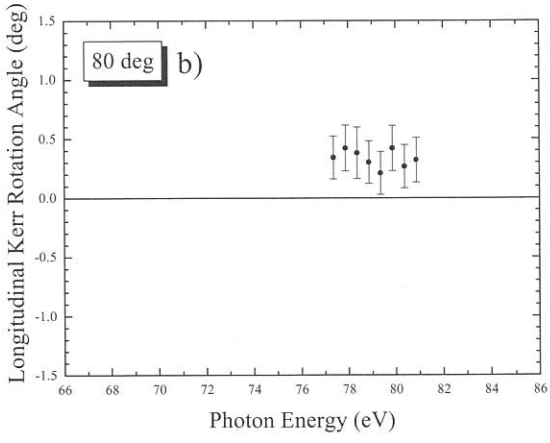

(BL5B)

Transmittance spectra of Self-standing Metal Thin Films for VUV Optical Filters

Kazutoshi Fukui[1], Yutaka Hamamura[2], Kiyoshi Kadomatsu[2], Hironobu Watanabe[3], Atsushi Motogaito[3] and Kazumasa Hiramatsu[3]

[1]*Research Center for Development of Far-Infrared Region, Fukui University, 3-9-1 Bunkyo, Fukui, Fukui 910-8507, Japan*

[2]*Nikon Corporation, Precision Equipment Company, 1-10-1 Asamizodai, Sagamihara, Kanagawa 228-0828, Japan*

[3]*Deptartment of Electrical and Electronic Engineering, Mie University, 1515 Kamihama, Tsu, Mie 514-8507, Japan*

The next generation photolithography will be exposed by using F_2 laser (λ=157 nm) or by using so-called EUV light (λ=13 nm). Especially, EUV (extreme ultraviolet) lithography requires new severe problems to the optical elements, because EUV light is so high photon energy light that the Quartz, which is one of the conventional and well-known optical materials, no longer transmit EUV light. In this background, we have been developing and measuring solar-blinded VUV optical filters.

The metal thin films are used for VUV low pass filter (LPF). If one keeps the throughput of those LPFs more than 10%, the thicknesses have to be from 10 to 100 nm. So they are supported by the metal meshes for reinforcement. However, mesh supported LPFs have some problems, such as 1) decrease of effective transmittance due to the existence of mesh itself, 2) scattering and non-uniformity of the intensity distribution due to mesh itself and/or the irregularity of the film surface between on-mesh and off-mesh, and 3) pin holes or cracks of thin film due to the stress between on- and off-mesh. Therefore, self-standing thin films are the best answer for those problems. However, in the actual usage conditions of LPFs, optical configuration requires some dimension to LPF, because optical filters are not able to insert at the focus points that are occupied by slits, samples, *etc*. In this report, transmittance spectra in VUV region of self-standing thin films, which are made by using both semiconductor and micromachine process technologies, are described.

Self-standing metal thin films are the applications of SiN membrane manufacturing technique on SiN/Si substrates. Si substrate is partially etched and metal thin film evaporated on the substrate is remained. Finally, LPF consists of integrated two parts; one is the part of self-standing metal thin film, and the other is thin film with Si substrate frame. Since metals are evaporated under the appropriate tensile stress, self-standing metal thin films are wrinkle-free flat as same as the surface of Si substrates. Shapes of self-standing metal thin films have some flexibility, maximum dimension is 12 x 6 mm^2 and the typical other sizes are 8 x 8, 4 x 4 mm^2. At present, Au, Al, Zr, Ti, SiN and their multi-layered films are fabricated and the minimum thickness is 18 nm of Au. Transmittance measurements at BL5B are carried out mainly from 50 to 100 eV at room temperature. Since SiN membrane is able to use as LPF (higher order light cut filter) in this energy region, high purity monochromatized light can be used.

Figure 1 shows the observed and calculated transmittance spectra of SiN membrane, which is used as LPF. The estimated thickness of SiN membrane is about 100 nm. The calculation results are derived from the complex index of refraction table of SiN [1]. The spectral feature of calculated curve is good agreement with that of observed curve, although calculated transmittance is uniformly lower than observed one. Figures 2 and 3 show the observed and calculated transmittance spectra of Ti (5nm)-Zr (44nm)-Ti (5nm) and Ti (5nm)-Al (50nm)-Ti (5nm) films, respectively. Transmittance measurements are carried out with SiN LPF shown in fig.1. Since the complex index of refraction of Zr metal has some differences among tables, two calculated curves derived from different tables [1,2] are presented in fig. 2. Ti sandwiched multi-layer structure is employed to prevent the oxidation of both Zr and Al metals. The spectrum features of observed and calculated results in Figs. 2 and 3 are agreement with each other. Those films also have a good solar-blinded character. It is concluded that the self-standing metal thin films are manufactured as designed and high throughput is easily obtained due to the meshless structure. The high throughput will give us the flexibility for designing the dedicated multilayered LPF with high contrast between transparence and non-transparence energy regions.

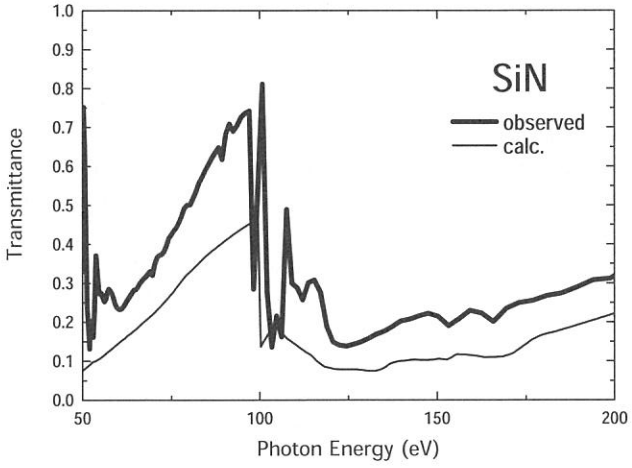

Figure 1 Observed and calculated Transmittance spectra of SiN 100nm single layer film.

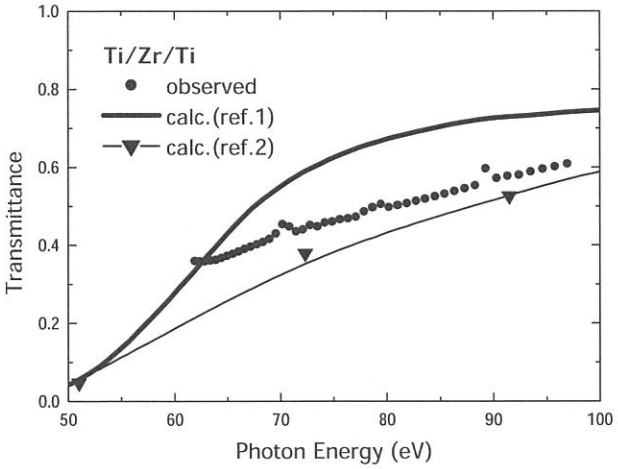

Figure 2 Observed and calculated Transmittance spectra of Ti/(5nm)/Zr(44nm)/Ti(5nm) multilayer film.

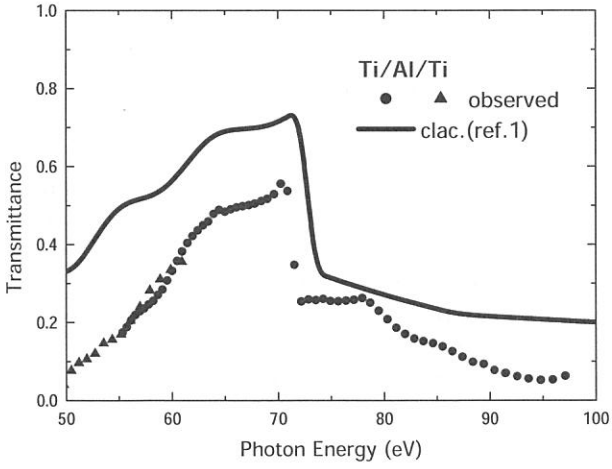

Figure 3 Observed and calculated Transmittance spectra of Ti/(5nm)/Al(50nm)/Ti(5nm) multilayer film.

References

[1] http://www-cxro.lbl.gov/optical_constants/getdb2.html

[2] D.L.Windt et al. : Applied Optics **27** (1988) 246.

(BL5B)

Reflection and Transmission Spectra of Amorphous Chalcogenide Films in the Vacuum Ultra-Violet Region

Koji HAYASHI

Department of Electrical and Electronic Engineering, Gifu University, Gifu 501-1193, JAPAN

Amorphous chalcogenide semiconductor materials, such as amorphous As_2S_3 (a-As_2S_3), amorphous As_2Se_3 (a-As_2Se_3), and amorphous Se (a-Se) etc., show a variety of photoinduced phenomena. Since these materials are very sensitive to the light, they are greatly expected as materials for optoelectronic devices, such as solar battery, photonic memory, and image sensors etc. Although a large number of studies[1,2] have been done on the photoinduced phenomena of these amorphous semiconductor materials, little is known about the details of these mechanisms. These phenomena were studied by exciting outer core electrons with the irradiation of light with the energy corresponding to the optical bandgap or subbandgap. The interest has been attracted for the change of the optical properties in the energy region of the visible light. Little attention has been given to photoinduced effects by exciting inner core electrons with the irradiation of higher energy photon. We are interesting for the change of the optical properties in the higher energy region. To obtain a wide knowledge of the photoinduced phenomena, it is necessary to investigate to the photoinduced effects on wide energy region. In previous reports[3], we reported the photodarkening in amorphous chalcogenide films by the vacuum ultra-violet(VUV) light. In our recent study, we observed interesting photoinduced change in the photoconductivity and the total photoyield of amorphous chalcogenide films by the irradiation of the VUV light and bandgap(BG) light[4]. In previous reports[5-7], we reported the photoinduced change at the VUV reflection spectra of the amorphous chalcogenide films induced by BG light. In present report, we report the examination on the more exact measuring method of the photoinduced change at the spectrum in the VUV region.

Samples used for the measurement were amorphous chalcogenide (a-As_2Se_3 and a-As_2S_3) films. Thin films of amorphous chalcogenide were prepared onto quartz substrates for the measurement of reflection spectrum and onto collodion films for the measurement of transmission spectrum by conventional evaporation technique. A typical thickness of an amorphous film was around 0.7 μ m. After evaporation, samples used for the measurement of reflection spectrum were annealed near the glass transition temperature for two hours in a vacuum with a pressure of 10^{-4} Pa. A xenon arc lamp or a high pressure mercury lamp with IR-cut-off filter were used as a light source. Before the measurement of the VUV reflection spectra, half area of the sample was irradiated with the BG light to the degree in which the sample sufficiently produced the photodarkening. The measurement of reflection and transmission spectra in the VUV region was performed at room temperature at the BL5B beam line of the UVSOR facility of the Institute for Molecular Science. For the measurement of the reflection spectra, the incident angle was near normal to the sample surface and the reflectivity was measured by a silicon photodiode. In present experiment, to eliminate the higher order light from the monochromator, a Al thin film was inserted between the monochromator and sample. We also monitored the spectrum of light source by measuring the photoyield of the gold mesh. The reflection and transmission spectra were obtained by normalizing the spectra by the spectrometer system response.

In until now measurement, we have noticed the relative change of the spectrum by irradiating the light. Therefore, the filter for giving priority to the optical intensity, and for removing the higher order light from the monochromator was not used. The effect of the higher order light is removed in order to examine the exact change of the spectrum, and in addition, calibration of the wavelength is also necessary. Then, the filter made of a thin film of aluminum was used the measurement of the reflection spectrum for purpose of the removal of the higher order light and wavelength calibration. Figure 1 shows the VUV reflection spectra of a-As_2Se_3 film at room temperature. Two main peaks of a-As_2Se_3 were observed in this region. One peak around 22nm corresponds to the 3d core level of Se atom. Another peak around 28nm corresponds to the 3d core level of As atom. However, the ratio of noise and signal becomes very bad, when the filter is inserted. The peak has been hidden, when the reflection spectrum is normalized with the intensity of the incident light. This time, the sample was deposited on the collodion film, and the

measurement of the transmission spectrum was also tried. Figure 2 shows the VUV transmission spectrum of a-As_2Se_3 film at room temperature. There are two absorption peaks at the transmission spectrum in the fig.2. Though the absorption was saturated, since the film thickness was thick, the ratio of signal and noise was good. It is necessary to examine the optimum film thickness of the sample of transmission spectrum. However, the annealing is future problem, because it is not possible for the sample on the collodion film. The detailed experiments and analysis will be done in the next step.

This work was partly supported by grants-in-aid for Scientific Research from the Ministry of Education, Science and Culture of Japan.

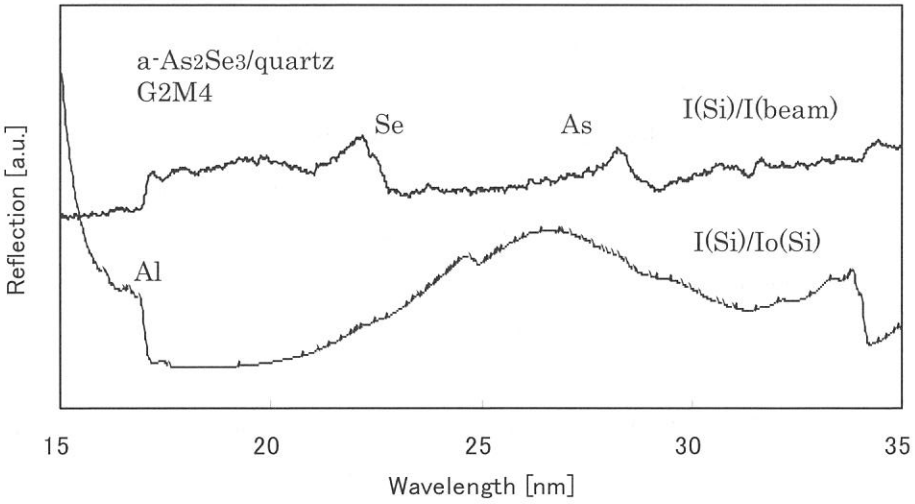

Fig. 1. VUV reflection spectra of a-As_2S_3 film at room temperature. (a) I(Si)/I(beam) and (b) I(Si)/Io(Si).

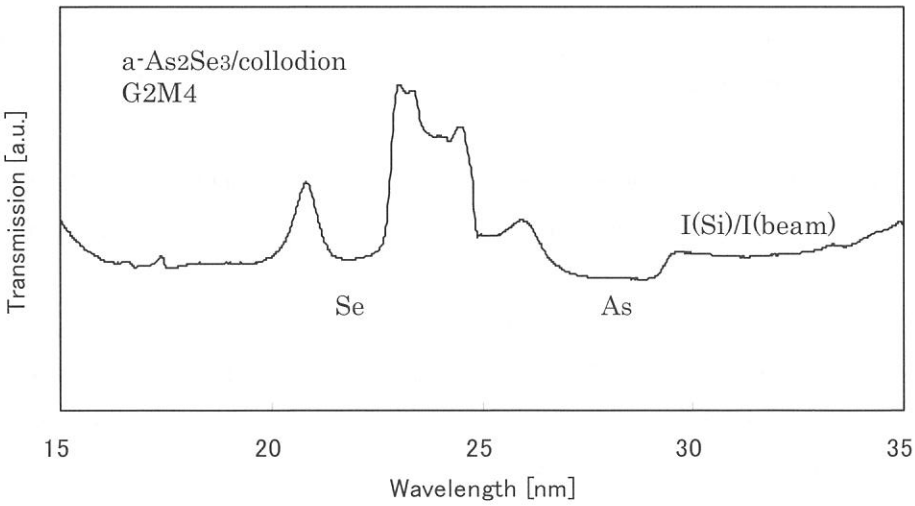

Fig. 2. VUV transmission spectrum of a-As_2S_3/collodion at room temperature.

REFERENCES

[1] Ke. Tanaka, Rev. Solid State Sci., 4(1990)641.
[2] K. Shimakawa, A. Kolobov, and S. R. Elliott, Adv. Phys., 44(1995)475.
[3] K. Hayashi, D. Kato, and K. Shimakawa, J. Non-Cryst. Solids., 198-200(1996)696.
[4] K. Hayashi, A. Hirai, and K. Shimakawa, UVSOR Activity Report 1996(1997)116.
[5] K. Hayashi, UVSOR Activity Report 1999(2000)90.
[6] K. Hayashi, Y. Naito, and S. Nakamura, UVSOR Activity Report 2000(2001)122.
[7] K. Hayashi, UVSOR Activity Report 2001(2002)126.

(BL5B)

Responsivity spectra of GaN based UV detectors in VUV and SX region

Atsushi Motogaito[1], Hironobu Watanabe[1], Kazumasa Hiramatsu[1], Kazutoshi Fukui[2],
Yutaka Hamamura[3] and Kazuyuki Tadatomo[4]

[1]Deptartment of Electrical and Electronic Engineering, Mie University,
1515 Kamihama, Tsu, Mie 514-8507, Japan
[2]Research Center for Development of Far-Infrared Region, Fukui University,
3-9-1 Bunkyo, Fukui, Fukui 910-8507, Japan
[3]Nikon Corporation, Precision Equipment Company,
1-10-1 Asamizodai, Sagamihara, Kanagawa 228-0828, Japan
[4]Telecommunication & Photonics Research Laboratory, Mitsubishi Cable Industries, Ltd.,
4-3 Ikejiri, Itami, Hyogo 664-0027, Japan

VUV and SX light are expected to be utilized in the new photolithography technique, such as using the light of an ArF laser (λ=193 nm), an F_2 laser (λ=157 nm) and an EUV light (extreme UV, λ=13 nm). Currently, for the detection of VUV or SX light, Si-based photodetectors (SPDs) [1] are mainly used. However, they have significant limitations due to some problems previously mentioned. III nitrides based photodetectors are expected to overcome these limitations. The fabricated GaN based UV photodetectors have possibilities of being used in steppers for future photolithography systems with short wavelength mentioned above. However there are only few reports on the detection of VUV light (<25 eV) by GaN based photodiodes [2-4] and there are no reports on that of VUV and SX light (>25 eV).

In this report, the responsivity spectra of GaN based Schottky type UV photodetectors with transparent electrode from the VUV region to SX region (10-100 nm, 124-12.4 eV) are described.

The UV detectors used in this study adopt the Schottky contacts with a transparent electrode. They consist of a 3-μm-thick n-GaN layer ($n=2.0\times10^{18}$ cm^{-3}) and a 1.5-μm-thick i-GaN layer ($n=1.0\times10^{16}$ cm^{-3}) on a (0001) sapphire substrate. These layers are grown by metalorganic vapor phase epitaxy (MOVPE). The Au/Ni Schottky contact is deposited on i-GaN. The thickness of Au and Ni are 10 nm and 1 nm, respectively. The diameter of detectors is 6.5 mm.

Prior to measuring responsivity, the transmittance of transparent Schottky electrode is estimated by measuring the transmittance of Ti/Au membrane. The transmittance of 10-nm-thick Ni/Au Schottky electrode is estimated to about 0.5-0.7 in the VUV and SX region (20-100 eV) as shown in Figure 1. Thus it is considered that the 10-nm-thick Ni/Au Schottky electrode is enough thickness to transmit VUV and SX light into transparent electrode. Figure 2 shows the responsivity spectra of samples The responsivity in VUV region (10-50 eV) is about 0.01 A/W. The larger responsivity is found in VUV-SX region (>50 eV). It is considered that the high responsivity in VUV-SX region is due to the increased transmittance of Ni/Au with increasing

photon energy. The value of responsivity in soft X-ray region (@13 nm for EUV lithography system) is about 0.05 A/W.

References

[1] E. M. Gullikson, R. Korde, L. R. Canfield and R. E. Vest: J. Elect. Spectr. Rel. Phenom. **80**, 313 (1996).

[2] A. Motogaito, M. Yamaguchi, K. Hiramatsu, M. Kotoh, Y. Ohuchi, K. Tadatomo, Y. Hamamura and K. Fukui: Jpn. J. Appl. Phys. **40**, L368 (2001).

[3] A. Motogaito, K. Ohta, K. Hiramatsu, Y. Ohuchi, K. Tadatomo, Y. Hamamura and K. Fukui: Phys. Stat. Sol. (a) **188**, 337 (2001).

[4] E. Monroy, T. Palacios, O. Hainaut, F. Omnès, F. Calle and J. F. Hochedez: Appl. Phys. Lett. **80**, 3198 (2002).

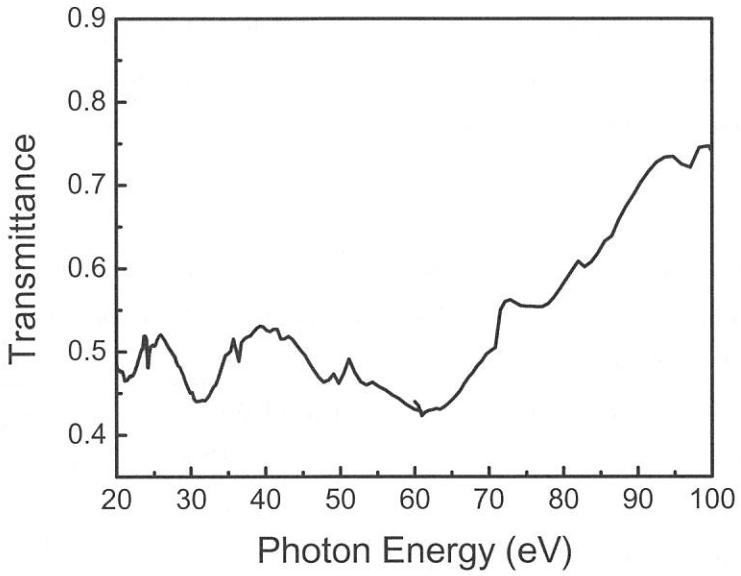

Fig.1 Transmittance spectra of transparent Schottky electrode calculated from that of Ti/Au membrane.

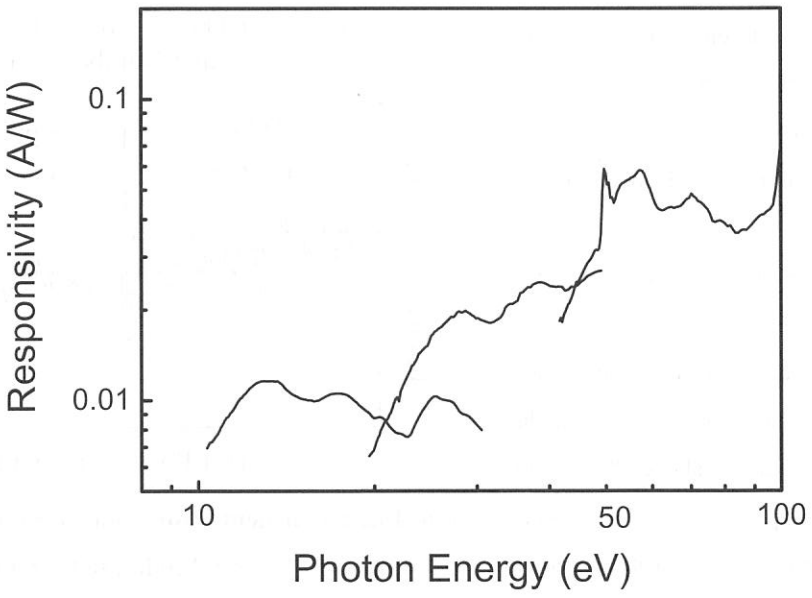

Fig.2 The responsivity spectra of UV detectors in VUV and SX region.

(BL6A1)

Laser-induced infrared absorption measurement in lead tungstate by using the laser-SR combined system.

J. Azuma, M. Koike[A], M. Itoh[A] and M. Kamada

Synchrotron Light Application Center, Saga University

Faculty of Engineering, Shinshu University [A]

In recent years, lead tungstate ($PbWO_4$) has been expected as a new scintillating material for high-energy physics experiments because of the fast luminescence response and the high density. For the improvement of the optical properties, the luminescence mechanism of this material has attracted considerable attention.

Transient absorption measurement is a powerful technique to investigate the photo-excited states in condensed matter. Therefore we have applied the technique of the infrared transient absorption measurement to $PbWO_4$.

In this experiment, photo-excited states were generated by two-photon excitation using the second harmonics of a regenerative amplified Ti:sapphire laser (Spectra Physics, Hurricane). The wavelength, average power, pulse width and repetition rate of the second harmonics were 400 nm, 250 mW, 120 fs, and 1 kHz, respectively. The measurement was performed in the energy range of 400～13000 cm^{-1} with the rapid-scan Michelson interferometer (Bruker, IFS-66V) by using a quartz or a KBr beam splitter. A HgCdTe detector was used. The transient absorption was obtained from the difference between the transmitted IR intensities with and without the laser excitation. The sample used in this measurement was a single crystal grown by the Czochralski method.

Figure 1(a) shows the transient absorption spectrum of lead tungstate at 16 K. A broad transient absorption band appears above 4000 cm^{-1}, with a peak around 9000 cm^{-1}. When the sample temperature is raised above 20 K, this absorption band disappears. The temperature dependence of the absorption intensity is shown in the inset of Fig. 1(a).

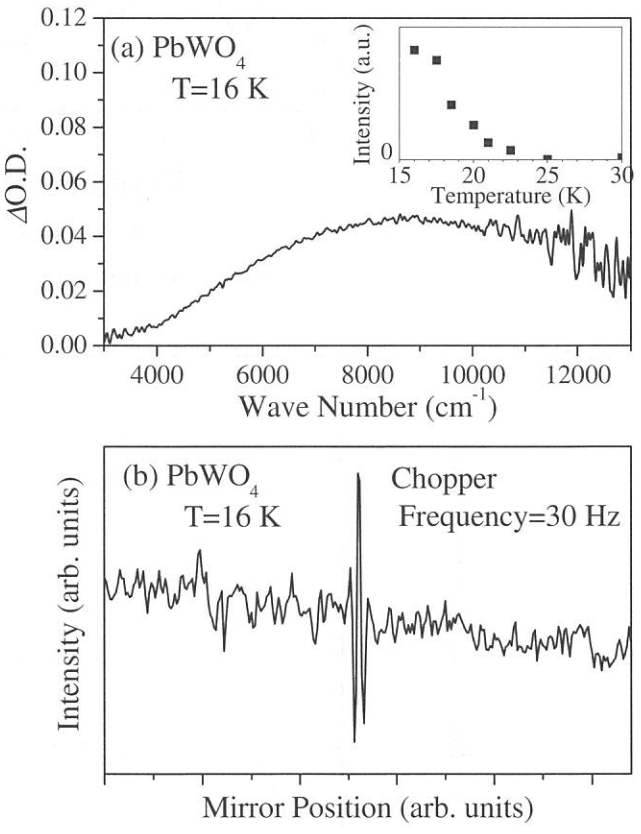

Fig. 1 (a): Transient absorption spectrum of $PbWO_4$ crystal at 16 K. (b): Modulated IR interferrogram obtained by the laser intensity modulation.

In order to obtain the information about the decay time of the transient absorption, we have modulated the laser intensity by using the optical chopper at 10～50 Hz. The modulated signal of IR transmittance synchronous to the laser modulation was detected by a lock-in amplifier.

Figure 1(b) shows the modulated IR interferrogram. This corresponds to the interferrogram of the IR light transiently absorbed by the photo-excited state. The intensity of the modulated IR interferrogram increases when the modulation frequency is around 30 Hz. This means that the lifetime of the photo-excited state, the origin of the transient absorption, is about 30 ms.

Martini *et al.* [1] have reported the thermally stimulated luminescence (TSL) of the lead tungstate. The ordinary luminescence is stimulated by the thermally activated recombination between the hole trap center and the electron trap center in this TSL process. In their paper, the TSL is found to appear around 20 K and 50 K. It means that one type of the trap center becomes unstable around 20 K and other type becomes unstable around 50 K. The transient absorption observed here is probably due to the trap center related to the TSL around 20 K. The lifetime of the transient absorption is much longer than the radiative lifetime around 16 K [2]. Therefore the observed transient absorption should be originated from the extrinsic shallow trap center, the nature of which has not been clarified yet. At low temperatures below 20 K, the photo-excited carriers partially relax into that center, which may be linked to small yield of the intrinsic luminescence in $PbWO_4$. The detail of this center is a future problem.

References

[1] M. Martini, F. Meinardi, G. Spinolo, A. Vedda, M. Nikl and Y. Usuki, Phys. Rev. B **60** (1999) 4653.

[2] M. Itoh, M. Horimoto and M. Fujita, J. Phys.: Condens. Matter **15** (2003) 193.

(BL6A1)

Infrared Spectra of protonic conductor $SrZrO_3$:Yb

Osamu Kamishima, Junichi Kawamura, Teruyoshi Awano[1], Takeshi Hattori
Institute of Multidisciplinary Research for Advanced Materials, Tohoku University Japan, Sendai 980-8577
Department of Applied Physics, Tohoku Gakuin University, Japan, Tagajo 985-8537

Strontium zirconate ($SrZrO_3$) is a typical material of proton conductors, when a few mol% Yb^{3+} ions are substituted for Zr^{4+} ions. Protons are located between two oxygen ions as if they made a hydrogen bond and migrate by hopping from a oxygen to another oxygen. Hempelmann and Karmonik[1] suggested that the proton diffusion process was characterized as a combination of trapping and escape events from neutron quasielastic scattering for $SrCeO_3$:Yb. The proton trapping events have been associated with the dopants. On the local structure around the dopant ions, it was suggested by EXASF measurement for the $SrZrO_3$:Yb that the doped Yb ions would be sifted from the center of the oxygen-octahedron.[2] The Zr ion locates at the inversion center and a charge balance with oxygen is maintained to be a neutrality. In the case of (YbO_6)-octahedron, however, it seems to make a significant polarization because of the different valence charge and the off-center location. The trapping state for the proton diffusion might be resulted from such a polarization in the vicinity of the Yb dopants. Therefore, it is expected to investigate an IR-active impurity band induce by the dopant Yb. To confirm the local polarization, we have measured the infrared spectra of $SrZrO_3$ with several Yb-concentrations.

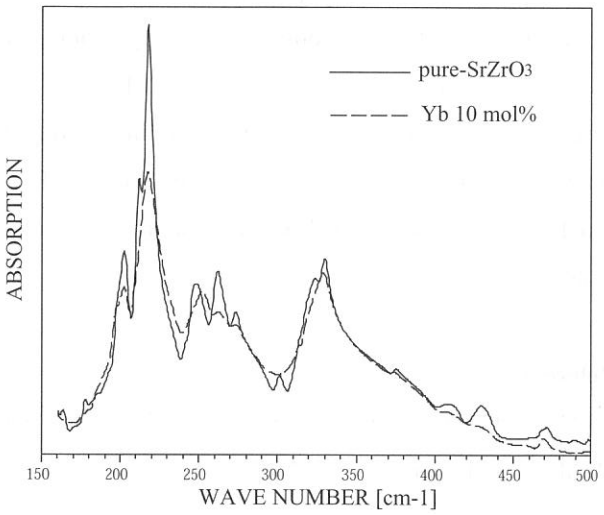

Figure 1. Absorption spectra of pure-$SrZrO_3$ (solid curve) and doped $SrZrO_3$ with Yb 10 mol% (dashed curve) at 30 K, calculated from the reflectivity spectra by Kramers-Kronig analysis.

$SrZrO_3$ belongs to the space group of *Pnma* containing 4 molecules in a unit cell. The irreducible representation Γ of the phonon modes at the zone center can be decomposed as follows by a factor group analysis:

$$\Gamma = 7A_g + 5B_{1g} + 7B_{2g} + 5B_{3g} + 8A_u + 10B_{1u} + 8B_{2u} + 10B_{3u}.$$

The above equation shows that there are 24 Raman-active modes ($7A_g + 5B_{1g} + 7B_{2g} + 5B_{3g}$), 25 infrared active modes ($9B_{1u} + 7B_{2u} + 9B_{3u}$) and three translational modes ($B_{1u} + B_{2u} + B_{3u}$), while the $8A_u$ modes are inactive in both Raman and infrared. It can be expected from Raman experiments[3] that the IR active B_{1u}, B_{2u} and B_{3u} in the range of 200 ~ 400 cm^{-1} are mainly composed by oxygen-strontium vibrations with the exception of a B_{3u} mode around 200 cm^{-1} due to zirconium vibration. $SrZr_{1-x}Yb_xO_3$ crystals of (x = 0.0, 0.01, 0.05 and 0.10) were prepared, and the IR measurements were carried out at 30K and room temperature. Figure 1 shows absorption spectra of pure-$SrZrO_3$ and doped $SrZrO_3$ with Yb 10 mol% at 30 K. When Yb ions were doped in $SrZrO_3$, the IR absorption spectrum is just broading even around 200 cm^{-1} associated with zirconium vibration. An impurity band related to the local polarization, alternatively Raman active band by a symmetry breaking could not be observed. It seems that the dopants Yb could not influence on the oxygen lattice so much in the present wave length. It is necessary to change the approach for the conformation of the lattice distortions.

[1] R. Hempelmann and Ch. Karmonik *Phase Transitions* **58** (1996) 175.
[2] O. Kamishima, K. Ohta, Y. Chiba and T. Hattori *J.Phys.: Condens.Matter* **13** (2001) 152.
[3] O. Kamishima, T. Hattori, K. Ohta, Y. Chiba and M. Ishigame *J.Phys.: Condens. Matter* **11** (1999) 5355.

(BL6A1)

Far-Infrared microspectroscopy of κ-(BEDT-TTF)$_2$Cu[N(CN)$_2$]Br

T. Nishi [1], S. Kimura [2], T. Takahashi [3], K. Miyagawa [4] and K. Kanoda [4]

[1]*Graduate School of Science and Technology, Kobe University, Nada-ku, Kobe 657-8501*
[2]*UVSOR, Institute for Molecular Science, Okazaki 444-8585*
[3]*Research Reactor Institute, Kyoto University, Osaka 590-0494*
[4]*Department of Applied Physics, The University of Tokyo, Hongo, Bunkyo-ku, Tokyo 113-8656*

κ-(BEDT-TTF)$_2$Cu[N(CN)$_2$]Br is a quasi-two-dimensional organic superconductor with T_C = 11.6K. The BEDT-TTF molecule has two ethylene groups at the end. By partially replacing all hydrogen of the ethylene end groups by deuterium, κ-(BEDT-TTF)$_2$Cu[N(CN)$_2$]Br shows superconductor-insulator (SC-I) transition. Hereafter the partially substituted one is denoted by d[*n*, *n*], where *n* means the number of the deuterium and *n* = 0 - 4. This SC-I transition is considered as Mott transition. κ-(BEDT-TTF)$_2$Cu[N(CN)$_2$]Br has two other SC-I transitions, one appears in d[2,2] by magnetic fields and the other in d[3,3] by fast cooling at around 80 K. [1]

In this study, we measured reflectivity spectra of d[*n*, *n*] (*n* = 0, 2, 3, 4) in the far-infrared region of ω = 220 - 700 cm^{-1} at UVSOR BL6A1 combined with an infrared microscope. The other regions are measured at SPring-8 BL43IR for magneto-optics, UVSOR BL7B for VUV reflectivity and a laboratory's instrument for mid-infrared reflectivity.

Figure 1 and 2 show the optical conductivity ($\sigma(\omega)$) spectra at 4 and 50 K after the fast cooling (17 K/min) and the slow cooling (0.05 K/min), respectively. They are obtained by a Kramers-Kronig transformation of the reflectivity spectra. In the d[0,0] spectra, the peak intensity at around 0.3 eV at 4 K is lower than that at 50 K. However, in the d[4,4] spectra, the temperature dependence is the opposite. In d[3,3] spectra, the peak intensity at 4 K is lower than that at 50K by the slow cooling, but the behavior is the opposite by the fast cooling. This means that the electronic structure of d[3,3] by the slow cooling is the same as that of d[0,0] and that by the fast cooling is the same as that of d[4,4], *i.e.*, the slow cooling d[3,3] is a superconductor and the slow cooling d[3,3] is an insulator. The cooling rate dependence is the same as the resistivity at zero magnetic field. Therefore it is concluded that the change of the $\sigma(\omega)$ spectra reflect that of the electronic structure due to the Mott transition.

Reference [1] A. Kawamoto, *et al.*, Synthetic Metals **133-134** (2003) 123.

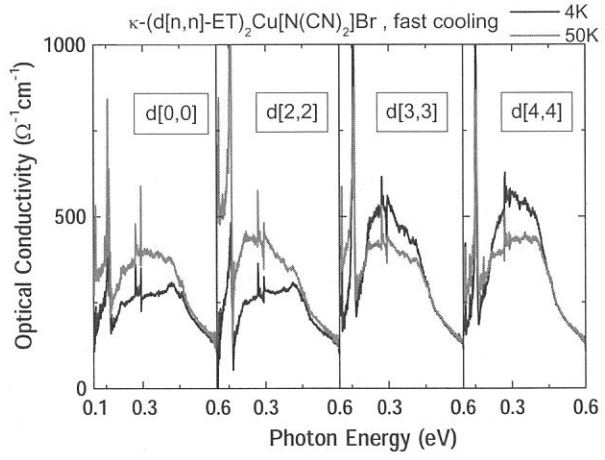

Fig. 1. Optical conductivity spectra of fast cooled (17 K/min) d[*n*,*n*] (*n* = 0, 2, 3, 4) at 4 and 50K.

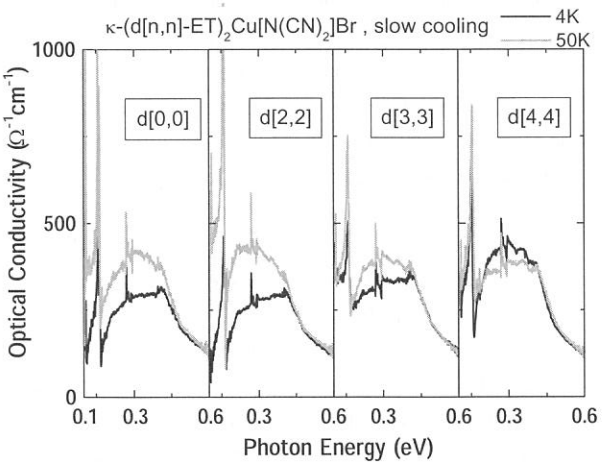

Fig. 2. Optical conductivity spectra of slow cooled (0.05 K/min) d[*n*,*n*] (*n* = 0, 2, 3, 4) at 4 and 50K.

(BL6A1)

Surface-Enhanced Infrared Absorption Spectroscopy at the Electrochemical Interface

Masatoshi OSAWA, Atsushi MIKI and Hiroto Miyake

Catalysis Research Center and Graduate School of Environmental Earth Science, Hokkaido University, Sapporo 060-0811

Infrared spectroscopy is one of the useful tools for *in situ* characterization of the electrochemical interface (solid/solution interface). Infrared reflection-absorption spectroscopy (IR-RAS) technique has been used widely for this purpose, as in surface studies in ultra-high vacuum and gas phase. However, there exist several problems in applying this technique to electrochemical systems. The most serious is the strong absorption of the solution. The electrode must be pushed against a cell window to reduce the thickness of the solution layer to a few μm. The thin-layer structure of the cell prevents free mass transportation between the thin layer and the reservoir, and also the quick response of the electrochemical system against externally applied potential modulation. Furthermore, even if the solution layer is thin enough for spectral measurements, it is still three orders of magnitude thicker than that of monolayers on the electrode surface, and hence complete subtraction of the solution background from the surface spectrum is not easy.

To remove such problems, we have developed surface-enhanced infrared absorption (SEIRA) spectroscopy using the Kretschmann ATR configuration (ATR measurements with a prism/metal (electrode)/solution geometry, Fig. 1). SEIRA is an effect that infrared absorption of molecules adsorbed on some rough metal surfaces is extremely enhanced [1,2]. The sensitivity of the SEIRA spectroscopy is over ten-times higher than IR-RAS, which enables time-resolved monitoring of electrode dynamics. Unfortunately, however, the SEIRA measurements have been limited to mid-IR range (> 1000 cm^{-1} for Si) due to the strong absorption of the prism (this is also the case in IR-RAS). In the present investigation, we aimed to extend SEIRA spectroelectrochemistry to far-IR range by using the strong IR beam from UVSOR.

Figure 1 shows the optics constructed for the present study. The infrared beam was taken from a service port on BL6A1 with a KRS-5 window after passing through an FT-IR spectrometer (Bruker IFS 66V). An MCT detector (for mid-IR range) and Si bolometer (for far-IR range) were used to detect the IR beam totally reflected from the electrochemical interface. The electrochemical cell was a three-electrode glass one with a Pt counter electrode and reversible hydrogen electrode (RHE) in the supporting electrolyte. The working electrodes were prepared by electroless (i.e., chemical) deposition of Pt [3] or Au [4] on the total reflecting plane of a Si hemicylinder (0.5 cm in radius and 2 cm long). The electrode potential was controlled with a potentiostat (Hokuto Denko, HAB-151). Solutions were prepared from ultra-pure water and analytical grade chemicals, and deaerated by Ar gas bubbling before use.

Figure 2 shows SEIRA spectrum of CO adsorbed on a Pt electrode in 0.5 M (= mol dm^{-3}) H_2SO_4 at 0.1 V. The CO adlayer was established by bubbling CO gas under a potential control at 0.05 V. Spectrum a and b were constructed by coadding 100 and 5000 interferograms, respectively. A reference spectrum was recorded before establishing the CO adlayer and all the spectra were calculated with the absorbance units defined as $-\log(R/R_0)$, where R and R_0 represent the intensities of the IR radiation reflected from the electrode surface with and without the CO adlayer. The very strong band at 2070 cm^{-1} and the weak band at 1860 cm^{-1} are the stretching modes of CO adsorbed at atop and bridge sites of Pt surface (linear and bridge CO), respectively. The weak band at 3660 cm^{-1} is the stretching mode of water. The very high frequency and sharp feature of this band implies that water molecules at the CO-covered electrode surface are free from hydrogen bonding. The down-going bands at 3550 and 1610 cm^{-1} are the stretching and bending modes of water removed from the interface by the adsorption of CO. The characteristic bands of "bulk" water (3400 and 1600 cm^{-1}) and of supporting electrolyte (mostly bisulfate) are completely missing.

It should be noted that the peak intensity of the linear CO band is 0.3 (50 % in the reflectance change units $\Delta R/R_0$). The observed intensity is about 50-times as strong as that observed by IR-RAS. Relatively large surface area of the chemically deposited Pt electrode (roughness factor of about 7 estimated by cyclic voltammetry) contributes to the extremely strong absorption, but is not decisive. Rather, the strong absorption arises from SEIRA effect.

Owing to the use of the strong IR beam from UVSOR, the spectral range could be extended down to 600

cm^{-1} with the MCT detector. We further tried to detect the Pt–CO stretching mode expected around 400 cm^{-1} with the Si bolometer. Although the intensity of the beam passing through the prism was strong enough in the spectral range of 200–500 cm^{-1}, we have not yet succeeded in detecting this mode. Two reasons exist. The one is the very small absorption coefficient of this mode; two orders of magnitude smaller than that of the stretching mode. However, expected intensity is well above the detection limit of conventional FT-IR spectrometers (10^{-5}–10^{-4} absorbance). The more serious is noise the source of which is unknown (probably, the electronic circuits in the FT-IR spectrometer and vibration of the flour). In fact, the signal-to-noise ratios (S/N) of the spectra obtained in the present experiment were much worse than those acquired in our laboratory with a ceramic source, as shown in Fig. 2c. Although the number of intermerograms coadded was only 100, the S/N of spectrum c is equivalent or better than spectrum b (5000 interferograms coaddition).

In conclusion, we succeeded for the first time in observing SEIRA using synchrotron radiation for CO adsorbed on a Pt electrode in acidic solution. Although no bands could be detected in the far-IR region due to noise of the system, SEIRA measurements in the far-IR range will be possible if the noise of the system can be reduced.

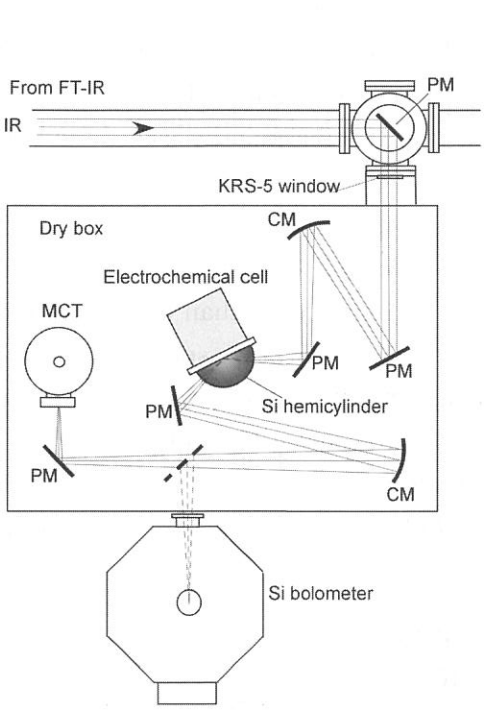

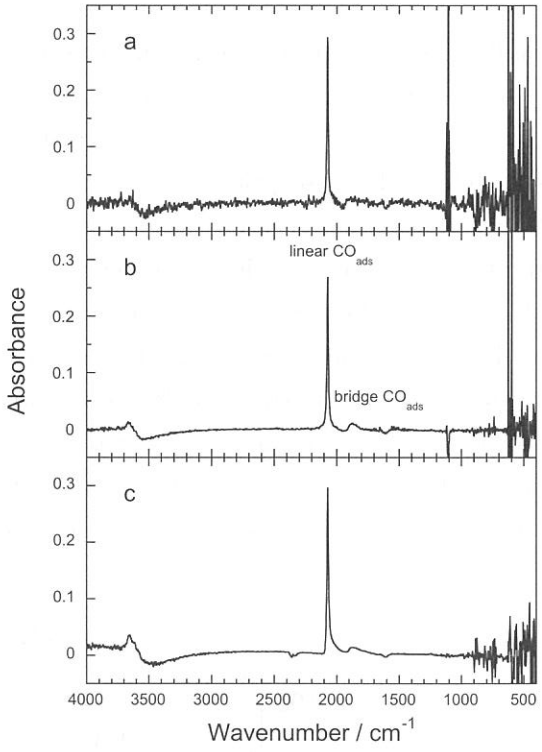

Fig. 1. (left) Experimental setup for *in situ* surface-enhanced spectroelectrochemistry using UVSOR. PM: plane mirror; CM: concave mirror, MCT: mercury-cadmium-telluride detector. The incident angle of the IR beam (p-polarization) is 70°.

Fig. 2. (right) SEIRA spectra of CO adsorbed on a Pt electrode in 0.5 M H_2SO_4 acquired with UVSOR (a and b) and a ceramic light source. The number of interferograms coadded was 100 for spectra a and c, and 5,000 for spectrum b. Spectral resolution was 4 cm^{-1}. The applied potential was 0.1 V vs. RHE.

References

[1] M. Osawa, *Bull. Chem. Soc. Jpn.*, **70**, 2861 (1997).

[2] M. Osawa, *Near-Field Optics and Surface Plasmon Plaritons,* S. Kawata (Ed.), Springer, Berlin (2001), p. 163-187.

[3] A. Miki, S. Ye and M. Osawa, *Chem. Commun.*, 1500 (2002).

[4] H. Miyake, S. Ye and M. Osawa, *Electrochem. Commun.* **4**, 973 (2002).

(BL6A1)

Absorption spectrum of GaP in the mid-infrared region

Ichiro Shoji and Takunori Taira

Laser Research Center for Molecular Science, Institute for Molecular Science, 38 Nishigonaka, Myodaiji, Okazaki 444-8585, Japan

Widely tunable mid-infrared (IR) coherent light sources are attractive for such applications as spectroscopy, chemical monitoring, biomedicine, and atmospheric and environmental sensing. Optical parametric oscillation (OPO) or difference-frequency generation (DFG) in which solid-state lasers are used as the pump sources are promising approaches to realize those sources. Especially, quasi-phase-matched (QPM) OPO/DFG devices using periodically-poled $LiNbO_3$ have been extensively studied and successfully developed for generation of 1 to 5 μm. However, it is difficult to obtain mid-IR light longer than 5 μm in high efficiency by use of $LiNbO_3$ due to its significant IR absorption.

We are developing QPM devices using compound semiconductors to access the mid-IR region because they have large optical nonlinearities [1] as well as longer absorption cutoff wavelengths than $LiNbO_3$. GaAs, the nonlinear-optical coefficient of which is more than 6 times as large as that of $LiNbO_3$, is one of good candidates. We measured the absorption spectrum of undoped semi-insulating GaAs in the mid-IR region and found that it is transparent as long as 16 μm [2]. Another promising material is GaP; it is less sensitive to two-photon absorption when pumped at 1 μm, although its nonlinear-optical coefficient is smaller than that of GaAs (but still larger than that of $LiNbO_3$). Previous measurements of mid-IR absorption spectra of GaP were carried

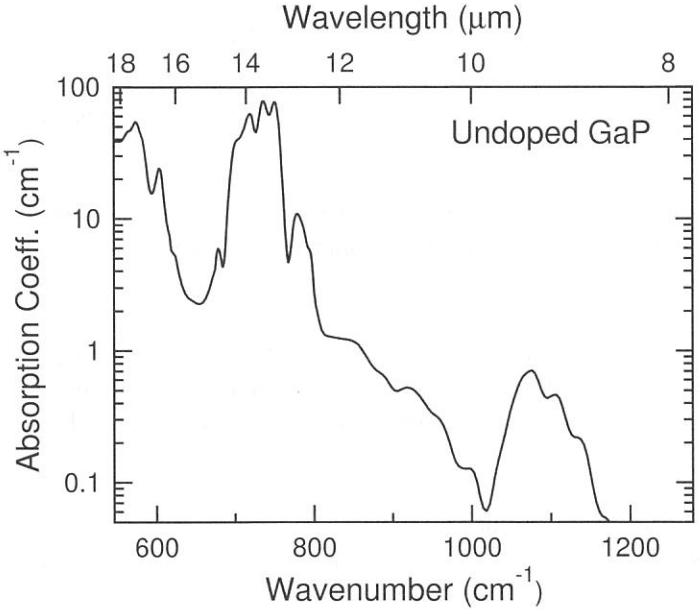

Fig 1. Absorption spectrum of the undoped GaP in the mid-IR region.

out only for n-type samples. Here we report the measurement for pure, i.e. undoped, semi-insulating samples, which are free from carrier-related absorption and suitable for nonlinear frequency-conversion devices.

We used undoped GaP samples grown by Sumitomo electric, the resistivity of which was $\geq 10^6\ \Omega\,\mathrm{cm}$. Two samples with different thicknesses, 75 μm and 5.3 mm, were prepared in order to accurately obtain the absorption coefficients both for high- and low-absorption regions. The absorption spectrum was measured with the rapid-scan Michelson FT-IR (Bruker) at the beam line BL6A1. Using the KBr beam splitter and a MCT detector, we made a measurement in the wavelength range of 400–7000 cm^{-1} (25–1.4 μm) at the resolution of 10 cm^{-1}.

Figure 1 shows the obtained absorption spectra. The wavelength range of 1280–7000 cm^{-1}, in which no absorption was observed, and the range of 400–550 cm^{-1}, in which absorption was too strong to obtain accurate absorption coefficients, are not shown. We found that GaP are highly transparent in the wavelength region shorter than 1200 cm^{-1} (8.3 μm), and still useful up to 1000 cm^{-1} (10 μm) although there is a small absorption peak around 1070 cm^{-1} (9.3 μm).

In conclusion, undoped, semi-insulating GaP is a promising material for highly-efficient OPO/DFG devices which generate mid-IR as long as 10 μm.

References

[1] I. Shoji, T. Kondo, A. Kitamoto, M. Shirane, and R. Ito, J. Opt. Soc. Am. B **14,** 2268 – 2294 (1997).

[2] I. Shoji, S. Kurimura, and T. Taira, "Infrared absorption spectrum of GaAs," UVSOR ACTIVITY REPORT 2000.

(BL6A1)

Millimeter Wave Reflection Measurements of Secondary Battery Substance $Li_{1-x}CoO_2$

Hitoshi Ohta, Tomoya Hirano[A], Yuta Nagasaka[A], Takao Nanba[A], Atushi Hirano[B] and Ryoji Kanno[C]

Molecular Photoscience Research Center, Kobe University, 1-1 Rokkodai, Nada, Kobe 657-8501
[A]The Graduate School of Science and Technology, Kobe University, 1-1 Rokkodai, Nada, Kobe 657-8501
[B]Faculty of Engineering, Mie University, 1515 Kamihama-cho, Tsu 514-8507
[C]Interdisciplinary Graduate School of Science and Engineering, Tokyo Institute of technology, 4259 Nagatsuda, Midori, Yokohama 226-8502

As $LiNiO_2$, which is known as a super ionic conductor, has attracted much attension as a promising material for the positive electrode of the Li ion secondary batteries, we have been studying the millimeter wave reflection measurements of $LiNiO_2$ and related substances using UVSOR and also the coherent SR of Kyoto University in Kumatori [1-7]. We found the drastic increase of the reflection of $LiNiO_2$ above 300 K in the millimeter wave region [1, 6], and we suggested that this increase of reflection is related to the motion of Li ion in the system. However, the positive electrode in the real application at the moment is the $LiCoO_2$. Therefore, it is worth trying the similar measurement on $LiCoO_2$ using UVSOR.

The reflection measurements of $LiCoO_2$ sintered sample with a diameter of 10 mm have been performed in the spectra region from 5 to 60 cm^{-1} using the beam line BL6A1 of UVSOR. The low pass filter was used for the measurement below 22 cm^{-1}. The temperature was changed from 300 to 380 K. The gold plate was used as a reference and InSb detector was used as a detector. However, the reflection of $LiCoO_2$ was almost flat and in the observed region and there was no temperature dependence. Therefore, we tried $Li_{1-x}CoO_2$, which corresponds to the state during the recharge and discharge process of $LiCoO_2$ electrode. Figure 1 shows our results for $Li_{1-x}CoO_2$ sample. The result shows that the reflectivity starts to rise clearly from 300 K but the rise does not increase very much in the temperature region from 300 to 380 K. The connection between the obtained results and the battery performance should be considered in the near future.

[1] H. Ohta *et al.*: UVSOR Activity Report 1996 (1997) 182.
[2] H. Ohta *et al.*: UVSOR Activity Report 1997 (1998) 128.
[3] H. Ohta *et al.*: UVSOR Activity Report 1998 (1999) 158.
[4] H. Ohta *et al.*: UVSOR Activity Report 1999 (2000) 93.
[5]H. Ohta *et al.*: UVSOR Activity Report 2000, (2001) 121.
[6] H. Ohta *et al.*: Jpn. J. Applied Phys. **39** (2000) Suppl. 39-1, 409-410.
[7] H. Ohta *et al.*: UVSOR Activity Report 2001, (2002) 138.

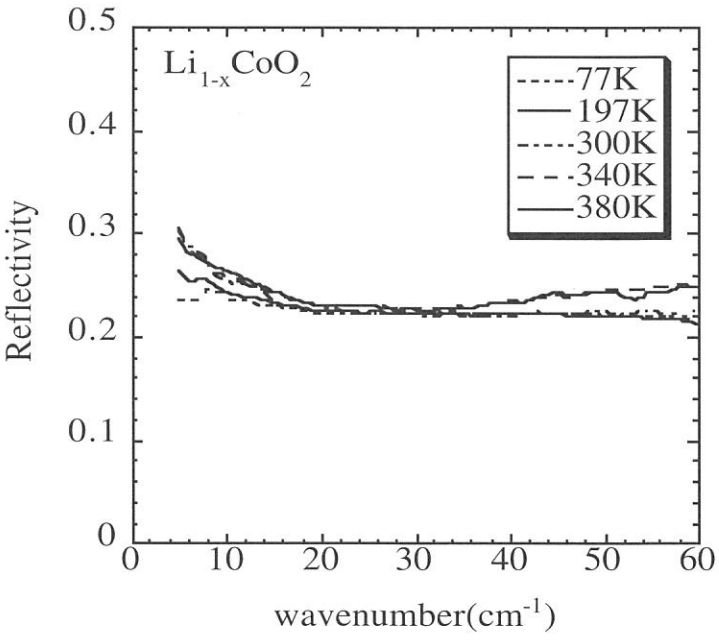

Fig. 1 Reflection spectra of $Li_{1-x}CoO_2$.

(BL6A1&7B)

Optical properties of monochalcogenide compound YbS

M. Matsunami[a], L. Chen[a], T. Nanba[a] and A. Ochiai[b]

a Graduate School of Science and Technology, Kobe University ,Nada-ku, Kobe 657-8501, Japan
b Center for Low Temperature Science, Tohoku University, Aoba-ku, Sendai 980-8578, Japan

Yb monochalcogenides (YbX, X=O, S, Se, Te), which crystallize in the NaCl structure, show semiconducting properties at ambient pressure and undergo a pressure-induced semiconductor-to-metal transition without any change in the crystal structure. Pressure-volume behavior on YbS suggests that Yb changes from a divalent state to a trivalent state through an intermediate valence state with Yb^{2+} and Yb^{3+} under high pressure , and exhibits finally metallic properties above 10 GPa due to a partial f-electron delocalization. Hitherto, the optical properties of YbX have not been investigated except the works by V. Narayanamurti et al.[1] and K. Syassen et al.[2] from a near IR to visible region. The fundamental optical spectrum at ambient pressure is important as the starting data to know the change in the electronic state under pressure. The optical spectra under pressure has been published elsewhere [3]. In this study, we have measured optical reflectivity spectra of cleaved YbS single crystals in the wide energy regions from 7 meV to 30 eV with use of synchrotron radiation light source as well as a conventional black body source. The measurements were performed using a Fourier-transform interferometer. The optical conductivity (σ) spectra were obtained by a Kramers-Kronig analysis of the measured reflectivity data.

Fig. 1 (a) shows the optical reflectivity spectra of YbS at room temperature and (b) corresponding conductivity spectra in a logarithmic scale. In the far-infrared region, a strong reststrahlen phonon band due to a NaCl structure was resolved. The threshold of the absorption due to the $4f^{14}$-$4f^{13}5d$ excitation across the energy gap was observed around 1.2 eV. Main peaks A-D denoted in the inserted figure in addition to many peak structure due to interband transition to the higher energy lying levels were observed. A weak peak of which intensity shows a strong temperature-dependence was observed around 0.27 eV. At 295 K, the peak is very weak and with decreasing temperature its intensity grew. The origin is still unknown. Fig.2 shows the schematic drawing of the energy diagram for the assignmernt of the A-D peaks. The 4*f* state in the conduction band suffers from the crystal splitting (10Dq) into the e_g and t_{2g} level, respectively. The each e_g and t_{2g} level further split into $^2F_{5/2}$ and $^2F_{7/2}$ levels due to a spin orbit coupling. The peak A and B were assigned to the excitation from the $4f^{14}$ ground state to the excited $^2F_{5/2}$ and $^2F_{7/2}$ spin-orbit pair of the t_{2g} state and the C and D to the excitation from the $4f^{14}$ ground state to the excited $^2F_{5/2}$ and $^2F_{7/2}$ spin-orbit pair of the e_g state .

References

[1] K. Syassen et al.:Phys. Rev. **B32**(1985) 8246.

[2] V. Narayanamurti et al.:Phys. Rev. **B9**(1974) 2521 .

[3] M.Matsunami, L.Chen, T.Nanba and A.Ochiai: Acta Physica Polonica B34(2002)1011.

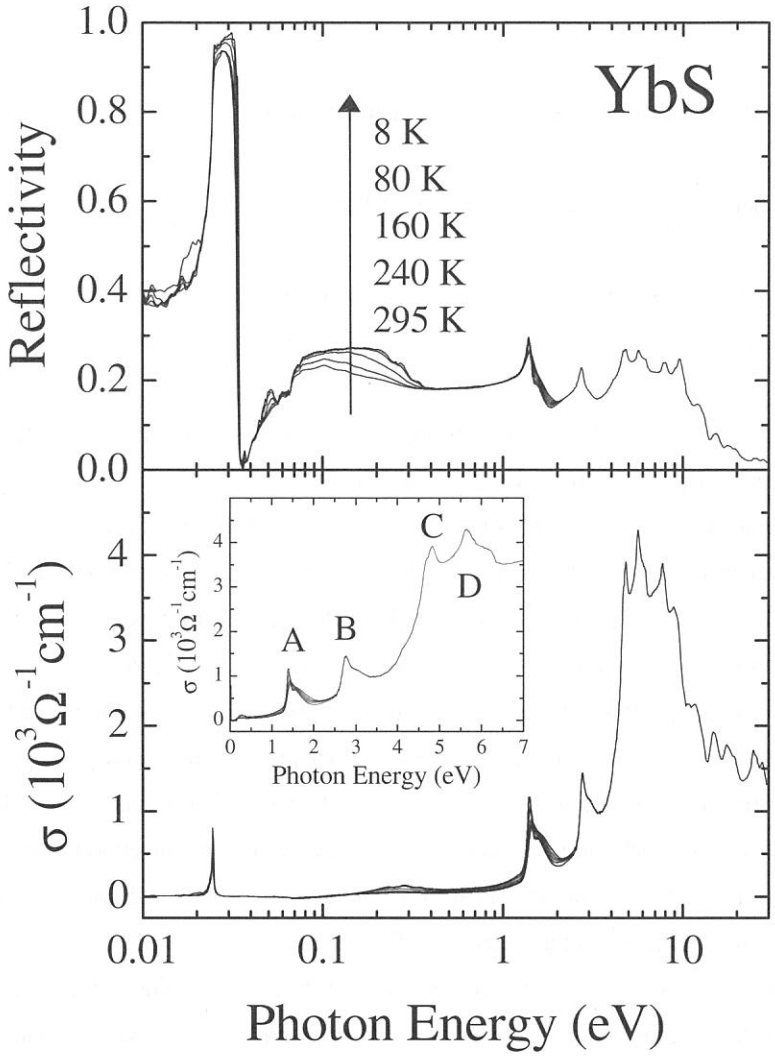

Fig.1 Optical reflection spectra (a) of YbS single crystal and corresponding optical conductivity spectra.(b).

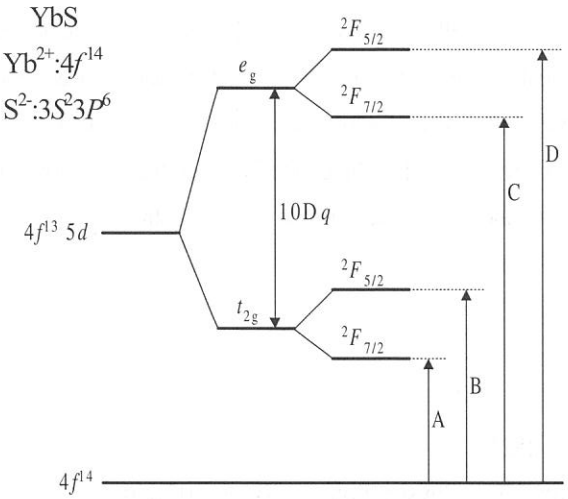

Fig.2 the Schematic drawing to represent the optical excitations between the g.s. and excited electronic states for the A-D peaks in the σ -spectrum.

(BL7B)

Reflectivity spectrum of $SrTiO_3$

H. Okamura, L. Chen, M. Matsunami, T. Nanba, K. Tanaka[A]

Graduate School of Science and Technology, Kobe University
Kobe 657-8501, JAPAN.
[A]Department of Physics, Graduate School of Science, Kyoto University,
Kyoto 606-8502, JAPAN

$SrTiO_3$ (STO) has been known to show a "quantum paraelectricity" at low temperatures: its static dielectric constant ε becomes extremely large, ~ 20000 at 4 K, without showing any ferroelectricity unlike the famous case of $BaTiO_3$. The absence of ferroelectricity in STO has been interpreted to arise from strong quantum fluctuations (zero-point oscillations) of the electric dipole moment, hence the term "quantum paraelectricity". Very recently, it has been found that an optical excitation with uv light (above band gap) further enhances the low temperature ε of STO by as much as two orders of magnitude. In addition, it is known that STO shows a very high photoconductivity under uv (above-gap) excitation. These phenomena are examples of light-induced electronic crossover, and attracting a lot of current interest. We are starting infrared and far-infrared studies of STO under UV laser excitations. To understand the very basic optical properties of STO, we have measured the reflectivity spectrum of STO at room temperature (without uv excitations) at BL7B of UVSOR. The obtained spectrum in the Figure shows many structures in uv and vuv regions. We are currently extending the measurement to lower energy regions.

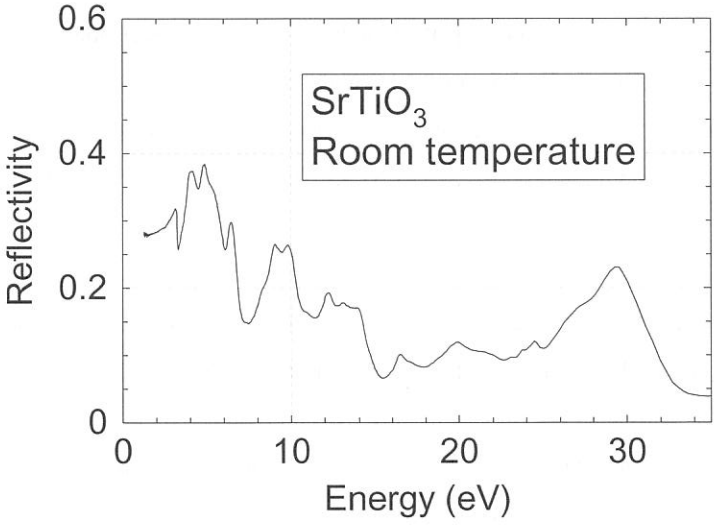

Figure. Reflectivity spectrum of $SrTiO_3$ at room temperature.

(BL7B)

Characterization of GaN Based UV Detectors in the Near UV and VUV Region using Annealed Schottky Electrode

Kazumasa Hiramatsu[1], Keiichi Ohta[1], Atsushi Motogaito[1], Youichiro Ohuchi[2], Kazuyuki Tadatomo[2], Yutaka Hamamura[3] and Kazutoshi Fukui[4]

[1]*Deptartment of Electrical and Electronic Engineering, Mie University, 1515 Kamihama, Tsu, Mie 514-8507, Japan*

[2]*Telecommunication & Photonics Research Laboratory, Mitsubishi Cable Industries, Ltd., 4-3 Ikejiri, Itami, Hyogo 664-0027, Japan*

[3]*Nikon Corporation, Precision Equipment Company, 1-10-1 Asamizodai, Sagamihara, Kanagawa 228-0828, Japan*

[4]*Research Center for Development of Far-Infrared Region, Fukui University, 3-9-1 Bunkyo, Fukui, Fukui 910-8507, Japan*

Ultraviolet (UV) detectors are one of the most attractive devices in the group III-nitride semiconductors. Currently, for the measurement of UV light, photodetector components with Si such as photodiodes are mainly used. However, light sensitivity often deteriorates due to radiation damage in the vacuum ultraviolet (VUV) region. Several groups have reported on GaN- or AlGaN-based UV detectors. They have good responsivity from 250 to 360 nm and clear cut-off characteristics at a cut-off wavelength of λ_c=360 nm. We reported responsivity spectra of GaN based UV detectors with comb-shaped electrode in VUV region for the first time [1]. Furthermore, the larger responsivity is obtained by using transparent Schottky electrode [2].

In this report, the reduction of dark current by annealing Schottky electrode and responsivity spectra applying reverse bias are described.

The UV detectors used in this study adopt the Schottky contacts with a transparent electrode. They consist of a 3-μm-thick n-GaN layer ($n=2.0\times10^{18}$ cm^{-3}) and a 1.5-μm-thick i-GaN layer ($n=1.0\times10^{16}$ cm^{-3}) on a (0001) sapphire substrate. These layers are grown by metalorganic vapor phase epitaxy (MOVPE). The Au/Ni Schottky contact is deposited on i-GaN. The thickness of Au and Ni are 10 nm and 1 nm, respectively. The diameter of detectors is 6.5 mm.

To examine the effect of annealing Schottky electrode on the Schottky characteristics, the I-V characteristics were carried out. Figure 1 shows I-V characteristics of the samples. Reverse dark current (I_{dark}) and photocurrent (I_{ph}) were measured as shown in Fig 1. In the low reverse voltage region (<2V), the dark current was about 10 nA (before annealing) and 100 pA (after annealing), respectively. Thus, the dark current of samples after annealing Schottky electrode is reduced by hundredth part of that of samples before annealing Schottky electrode. The ratio of I_{ph} to I_{dark} was 1 (before annealing) and 100 (after annealing),

respectively. This means S/N ratio can be improved by annealing Schottky electrode.

The responsivity spectra applying reverse bias were characterized. Figure 2 shows responsivity spectra of samples with annealing Schottky electrode. No responsivity was observed under 3.4 eV because the band gap of GaN was 3.4 eV. Responsivity is increased by absorbing the near UV and VUV light in i-GaN layer. The contrast of responsivity between the near UV region and the visible region is about 10^4 at 0.5 V. The maximum responsivity was 0.1 A/W at 3.5 eV. The responsivity for the VUV light was about 0.01 A/W. The small dark current and stable responsivity spectra were observed when the reverse voltage was less than 2V. In the case of large reverse voltage (>2V), the dark current was increased and the responsivity spectra were not stable. These results are related with Figs. 1. In the low reverse voltage region (<2V), good responsivity spectra are obtained because of large ratio of I_{ph} to I_{dark}.

References

[1] A. Motogaito, M. Yamaguchi, K. Hiramatsu, M. Kotoh, Y. Ohuchi, K. Tadatomo, Y. Hamamura and K. Fukui: Jpn. J. Appl. Phys. **40**, L368 (2001).

[2] A. Motogaito, K. Ohta, K. Hiramatsu, Y. Ohuchi, K. Tadatomo, Y. Hamamura and K. Fukui: Phys. Stat. Sol. (a) **188**, 337 (2001).

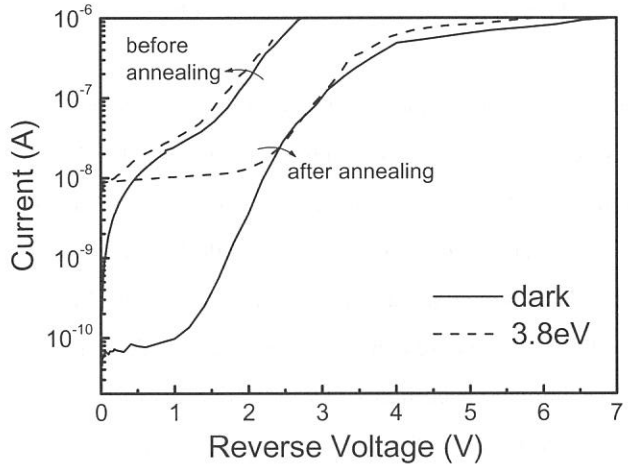

Fig.1. I-V characteristics of GaN based UV detectors using transparent electrode.

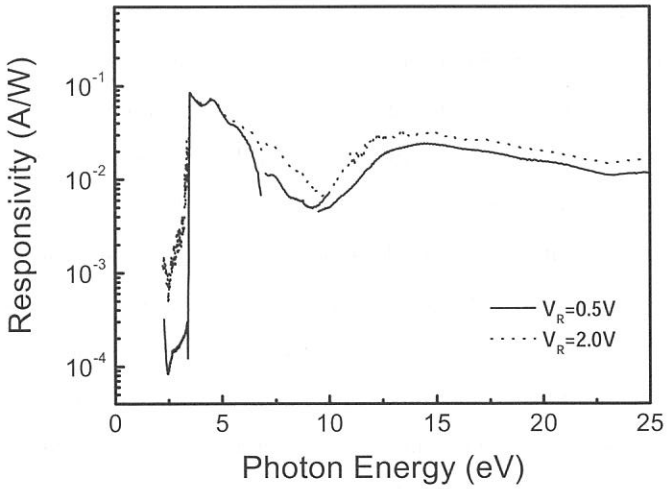

Fig. 2. Responsivity spectra with various reverse voltage.

(BL7B)

VIS-UV luminescence and time resolved measurements of the III-V nitride alloys

Kohji KIMURA[1], Kazutoshi FUKUI[2], Satoru TANAKA[3],

Hideki HIRAYAMA[4] and Yoshinobu AOYAGI[4]

[1]*Department of Electric and Electronic Engineering, Fukui University, Fukui 910-8507, Japan*

[2]*Research Center for Development of Far-Infrared Region, Fukui University, Fukui 910-8507, Japan*

[3]*Research Institute for Electronic Science, Hokkaido University, Sapporo 060-0812, Japan*

[4]*The Institute of Physical and Chemical Research, Wako 351-0198, Japan*

The group III-nitride semiconductors (AlN, GaN and InN) are promising materials for applications in opt-electronic devices. The ternary alloy system $Al_xGa_{1-x}N$ (AlGaN) is complete solid solution and varies its band gap from 3.4 eV (blue) to 6.2 eV (ultraviolet). We have been performed the reflectance measurements at the visible – vacuum ultraviolet region [1], and luminescence and time resolved measurements [2-3]. In this report, we represent the decay profiles.

AlGaN samples were made by MOCVD method at RIKEN on SiC substrates. The photo luminescence (PL) experiments were carried out as follows; a) excitation light source : BL7B (3.4 – 25 eV) b) detection of luminescence : 30cm Czerny-Turner type VIS – UV monochromator (1.5 – 6.2 eV) with a CCD array c) vacuum condition : in the range of 10^{-9} Torr d) temperature range : 22 K – 100 K e) time resolved measurement : TAC method with MCP-PMT under the single bunch operation. A single UV optical fiber cable, which was dedicated for ultra high vacuum (UHV) and had 0.6 mm core diameter, were used for detecting VIS and UV luminescence in the UHV chamber. VIS and UV luminescence lights were introduced to the VIS-UV monochromator with CCD array detector via both a UHV fiber optic feedthrough and a flexible optical fiber. The period and the observed FWHM of the excitation SR light under single bunch operation are 178 ns and about 450 ps, respectively.

PL spectra of AlGaN consist of two luminescence bands. One is B-band whose peak energy is almost same energy as the band gap. The other is Y-band and its peak energy is located about 2 ~ 2.5 eV. Figure 1 shows the B-band PL decay profiles measured at the peak energy position of the emission spectra at $T = 22$ K. The decay profiles of higher Al content samples have sharp peaks at around 0 time which are similar to the time structure of the excitation SR light. It means that there are short decay time components less than 1 ns. To ensure the time component analysis of B-band PL of AlGaN materials, deconvolution method has been performed. Deconvolution of decay profiles reveals that there are three decay time components (fast, middle and slow) in each decay profiles. Figure 2 shows those decay time, as a function of the Al content at 22 K. Both the fast component with its lifetime less than 1 ns, and the middle one with the order of 1 ns show little dependent on Al content. The decay time of the slow component, on the other hand, which has the order of 10 ns, increase with increasing Al content. The ratio among the integrated intensity of three components shows that the slow

component becomes dominant with increasing Al content, while the fast component becomes clear with increasing Al content in fig 1. Those results suggest that the time structure of B-band PL of AlN, which is yet to be reported, mainly consist of slow component (> 100 ns).

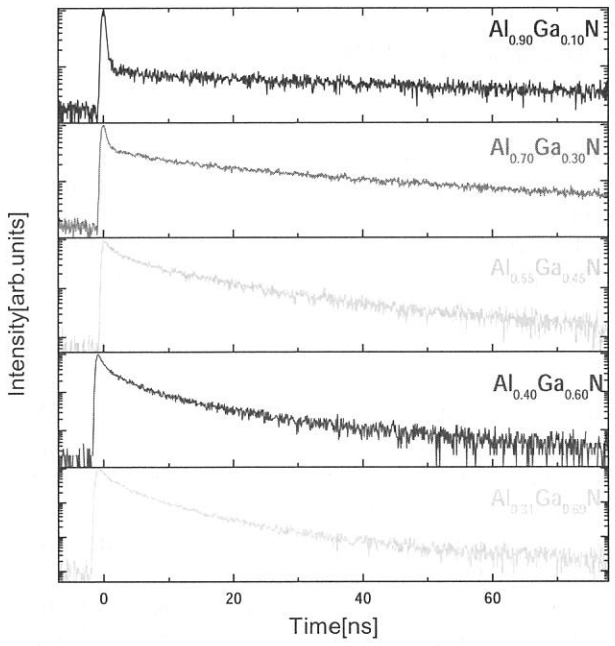

Fig.1

Decay profiles measured at the peak energy position of the emission spectra at 22K.

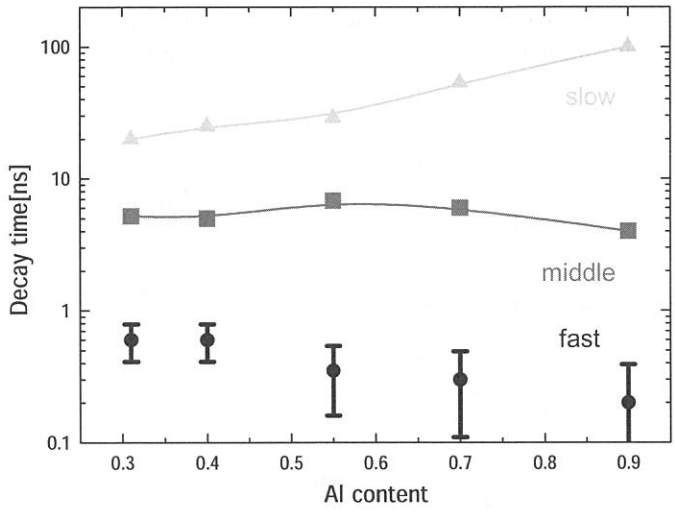

Fig2.

PL decay times, as a function of the Al content at 22 K.

References

[1] K. Fukui, H. Miura, A. Okada, Q. Guo, S. Tanaka, H. Hirayama and Y. Aoyagi : ,Proceedings of International Workshop on Nitride Semiconductors, IPAP Conference Series 1, (2000.11) 647.

[2] K. Fukui, H. Hirayama, S. Tanaka, Y. Aoyagi : UVSOR Activity Report 2000, 142 (2001).

[3] K. Fukui, K. Ebisu, S. Oda, K. Kimura : UVSOR Activity Report 2001, 146 (2002).

(BL7B)

Optical conductivity of a non-Fermi-liquid material $YbRh_2Si_2$

S. Kimura[1,2], T. Nishi[2], J. Sichelschmidt[3], V. Voevodin[3], J. Ferstl[3], C. Geibel[3] and F. Steglich[3]

[1]*UVSOR Facility, Institute for Molecular, Science, Okazaki 444-8585*
[2]*Department of Structural Molecular Science, The Graduate University for Advanced Studies, Okazaki 444-8585*
[3]*Max Planck Institute for Chemical Physics of Solids, D-01187 Dresden, Germany*

$YbRh_2Si_2$ shows a non-Fermi liquid (NFL) behavior in the wide temperature range of 0.1 – 10 K at ambient pressure and zero magnetic field. [1] Then the material is suitable for the investigation of the fundamental properties of NFL. In this study, we measured reflectivity spectra in the temperature range of 2.7 – 300 K and in the photon energy range of 0.01 – 30 eV. We investigate the NFL properties in the optical conductivity ($\sigma(\omega)$) spectra as well as whether the $\sigma(\omega)$ spectrum differs from that of Landau Fermi liquid (LFL) materials or not.

The material was grown by an indium flux method. The *c*-plane of the tetragonal structure of the sample with a size of $0.8 \times 0.8 \times 0.1$ mm^3 was measured. The optical spectra in $\hbar\omega$ = 0.01 - 1.5 eV was detected at eight temperatures of 2.7 – 300 K by using two conventional FTIR spectrometers in Dresden and Okazaki. The spectrum in the photon energy range of $\hbar\omega$ = 1.2 – 30 eV was obtained only at room temperature using a synchrotron radiation in Okazaki. The $\sigma(\omega)$ spectra were obtained from the Kramers-Kronig analysis of the reflectivity spectra in $\hbar\omega$ = 0.01 – 30 eV.

The temperature dependence of $\sigma(\omega)$ spectrum is shown in Figure 1. Two characteristic structures appear in the figure, one is a dip structure at around $\hbar\omega$ = 0.02 eV the other a broad peak at $\hbar\omega$ = 0.2 eV. In the former structure, the extrapolation to 0~eV of the $\sigma(\omega)$ at 300 K seems to correspond to the σ_{DC} value. The $\sigma(\omega)$ curve seems to be roughly explained by a Drude model but a broad interband transition component due to the *cf* hybridization as discussed later appears at around $\hbar\omega$ = 0.2 eV. However, at low temperature, the temperature dependence is the opposite to the σ_{DC}. This indicates that a steep rise $\sigma(\omega)$ structure close to the σ_{DC} should appear below $\hbar\omega$ = 0.01 eV. The structure clearly originates from the creation of heavy quasiparticles due to the *cf* hybridization (so-called "coherent part"). On the other hand, the structure corresponding to the latter grows up with decreasing temperature. The structure is commonly observed in dense-Kondo systems such as Ce- and Yb-based compounds, *i.e.*, the origin is the interband transition between the bonding and antibonding *cf* hybridization states ("incoherent part").[2]

The temperature dependence of the peak intensity of the incoherent part is shown in Figure 2 (a).

The figure indicates that the incoherent part rapidly increases with decreasing temperature from 300 to 80 K, slightly increases from 80 to 20 K and becomes almost constant below 20 K. The increase of the incoherent part indicates the growth of the *cf* hybridization, *i.e.*, the *cf* hybridization rapidly and slightly grows up above 80 K and between 80 and 20 K, respectively, and becomes constant below 20 K. The 80 K is consistent with the temperature at which the electric resistivity turns down with decreasing temperature [1] and also the temperature dependence of the ^{29}Si Knight shift changes.[3] In addition,

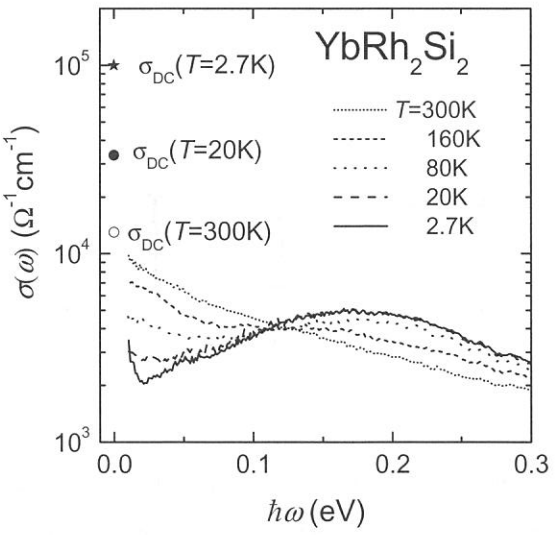

Fig. 1. Temperature dependence of optical conductivity ($\sigma(\omega)$) spectrum of $YbRh_2Si_2$. The direct current conductivities (σ_{DC}) at 300, 20 and 2.7 K are also plotted. The σ_{DC} at 160 and 80 K are similar to that at 300 K.

the constant *cf* hybridization intensity is consistent with a characteristic spin-fluctuation temperature (~ 15 K) determined by the NMR.

Next, the temperature dependence of the tail of the coherent part at around 0.02 eV is discussed. In general, the $\sigma(\omega)$ due to carriers is explained by the Drude model as the following, $\sigma(\omega) = \omega_P^2\tau / \{4\pi (1 + \omega^2\tau^2)\}$. Here, ω_P is the plasma frequency and τ the relaxation time. At frequencies (ω_1) being sufficiently higher than $1/\tau$, $\omega_1\tau \gg 1$. Then $\sigma(\omega_1) = \omega_P^2 / (4\pi\, \omega_1^2\tau) \propto 1/\tau$. Since $\rho \propto 1/\tau \propto T^n$ ($n = 2$ for LFL, < 2 for NFL), $\sigma(\omega_1) \propto T^n$. In the case of $YbRh_2Si_2$, $n = 1$.

The temperature dependence of $\sigma(\omega)$ at $\hbar\omega = 0.02$eV is shown in Figure 2 (b). We recognize that the $\sigma(\hbar\omega = 0.02\text{eV}) \propto T$ is realized below 20 K in the inset of the figure. This is consistent with the appearance of NFL character below 20 K in the electric resistivity and the specific heat.[1]

In conclusion, the temperature dependence of the optical conductivity spectrum of $YbRh_2Si_2$ was measured for the investigation of the NFL property. There are two temperature dependent structures, in which NFL character appears, in the spectrum, one is the coherent part of heavy quasiparticles due to the *cf* hybridization below $\hbar\omega = 0.02$ eV and the other the incoherent part at around 0.2 eV.

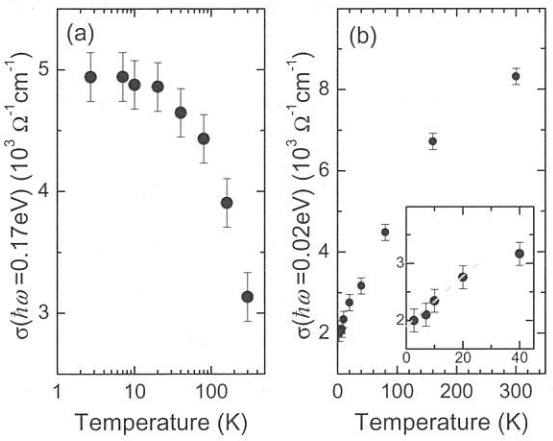

Fig. 2. Temperature dependence of optical conductivity ($\sigma(\omega)$) at two photon energies of 0.17 eV (a) and 0.02 eV (b) of $YbRh_2Si_2$. The temperature dependences of $\sigma(\hbar\omega = 0.17$ eV) and $\sigma(\hbar\omega = 0.02$eV) indicate that of the *cf* hybridization intensity and that of the Drude tail of the heavy quasiparticles, respectively. We recognize the *T*-linear part, which is the evidence of the NFL character, appears below 20 K in the inset of (b).

This work was partially supported by a Grants-in-Aid for Scientific Research from MEXT of Japan.

References

[1] O. Trovarelli *et al.*, Phys. Rev. Lett. **85** (2000) 626.
[2] P. Wachter, *Handbook on the Physics and Chemistry of Rare Earths*, Vol. 19 Ch. 132 (1993) (North Holland).
[3] K. Ishida *et al.*, Phys. Rev. Lett. **89** (2002) 107202.

(BL7B)

Reflectivity Spectra of $La_3Ga_5SiO_{14}$ Crystals

M. Kitaura, K. Mochizuki[A], Y. Inabe[B], M. Itoh[B], H. Nakagawa[C] and S. Oishi[D]

Fukui National College of Technology, Sabae, 916-8507

[A] *Crystal Growth R&D Group, Shinkosha Co., Ltd, Yokohama, 247-0007*

[B] *Department of Electrical and Electronic Engineering, Shinshu University, Nagano 380-8553*

[C] *Department of Electrical and Electronics Engineering, Fukui University, Fukui 910-8507*

[D] *Department of Environmental Science and Technology, Shinshu University, Nagano, 380-8553*

$La_3Ga_5SiO_{14}$ (LGS) attracts great attention as a promising material for surface acoustic wave (SAW) filters in advanced digital communication systems [1,2]. The crystal of LGS belongs to the trigonal system of P_{321} space group. This crystal is characterized by the $Ca_3Ga_2Ge_4O_{14}$ structure [3], in which there are four kinds of cation sites named A, B, C and D; i.e., $A_3BC_3D_2O_{14}$. Owing to a variety of cation sites, the substitutions of isovalent elements for the four cation sites are considered to be a reasonable way for the improvement of its function. From this viewpoint, the effect of substitutions on the piezoelectric properties has been studied [4–6]. However, the growth method of LGS-based crystals seems not to be cleared at present. This is presumably because the fundamental properties needed in understanding the change due to substitutions, e.g., electronic properties, have not yet been investigated.

In the present study, we have investigated the electronic structure of LGS by measuring the reflectivity spectra and the X–ray photoelectron spectroscopy (XPS) spectra. The crystal plates of LGS were supplied from Shinkosha Co., Ltd. They were grown from the melt by Czochralski technique. The surface of samples used in the present experiment was prepared by mechanical polishing. The measurements of reflectivity spectra were carried out at the BL7B using a 3-m normal incidence monochromator. The band–pass of the monochromator was set to be less than 0.3 nm. The incident angle of the SR light for the sample surface was held at 15 degrees. The incident and reflected light were detected using a calibrated silicon diode sensor (IRD AXUV–100). The measurements of XPS spectra were performed using an ESCA instrument at Shinshu University.

Figure 1 shows a typical reflectivity spectrum of LGS at 10 K. The absolute values of reflectivity were determined by referring to the reflactive index at 4.96 eV. The reflectivity spectrum is composed of four large structures labeled by I (5–11 eV), II (11–18 eV), III (18–23 eV) and IV (23–30 eV). The lowest energy peak at 6.02 eV in the structure I most likely originate from the excitonic transition from the top of the valence band (VB) to the bottom of the conduction band (CB). From the analysis of XPS spectra, it was turn out that the base width of the VB is about 11 eV, in agreement with those of the structures I and II. Therefore, we suppose that the structures I and II mainly reflect the density of states (DOS) in the VB. In analogy with metal oxides, it seems likely that the VB of LGS is of O $2p$ character. In the structure III, three fine peaks are observed at

19.59, 20.40 and 22.37 eV, as indicated by bars. In the XPS spectra, it was clarified that the $5p$ level of La is located at around 16 eV below the top of the VB. In addition to this finding, as the band gap energy of LGS is assumed to be 6.5 eV, the transitions from the $5p$ level to the bottom of the CB are expected to take place around 22.5 eV. This photon energy is close to the energies of the three peaks. On this basis, the three peaks are reasonably attributed to the electronic transitions from the $5p$ core level to the $5d$ conduction level in La atoms, which would result in the creation of core excitons. According to the atomic excitation picture of $(5p)^6 \rightarrow (5p)^5(5d)^1$ transitions in La atoms, the transitions from the ground state of $^1S_0$ to the $J=1$ excited states of $^3P_1$, $^1P_1$ and $^3D_1$ are allowed through the electron-hole exchange and spin-orbit interactions. This fact explains well the appearance of three peaks in the structure III. The structure IV appears at the energy equal to the difference between the O $2s$ level and the bottom of the CB, and it is thus assigned to the electronic transitions from the O $2s$ level to the CB with p–like symmetry.

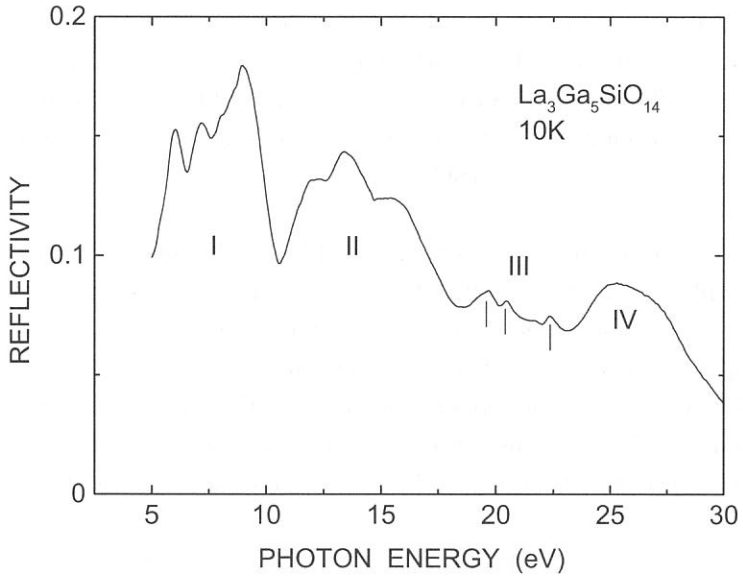

Fig.1 Reflectivity spectrum of $La_3Ga_5SiO_{14}$ at 10 K.

References

[1] A.N. Gotalskaya, D.I. Drezin, V.V. Bezdelkin and V.N. Stassevich, Proc. 1993 IEEE Int. Freq. Conf. Symp. p.339.

[2] K. Shimamura, H. Takeda, T. Kohno and T. Fukuda, J. Crystal Growth **163** (1996) 388.

[3] B.V. Mill, A.V. Butashin, G.G. Khodzhabagyan, E.L. Belokoneva and N.V. Belov, Dokl. Akad. Nauk SSSR **264** (1982) 1385.

[4] H. Takeda, K. Shimamura, T. Kohno and T. Fukuda, J. Crystal Growth **169** (1996) 503.

[5] H. Kawanaka, H. Takeda, K. Shimamura and T. Fukuda, J. Crystal Growth **183** (1998) 274.

[6] J. Sato, H. Takeda, H. Morikoshi, K. Shimamura, P. Rudolph and T. Fukuda, J. Crystal Growth **191** (1998) 746.

(BL7B)

Reflectivity and Optical Conductivity Spectra in $(Nd_{1-x}Sr_x)MnO_3$ and $(Sm_{1-y}Ca_y)MnO_3$

H. Kuroe, A. Sakuta, Y. Hirobe, H. Kuwahara and T. Sekine

Department of Physics, Sophia University, 7-1 Kioi-cho, Chiyoda-ku, Tokyo 102-8554, Japan

In $(Nd_{0.5}Sr_{0.5})MnO_3$, (NSMO $x = 0.5$, where x is the Sr concentration) a phase transition from the paramagnetic insulator phase to the ferromagnetic metal (FM) one and a successive phase transition to the charge-ordered (CO) one respectively occur at $T_C = 250$ K and $T_{CO} = 158$ K.[1] In the CO phase, the CE-type antiferromagnetic order appears, the Mn^{3+} and Mn^{4+} sites become unequivalent and the $d_{3x^2-r^2}$ and $d_{3y^2-r^2}$ orbitals are ordered together with the formation of an $a \times 2b \times c$ superlattice.[2] The FM phase survives even at low temperature when $x = 0.48$ and a metallic phase with the A-type antiferromagnetic order appears when $x = 0.52$. We have already reported Raman-scattering study in NSMO ($x \approx 1/2$).[3, 4] In the CO phase, we observed several new Raman peaks originating from the change of lattice symmetry and the folding of Brillouin zone due to the CO phase transition. In this work, we measure optical reflectivity in NSMO ($x = 0.35$, 0.48, 0.49, 0.50, 0.51, 0.52 and 0.55) to study the phonons and electronic excitations in these systems. We also measured the reflectivity spectrum between 2 and 30 eV in $(Sm_{1-y}Ca_y)MnO_3$ (SCMO $y = 0.5$, where y is the Ca concentration) to study the electronic structure.

The single crystals of NSMO and SCMO were prepared by the floating-zone method. The crystal axes were checked by x-ray diffraction. It was difficult to distinguish the a, b and c axes of crystals because the lattice constants are very close to each other at room temperature and the microdomains exist. The crystals were cut and polished carefully and the post annealing was performed in O_2 with a cooling rate of 10 K/hour from 1050 °C. To obtain an optical conductivity, the precise reflectivity spectrum between far infrared and vacuum ultraviolet regions is necessary. Then we measured the reflectivity spectra below 2 eV with Bruker 113V spectrometer in Sophia Univ. and those above 2 eV with the 3 m McPherson spectrometer at BL7B in UVSOR.

Figures 1 and 2 show the reflectivity spectra in NSMO ($x = 0.35$, 0.48, 0.49, 0.50, 0.51, 0.52 and 0.55) at room temperature between 2 and 30 eV and the optical conductivity one in NSMO ($x = 0.50$) below 1 eV, respectively. The calculated optical conductivity spectrum is consistent with that in the previous report.[5] Figure 3 compares the reflectivity spectrum of NSMO ($x = 0.5$) to that of SCMO ($y = 0.5$). The energies of the reflectivity peaks due to the electronic excitations in these systems are different from each other because of the different oxygen alignments around Mn ion, i.e. the strength of a ligand field. Moreover, the effects of energy-level mixing and/or charge transfer between the Mn $3d$ and O $2p$ orbitals may play an important role.

References

[1] H. Kuwahara *et al.*, Science **270** (1995) 961.

[2] S. Shimomura *et al.*, J. Phys. Soc. Jpn. **68** (1999) 1943.

[3] H. Kuroe *et al.*, Physica B **316-317** (2002) 575.

[4] H. Kuroe *et al.*, in press in Physica B.

[5] J. H. Jung *et al.*, Phys. Rev. B **62** (2000) 481.

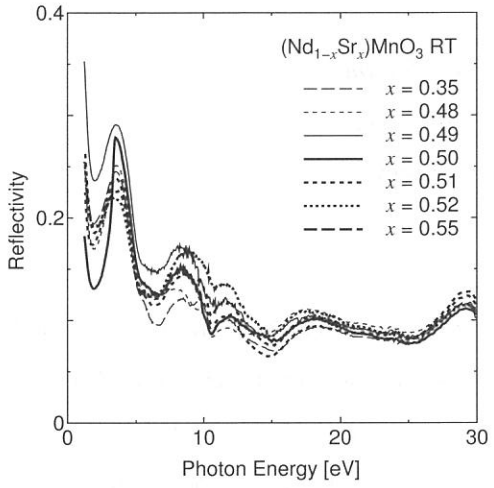

Figure 1: Reflectivity spectra in $(Nd_{1-x}Sr_x)MnO_3$ (x = 0.35, 0.48, 0.49, 0.50, 0.51, 0.52 and 0.55) at room temperature.

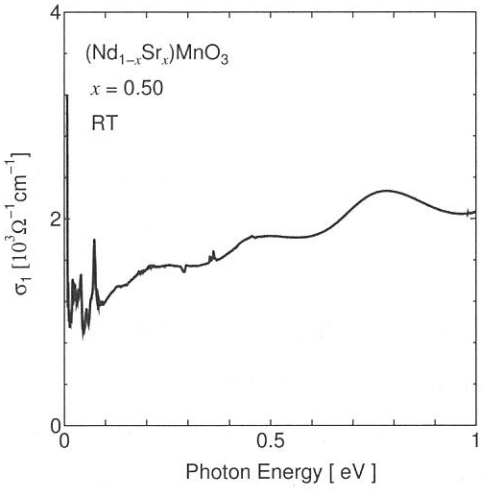

Figure 2: Optical conductivity spectrum in $(Nd_{1-x}Sr_x)MnO_3$ (x = 0.50) at room temperature.

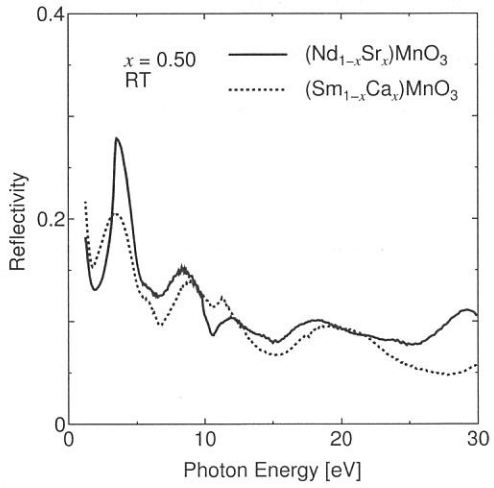

Figure 3: Reflectivity spectra in $(Nd_{0.5}Sr_{0.5})MnO_3$ and $(Sm_{0.5}Ca_{0.5})MnO_3$ at room temperature.

(BL7B)

Reflectivity spectra measurement of ZrB_2

Satoru ODA [1], Kazutoshi FUKUI [2]

[1] *Department of Electric and Electronic Engineering, Fukui University, Fukui 910-8507, Japan*

[2] *Research Center for Development of Far-Infrared Region, Fukui University, Fukui 910-8507, Japan*

ZrB_2 is one of the promising materials for the substrate of GaN , because the lattice constants and thermal expansion coefficient of ZrB_2 are similar to those of GaN. The electric property of ZrB_2 is metal, so that it also becomes the electrode and has the advantage for substrate of GaN devices[1]. ZrB_2 belongs to the AlB_2-type hexagonal crystal structure, and MgB_2 that is one of the attractive superconducing materials also belongs to the AlB_2-type structure. The differences among the properties of metal diborides are also interesting[2]. On the other hand, its basic optical properties, such as dielectric constants, have not been clarified until now. Therefore, reflectivity spectra over wide photon energy region have been performed, and the optical constants calculated by using the Kramers-Kronig analysis.

Single crystals of ZrB_2 were obtained from National Institute for Materials Science and Meijo University. The reflectivity spectra of ZrB_2 on the (0001) plane have been measured from 1.4 eV to 25 eV at room temperature using BL7B. The incidence angle is about four degrees.

Figure 1 shows typical reflectivity spectum of ZrB_2 in 1.4 - 25 eV region. The high reflectivity of the lower energy side is due to the plasma reflection with the valence electron. It is consistent with the metallic character of this material. Reflectivity becomes low at the higher energy side due to the normal incidence configuration.

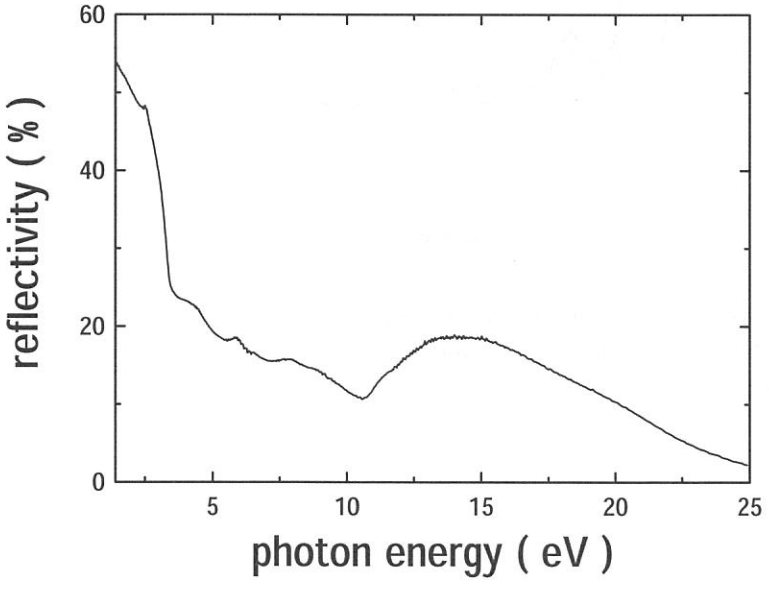

Fig. 1 Reflectivity spectrum of ZrB_2 from 1.4 to 25 eV at room temperature.

The dielectric constants calculated from the Kramers-Kronig analysis are shown in Figure 2 as the function of the photon energy. Crossing point of those two curves near 20 eV suggests that the plasmon energy is 20 eV which is consistent with our photoelectron result [3].

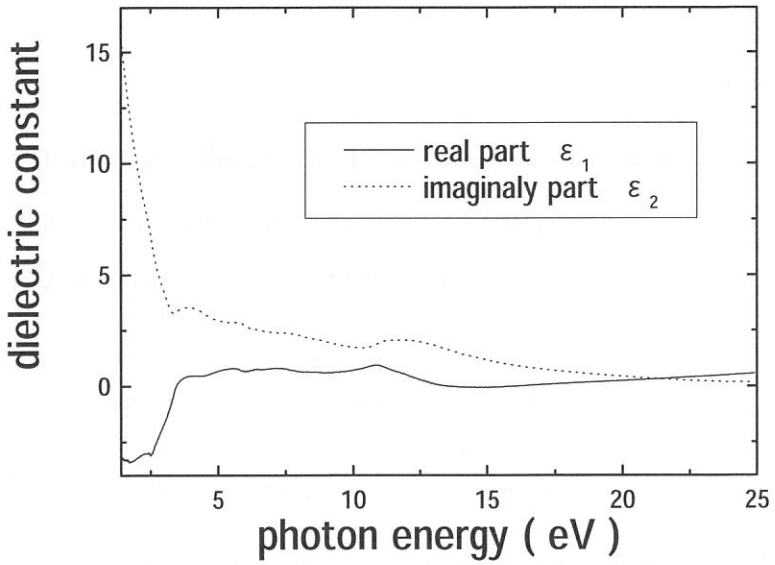

Fig. 2 Dielectric constants spectra obtained by the Kramers-Kronig analysis.

References

[1] H.Kinoshita, S.Otani, S.Kamiyama, H.Amano, I.Akasaki, J.Suda, and H.Matunami : Jpn. J. Appl. Phys. 40 (2001) L1280.

[2] J.R. Shein, A.L. Ivanovskii : cond-mat / 0109445

[3] K. Takahashi, K. Fukui, K. Takarabe : submitted to UVSOR activity report 2002

(BL8B1)

Core electron excited VIS-UV luminescence of the III－V nitride alloys

Kuniya OKADA, Kazutoshi FUKUI[2], Shun-ichi NAOE[3], Satoshi HAMAURA[1]

Hideki HIRAYAMA[4] and Yoshinobu AOYAGI[4]

[1]*Department of Electric and Electronic Engineering, Fukui University, Fukui 910-8507, Japan*

[2]*Research Center for Development of Far-Infrared Region, Fukui 910-8507, Japan*

[3]*Faculty of Engineering, Kanazawa University, Ishikawa 920-1192, Japan*

[4]*The Institute of Physical and Chemical Research, Wako 351-0198, Japan*

The group III-V nitride semiconductors (AlN, GaN and InN) and their alloys (AlGaN, InGaN, AlInN and InAlGaN) are promising materials for opt-electronics device application, since band gap varies from 0.8eV to 6.2eV. The emission spectra, which are excited by the band-to-band transition energy, give us the information of luminescence relaxation process. The core electron excited VIS (visible)-UV (ultraviolet) luminescence measurements also give us the ion-site dependence of the luminescence relaxation process. In this report, we represent nitrogen 1s core electron excited VIS-UV luminescence.

The experiments were carried out at BL8B1 in the range of 10^{-9} Torr from 15K to 300K. A single UV optical fiber cable, which was dedicated for ultra high vacuum (UHV) and had 0.6 mm core diameter, were used for detecting VIS and UV luminescence in the UHV chamber. VIS and UV luminescence light were introduced to the VIS-UV monochromator with CCD array detector via both a UHV fiber optic feedthrough and a 0.3 m single optical fiber (0.6 mm core diameter). Thin films were made by the MOCVD method on SiC substrate at RIKEN. Sample was cleaned with organic solvents just before the installation in the vacuum chamber. No specific surface cleaning of the samples was performed in the vacuum chamber.

Figure 1 shows the luminescence spectrum of $In_{0.04}Al_{0.35}Ga_{0.61}N$ thin film. The excitation energy is 404.02eV. Two emission bands were observed at 3.75eV (B-band) and 2.25eV (Y-band). A peak around 1.87eV is second order of B-band. The excitation spectra of both Y-band and B-bands are shown in Figure 2(a) and 2(b) with total photoelectron yield spectrum, respectively. Those three spectra are basically similar spectrum feature with each other, and suggest that p-states in the conduction band around N ion site are the initial states of both B and Y emission bands.

Figure 3(b) shows the integrated intensity of B-band as the function of the temperature, which represents the typical temperature quenching process. On the other hand, temperature dependence of the integrated intensity of Y-band, which is shown in fig. 3(a), shows more complicated manner, since Y emission band spectrum feature is affected by both the luminescence from SiC substrates and the second order peak of B-band. Although more precise measurements and analysis with time resolved measurements will be expected, those results will be examined by comparison with both Al 1s excited and band-to-band excited VIS-UV luminescence spectra.

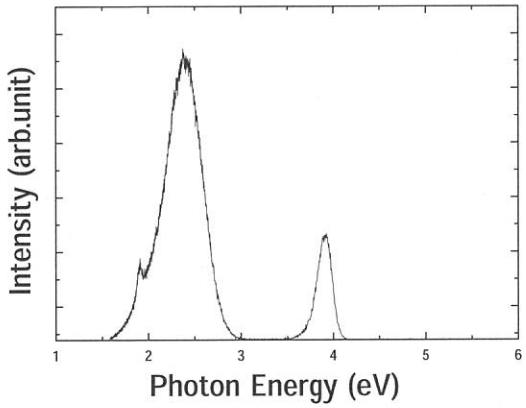

Fig. 1

Luminescence spectrum of $In_{0.04}Al_{0.35}Ga_{0.61}N$ at 15K. Excitation energy is 404.02eV.

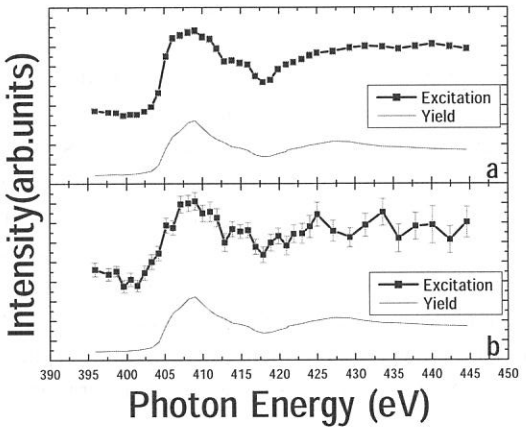

Fig.2

Excitation spectra of both Y-Band (a) and B-band (b) compared with total photoelectron yield spectrum, respectively.

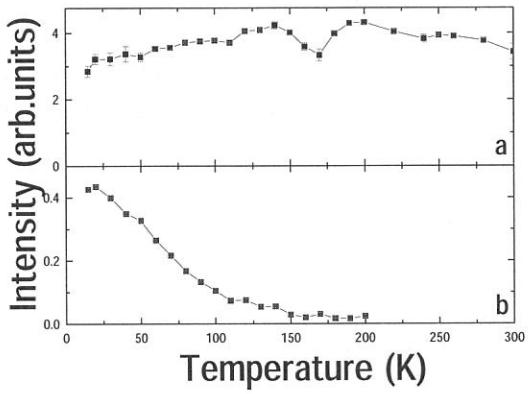

Fig.3

Temperature dependence of Y-Band (a) and B-band (b) integrated intensity. Temperature range is from 15K to 300K

(BL8B1)

Extreme Ultraviolet Faraday Rotation Spectra of Co/Pt Multilayers (II)

K. Saito, T. Ejima, T. Hatano, A. Arai and M. Watanabe

Institute of Multidisciplinary Research for Advanced Materials, Tohoku University
Katahira 2-1-1, Aoba-ku, Sendai 980-8577, Japan

Faraday rotation spectra of Co/Pt multilayers were obtained at room temperature in 50-80eV region. The apparatus is the same as the previous one.[1] In the last year, the measurements were performed on the Co/Pt multilayers deposited on collodion films. In this case, it was uncertain whether the samples on the collodion films were real multilayers or not. Therefore, in the present study, the multilayer samples were prepared onto thin Si films made from Si wafers. An area of ϕ 8 mm of a 18×18×0.2 mm wafer was etched chemically and milled by ion beam. The thickness was less than 1 μm. Five samples, Co(4Å)/Pt(t_{Pt} Å) with t_{Pt}= 8, 10, 16 and Co(t_{Co} Å)/Pt(16 Å) with t_{Co} = 4, 10, 16 multilayers were prepared by ion beam sputtering. Among them, Co(4 Å)/Pt(16 Å) multilayer shows the perpendicular magnetic anisotropy, which confirmed by the use of a vibrating sample magnetometer (VSM).

Figure 1 shows the typical Faraday rotation spectrum of the Co/Pt multilayers. One can see Faraday rotation around Co $M_{2,3}$ and Pt $N_{6,7}$ edges. Pt is magnetized even though it is paramagnetic in usual state. Figures 2 and 3 show the dependence of the Faraday rotation angle on the layer thickness. Here, we assume that the peak-to-peak values of Faraday rotation angles around Co-$M_{2,3}$ and Pt-$N_{6,7}$ edges are proportional to the average magnetic moments of Co and Pt layers, respectively. In Fig.2, the peak-to-peak values of the rotation angles around Co $M_{2,3}$ edges per a) period (normalized by the number of the periods) and b) unit thickness of Co layer (normalized by the total thickness of the Co layers) are plotted against the Co and Pt one-layer thickness (t_{Co} and t_{Pt}), respectively. The values of vertical axes in Fig.2 are proportional to a) the total magnetization of Co one-layer and b) the average magnetization of Co atoms. For the multilayers with t_{Co} = 4 Å, rotation angles per unit period and thickness are almost constant independent of t_{Pt}(= 8,10,16 Å) as seen in left side of Figs.2 a) and b). For the multilayers with t_{Pt} = 16 Å, rotation angles per unit period linearly increase with increase in t_{Co}(= 4,10,16 Å) as seen in right side of Fig.2a) and those per unit thickness are nearly constant independent of the t_{Pt}(= 8,10,16 Å) as seen in right side of Fig.2b). This indicates that the magnetic moment of Co atoms was almost constant in every multilayer. Similar plots for Pt around its $N_{6,7}$ edges are shown in Fig.3. For the multilayers with t_{Pt} = 16 Å, rotation angles per unit period and thickness are almost constant independent of t_{Co}(= 4,10,16 Å), as seen in right side of Figs. 3a) and 3b). This suggests that the contribution of Co atoms to the Co 3*d* - Pt 5*d* hybridization are confined at neighborhood of interface. On the other hand, for the multilayers with t_{Co} = 4 Å rotation angles per unit period are nearly constant independent of t_{Co}(= 4,10,16 Å) as seen in left side of Fig.3a), which contrasted with the case for Co as seen in right side of Fig.2a). As seen in left side of Fig.3b), the rotation angle per unit thickness is large when t_{Pt} is small, but decreases when t_{Pt} increases, which contrasted with the case for Co as seen in right side of Fig.2b). This means that the induced magnetization of Pt is localized around the interface as suggested previously.[2]

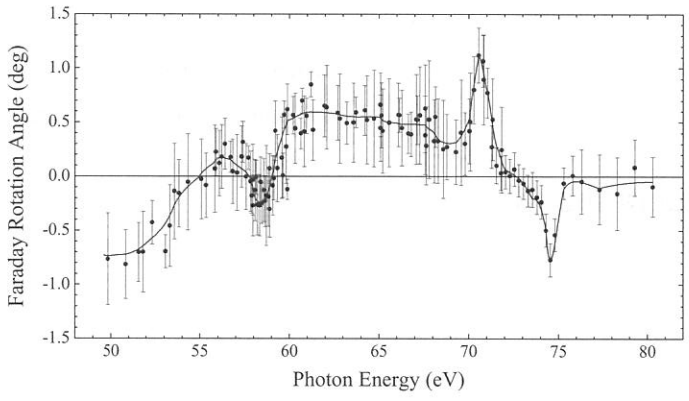

Fig.1. Faraday rotation spectrum of Co(4 Å)/Pt(16 Å) multilayer in 50-80 eV region.

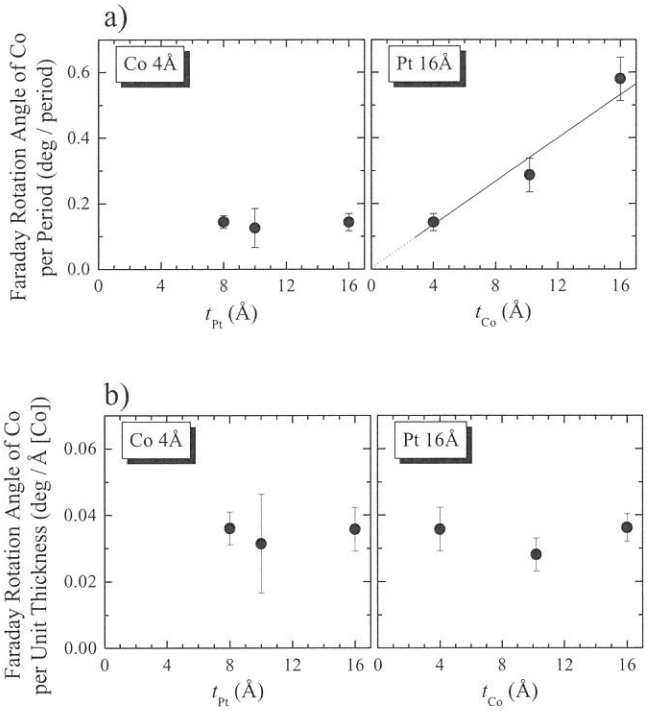

Fig.2. Peak-to-peak value of Faraday rotation angle around Co $M_{2,3}$ absorption edges per a) period and b) unit thickness of Co layer against the Co and Pt one-layer thickness (t_{Co} and t_{Pt}).

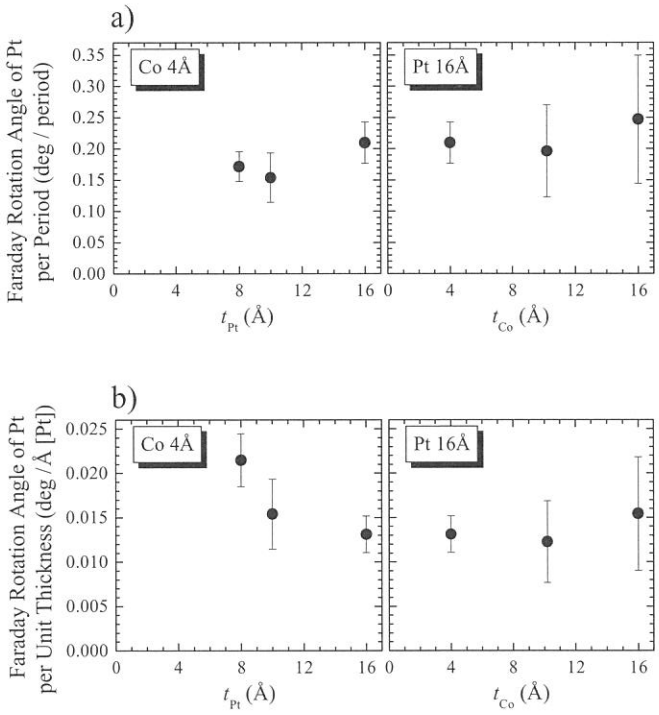

Fig.3. Peak-to-peak value of Faraday rotation angle around Pt $N_{6,7}$ absorption edges per a) period and b) unit thickness of Pt layer against the Co and Pt one-layer thickness (t_{Co} and t_{Pt}).

References

1) M. Igeta, K. Saito, T. Ejima, T. Hatano and M. Watanabe, UVSOR Activity Report 2001 (2002) 152.
2) C. Ederer, M. Komelj, M. Fähnle and G. Schütz, Phys. Rev. B **66** (2002) 094413.